Technical Report

TR-08-01

Validation of coastal oceanographic models at Forsmark

Site descriptive modelling SDM–Site Forsmark

Anders Engqvist, A & I Engqvist Konsult HB

Oleg Andrejev, Finnish Inst. of Marine Research

January 2008

Svensk Kärnbränslehantering AB
Swedish Nuclear Fuel
and Waste Management Co
Box 250, SE-101 24 Stockholm
Tel +46 8 459 84 00

Validation of coastal oceanographic models at Forsmark

Site descriptive modelling SDM–Site Forsmark

Anders Engqvist, A & I Engqvist Konsult HB

Oleg Andrejev, Finnish Inst. of Marine Research

January 2008

Keywords: Numerical model, 3D, Oceanographic measurement, Validation, Water velocity, Salinity, Temperature, Öregrundsgrepen, Baltic Sea.

Abstract

The Swedish Nuclear Fuel and Waste Management Company (SKB) is undertaking site characterisation at two different locations, the Forsmark and the Simpevarp areas, with the objective of siting a geological repository for spent nuclear fuel. The characterisation work is divided into an initial site investigation phase and a complete site investigation phase /SKB 2001/. In this context, the water exchange of the coastal zone is one link of the chain of possible nuclide transport mechanisms that must be assessed in the site description of potential repository areas /Lindborg et al. 2006/.

For the purpose of validating the pair of nested 3D-models employed to simulate the water exchange in the near-shore coastal zone in the Forsmark area, an encompassing measurement program entailing six stations has been performed. The design of this program was to first assess to what degree the forcing of the fine resolution (FR) model of the Forsmark study area at its interfacial boundary to the coarse resolution (CR) model of the entire Baltic was reproduced. In addition to this scrutiny it is of particular interest how the time-varying density-determining properties, salinity and temperature, at the borders are propagated into the FR-domain, since this corresponds to the most efficient mode of water exchange.

An important part of the validation process has been to carefully evaluate which measurement data that can be considered reliable. The result was that several periods of foremost near-surface salinity data had to be discarded due to growth of algae on the conductivity sensors. Lack of thorough absolute calibration of the salinity meters also necessitates dismissal of measurement data.

Relative the assessed data that can be accepted as adequate, the outcome of the validation can be summarized in five points: (*i*) The surface-most salinity of the CR-model drifts downward a little less than one practial salinity unit (psu) per year, requiring that the ensuing correlation analysis be subdivided into periods of a few months; (*ii*) Both 3D-models miss some rapid up- and down-welling episodes that were clearly registered on all salinity- and temperature-meters near the northern interface; (*iii*) The velocity profiles measured at the interface between the two nested models display a low but mainly positive correlation; (*iv*) The salinity dynamics in the interior station is fully acceptably simulated with improved correlation coefficients towards the surface; (*v*) The temperature profiles also generally display a high correlation between measurements and simulated data, certifying that the heat transfer through the surface is acceptably well simulated to render the salinity the dominating factor determining the density, but yet leaving room for further improvements.

It seems safe to conclude that the validation of velocity components has confirmed what has been found in many instances previously, namely that this is a challenge that demands considerably more measuring effort than has been possible to muster in this study in order to average out sub-grid eddies that the model grid does not resolve. For the scalar fields temperature is acceptably well captured by the models, but this is judged to be more an effect of the seasonal variation than an expression of the virtue of the actual models. The internal salinity dynamics is the strong point of the model. Its temporal development at the inner station is convincingly well reproduced by this model approach. This means that the overall computed water exchange of the Öregrundsgrepen can continued to be invested with due confidence.

Sammanfattning

Svensk Kärnbränslehantering AB genomför platsundersökningar vid två olika platser: Forsmarks- och Simpevarpsområdet. Syftet är att lokalisera en långsiktig förvaringsplats för utbränt kärnbränsle. Karaktäriseringsarbetet är uppdelat i två faser varav den första är en initial platsundersökning och den andra en komplett sådan /SKB 2001/. I detta sammanhang utgör vattenutbytet genom kustzonen en länk i en lång transportkedja av möjligt utläckande radionuklider /Lindborg m fl 2006/.

Ett omfattande mätprogram har genomförts i syfte att validera det par av två sammankopplade 3D-modeller som har använts för att simulera vattenutbytet i den strandnära kustzonen i Forsmarksområdet. Modellansatsen består av en grövre upplöst (GU) modell över hela Östersjön och en högupplöst (HU) modell över det studerade kustområdet i Forsmark. Utformningen av detta program syftade i första hand till att utröna i vilken omfattning drivningen över gränssnittet mellan dessa två modeller bestämmer vattenutbytet i det inre högupplösta området. Utöver denna granskning, omfattande sex mätstationer, har det varit av speciellt intresse att se hur densitetsbestämmande egenskaperna salinitet (S) och temperatur (T) vid dessa modellränder propagerar in till de inre delarna av HU-domänen.

En viktig del av valideringsprocessen har varit att noggrannt utvärdera vilka mätdata som kan betraktas som tillförlitliga. Resultatet blev att företrädesvis ytnära salinitetsdata måste förkastas på grund av algpåväxt som inverkar menligt på konduktivitetssensorerna. Brister avseende absolutkalibrering av salinitetsinstrumenten har också medfört att vissa sammanhörande data måst utelämnas från den fortsatta statistiska analysen av uppenbara skäl.

I förhållande till de insamlade data som kan accepteras såsom rättvisande, kan resultatet av denna validering summeras i fem punkter: (*i*) Ytsaliniteten för HU-modellen driver mot avtagande saliniteter av storleksordningen 1 psu-enhet per år. Detta medför att den efterföljande korrelationsanalysen måste delas upp i perioder av några månader. (*ii*) Båda 3D-modellerna missar några upp-/nervällningshändelser med snabbt förlopp som otvetydigt registrerades på samtliga salinitets- och temperaturinstrument i anslutning till den norra randen. (*iii*) Hastighetsprofilerna som registrerades på randen mellan de två sammankopplade modellerna visar små men huvudsakligen positiva korrelationer. (*iv*) Salinitetsdynamiken vid den inre stationen simuleras på ett fullt acceptabelt sätt med förbättrade korrelationsnivåer närmare ytan. (*v*) Temperaturprofilerna visar generellt höga korrelationsnivåer mellan uppmätta och simulerade data, vilket främst visar att värmeöverföringen mellan luften och vattnet simuleras acceptabelt väl så att saliniteten främst blir bestämmande för densiteten, även om utrymme finns för ytterligare förbättringar av värmedynamiken.

Det förefaller som en säker sammanfattning att valideringen av hastighetskomponenterna har bekräftat vad som har visats i många tidigare studier, nämligen att detta utgör en krävande utmaning som fordrar väsentligt mer mätansträngning än vad som varit möjligt att mobilisera i denna studie för att kunna medelvärdesbilda över tids- och rumsskalor som modellerna inte upplöser. Även om temperaturvariationerna modelleras acceptabelt väl, hör detta också samman med den uttalade säsongsdynamiken. Salinitetsdynamiken utgör modellernas starka sida. Dess variationer vid den inre stationen reproduceras övertygande väl av denna modellansats, vilket betyder att det beräknade övergripande vattenutbytet för Öregrundsgrepen med tillförsikt även fortsättningsvis kan betraktas som trovärdigt.

Contents

1 Introduction

1.1 The cascaded 3D-model approach

The Baltic model (AS3D) employed in this study /Andrejev and Sokolov 1989, 1990/ has been developed for the main purpose of providing insight into the circulation of the central Baltic. Its present horizontal resolution is set to 2′×2′ (nautical miles) based on the Warnemünde hypsographic data, see Figure 1-1. This is conveniently referred to as the coarse-resolution (CR) model. In spherical coordinates the model spans the area defined by the southwest corner (53° 48’ N, 9° 27’ E) and the northeast (65° 52’ N, 30° 27’ E). The horizontal diffusivity is nominally set to 30 [m^2/s], consistent with assuming the grid cells to be well mixed. This model is presently involved in several ongoing Baltic hydrographic studies /e.g. Andrejev et al. 2004ab/. A thorough testing of this model in comparison to measured data /Engqvist and Andrejev 2003/ revealed that along an interface to a model area comprising the Stockholm archipelago, the measured salinity and temperature profiles were acceptably well reproduced, with the main difference being an offset in salinity. This evaluation thus increased confidence in the realism of the AS3D model. The heat exchange with the atmosphere is mainly determined by the air temperature; likewise the ice formation and melting processes are formulated in a simple but straightforward manner. This would be a liability if the main concern were to correctly predict the ice situation /e.g. Omstedt 1999/, but in this present study the presence of ice cover has been prescribed by independent observation data. For projection into a distant future, climate scenarios could more likely produce a prognosis of shifting air temperatures, while other factors determining the heat exchange (insolation, relative humidity and nebulosity) would probably be more inaccessible.

The grid of the local fine-resolution (FR) 3D-model has been computed from a Digital Elevation Model (DEM) based on national digitized charts, complemented with shoreline information from economical maps. The grid has been specified in spherical coordinates WGS84 (sweref 99 long lat ellh) with the constraint that to be considered as a wet grid cell at least 50% of the covered area must consist of water. The numerical scheme is identical to the Baltic (CR) model but the horizontal diffusivity is nominally set to 20 [m^2s^{-1}] compared to 30 [m^2s^{-1}] for the Baltic model. The Forsmark coastal area was resolved horizontally into grid cells with a side length of 0.1×0.1 nautical mile (Figure 1-2) defined by the SW corner with spherical coordinates (60° 08’ N; 17° 59’ E) and the NE corner (60° 32’ N,18° 47’ E). The final choice of the actual model area includes a large section east of the Gräsö island that would barely seem to influence the strait connection to the southern section of model area that connects to Öregrundsgrepen through Öregrundsund. These waters east of Gräsö are subject to military restrictions and the bathymetry has therefore been only coarsely charted. It is thus advantageous to include these bathymetric uncertainties in a large buffer area that interfaces to the Baltic. The grid resolves the main underwater features of this coastal section, but does more poorly for the near-shore island clusters and for the landlocked waters in the vicinity of Östhammar. In fact, when using the objective gridding criterion that at least 50% of area must consist of water meant that these interior waters were disconnected at a few locations. In order to attach these to the main computational domain, manual corrections were performed.

The overall objective has been to evaluate the two nested numerical models with differing resolution (CR and FR) regarded as an operational entity and to investigate their combined capacity to simulate the measured oceanographic data that were assessed to this end.

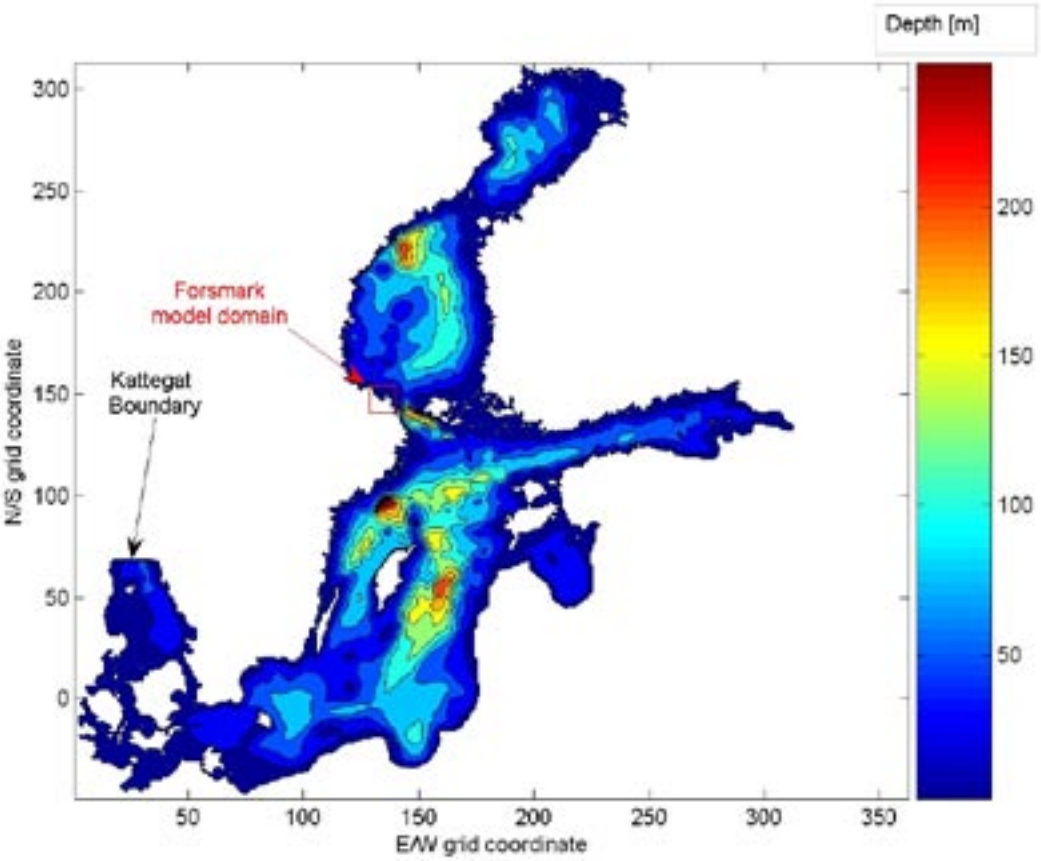

Figure 1-1. *Bathymetry of the Baltic model resolved into a grid with 2×2 nautical mile side length. The fine-resolution model of the Forsmark area and its approximate interface to the Baltic model in indicated with a red box. The Baltic model's open boundary between the Kattegat the Skagerrak is also indicated.*

1.2 Design of the field program

The general design idea of the field program was primarily to assess the oceanographic state parameters at some locations distributed as evenly as possible on the boundaries of the local model (FR-) grid which are coincidental with the interfaces to the nested (CR-) grid of the Baltic model. These stations are listed in Table 1-1 and their positions are shown in Figure 1-2 and supposedly they should represent the forcing of the large-scale events onto the fine-resolved local model domain. The oceanographic measurements consist of both vector entities, i.e. current velocities, and the scalar properties temperature and salinity.

Temperature is measured directly by use of thermistors but salinity is indirectly inferred from measured conductivity. All salinities in the following are thus presented dimensionless in the psu-scale. These scalar properties determine (together with pressure) the density of the sea water. Assessment of these at the periphery together with heat exchange with the atmosphere and freshwater discharge makes it possible to model their propagation into the centre of the domain where an evaluation relative other measurement sites can be performed. The measurement procedures of oceanographical parameters have been specified by /Johansson and Morosini 2002/.

Table 1-1. Overview of the naming and locations of the measurement stations. The RT90 coordinates differ from corresponding positions stated in /Lindow 2005/.

Location name	Station ID		Position				Depth	
			Northing	Easting	lat	long	desired	realized
	SKB	SMHI	(RT90 2.5 gon V (Ø:-15))		(WGS 84 Sweref 99)		[m]	[m]
Northen boundary East	PFM002653	Fo11	6715605	1639787	60° 32.0'N	18° 20.8'E	30	36
Northen boundary West	PFM002654	Fo12	6715233	1630543	60° 32.0'N	18° 11.0'E	23	24
Inner station I	PFM002655	Fo13	6699922	1638914	60° 23.6'N	18° 19.5'E	19	21
Strait of Öregrundssund	PFM002656	Fo14	6693919	1647130	60° 20.2'N	18° 27.9'E	20	27
Inner station II	PFM002657	Fo15	6701336	1641895	60° 24.3'N	18° 22.8'E	30	28
Southern boundary	PFM002658	Fo16	6684497	1657318	60° 14.86'N	18° 38.56'E	25	19

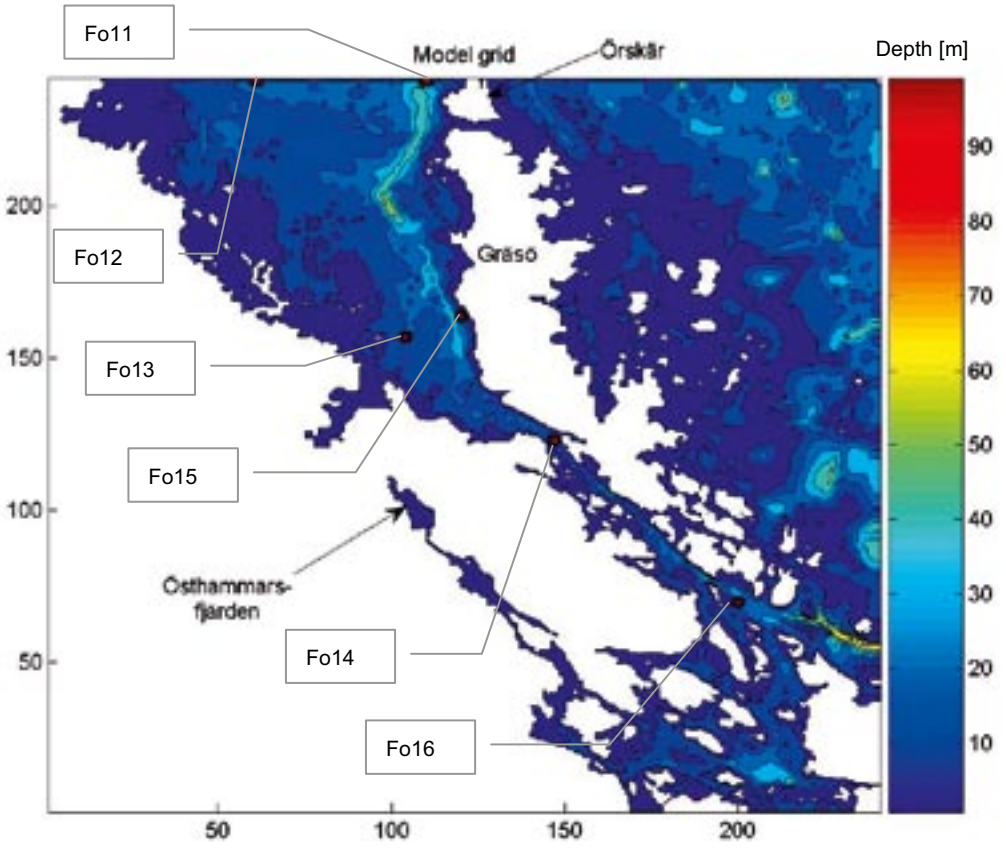

Figure 1-2. *The chosen model area with some of the grid cells manipulated manually. In particular the channel connecting Östhammarsfjärden with the southern basins has been made sufficiently wide in a few sections to permit through flow. The six red spots mark the sites of deployed oceanographic instruments during the validation year 2004 and are labelled with the reference naming of these stations. Some geographical names referred to in the text have been indicated.*

Based on experience from other similar validation endeavors, it was anticipated that for the scalar data, it should be unproblematic to make a direct and fair evaluation, while vector comparisons would be considerably more difficult. In negotiations with the contracted executioner of the field program, Swedish Meteorological and Hydrological Institute (SMHI), bottom-placed ADCP-instruments were recommended over RCM-instruments that also normally can be equipped to measure salinity and temperature. The argument was partly that bottom-placed instruments are less vulnerable to interfering with other maritime activities and partly that they are less expensive to deploy and operate.

The agreed understanding was that the executioner of the field programme should also have a say on the location of instrument deployment because they take the economic risk. For both instruments deployed on Fo11 and Fo15 their relocation from the recommended positions (60º 32.0'N, 18º 19.0'E respectively 60º 24.3'N, 18º 22.5'E) were agreed on beforehand due to navigational hazard considerations, but Fo14 was tacitly moved in stages from its desired position in the middle of Öregrundsund channel (60º 21.1'N, 18º 27.2'E) to decisively more secluded lateral positions.

In order to secure data, the one-year measurement period was subdivided into four sections with approximately equal duration but open to allowances due to bad weather conditions and other incidents that are difficult to apprehend. This plan was specified in detail in the Activity plan AP PF 400-03-105 with Sara Karlsson as the contemporary SKB representative.

1.3 Overview of the measurement program

The measurement program was originally planned to start on January 1, 2004, but due to the ice situation, this was delayed until mid-April the same year. In Table 1-2 the field program is specified in detail regarding the measured parameters and their deployment with regard to depth. This table also gives a first rough presentation of the data yield and also lists the names of the resulting 67 data files.

It seems safe to state that the actual handling and deployment of the instruments has been conducted professionally and with meticulous care. The handling and communication of data has on the other hand left more to be desired. Initially there was a complete abandonment of the specified protocol and even in the same file (e.g. time denoting), data format could be changed several times in the same file. No inspection of the presumed validity of data was performed by SMHI, but was passed over to be performed by SKB. It is also fair to state that by the end of the validation year, the accumulated criticism also led to a noticeable improvement on SMHI's performance in this regard.

The report on the assessment of oceanographic data conducted by SMHI /Lindow 2005/ admits most of the shortcomings, but not all. In Table 1-3 some of the additional sources of consternation have been commented upon.

1.4 Validation strategy

The overall validation plan is straightforward and consists of first inspecting the measurement data to dismiss the sections that for various reasons cannot be trusted. Then follows an encompassing investigation of the spectral appearance of the remaining data in order to determine an appropriate sampling frequency for the comparison with matching simulated data. Finally the actual comparisons are performed, which in most cases result in cross-correlation analysis. The six measurement locations, Fo11 through F16, are treated in order. Since there are no reliable sea level data available, an examination of this part has been omitted.

Table 1-2. Overview of the naming of the data files and what measured entity they denote.

Station ID				Instrument	Meas.	File	Naming		
SMHI	SKB	period	depth	type	param.	number	Original SMHI file name	Systematic name	SICADA_06_104_7
Fo11	PFM002653	1st	1.5 m	CTD	T,C	1	AaCTD 107 Fo11-1,5m.xls	Fo11_1of4_N1_TC_02m_hr.csv	OC010\temp_cond_salinity.csv
	PFM002653	1st	10 m	CTD	T,C	2	AaCTD 108 Fo 11-10m.xls	Fo11_1of4_N1_TC_10m_hr.csv	OC010\temp_cond_salinity.csv
	PFM002653	1st	17.5 m	CTD	T,C	3	AaCTD109 Fo11-17,5m.xls	Fo11_1of4_N1_TC_17m_hr.csv	OC010\temp_cond_salinity.csv
	PFM002653	1st	25 m	CTD	T,C	4	AaCTD110 Fo11-25 m.xls	Fo11_1of4_N1_TC_ 25m_hr.csv	OC010\temp_cond_salinity.csv
	PFM002653	1st	5:2:33 m	ADCP	15x(U,V)	5	FSMD0407_ver3.xls a)	Fo11_1of4_N1_15xUV_hr.csv	OC002\current_data_adcp.csv
	PFM002653	2nd	1.5 m	CTD	T,C	6	AaCTD 126 Fo 11-1,5m.xls	Fo11_2of4_N1_TC_02m_hr.csv	OC010\temp_cond_salinity.csv
	PFM002653	2nd		CTD	T,C	7	AaCTD 112 Fo11-10m.xls	Fo11_2of4_N1_TC_10m_hr.csv	OC010\temp_cond_salinity.csv
	PFM002653	2nd	17.5 m	CTD	T,C	8	AaCTD 113 Fo 11-17,5m.xls	Fo11_2of4_N1_TC_17m_hr.csv	OC010\temp_cond_salinity.csv
	PFM002653	2nd	25 m	CTD	T,C	9	AaCTD114-Fo11-25m.xls	Fo11_2of4_N1_TC_25m_hr.csv	OC010\temp_cond_salinity.csv
	PFM002653	2nd	5:2:33 m	ADCP	15x(U,V)	10	FSMD0410_ver3.xls b)	Fo11_2of4_N1_15xUV.csv	OC002\current_data_adcp.csv
	PFM002653	3rd	1.5 m	CTD	T,C & P	11	AaCTD 126 Fo 11-1,5m.xls	Fo11_3of4_N1_TC_02m_hr.csv	OC010\temp_cond_salinity.csv
	PFM002653	3rd	10 m	CTD	T,C	12	AaCTD 127 Fo11-10m.xls	Fo11_3of4_N1_TC_10m_hr.csv	OC010\temp_cond_salinity.csv
	PFM002653	3rd	17.5 m	CTD	T,C	13	AaCTD 128 Fo 11-17,5m.xls	Fo11_3of4_N1_TC_17m_hr.csv	OC010\temp_cond_salinity.csv
	PFM002653	3rd	25 m	CTD	T,C	14	AaCTD 129 Fo11-25m.xls	Fo11_3of4_N1_TC_25m_hr.csv	OC010\temp_cond_salinity.csv
	PFM002653	3rd	4:2:32 m	ADCP	15x(U,V)	15	BBSC3A_ver3.xls	Fo11_3of4_N1_15xUV_hr.csv	OC002\current_data_adcp.csv
	PFM002653	4th	5 m	CTD	T,C & P		missing		
	PFM002653	4th	10 m	CTD	T,C	16	AaCTD 130 Fo11-10m.xls	Fo11_4of4_N1_TC_10m_hr.csv	OC010\temp_cond_salinity.csv
	PFM002653	4th	17.5 m	CTD	T,C	17	AaCTD 131 Fo 11-17,5m.xls	Fo11_4of4_N1_TC_17m_hr.csv	OC010\temp_cond_salinity.csv
	PFM002653	4th	25 m	CTD	T,C	18	AaCTD 132 Fo11-25m.xls	Fo11_4of4_N1_TC_25m_hr.csv	OC010\temp_cond_salinity.csv
	PFM002653	4th	4:2:32 m	ADCP	15x(U,V)		missing		
Fo12	PFM002654	1st	12 m	RCM+	U,D,T,C,S	19	S 3033 Fo12-12m.xls	Fo12_1of4_N1_UDCT_12m_hr.csv	OC010\temp_cond_salinity.csv
	PFM002654	2nd	12 m	RCM+	U,D,T,C,S	20	S3035 Fo12-12m.xls	Fo12_2of4_N1_UDCT_12m_hr.csv	OC010\temp_cond_salinity.csv
	PFM002654	3rd	12 m	RCM+	U,D,T,C,S,P	21	AaS3037 Fo12-12m.xls	Fo12_3of4_N1_UDCT_12m_hr.csv	OC150\current_cond_salin.csv
	PFM002654	4th	15 m	RCM+	U,D,T,C,S,P	22	Fo12-4_AaS3040_15m.xls	Fo12_4of4_N1_UDCT_15m_hr.csv	OC150\current_cond_salin.csv
Fo13	PFM002655	1st	1.5 m	CTD	T,C	23	AaCTD104 Fo13-1,5m.xls	Fo13_1of4_I1_TC_02m_hr.csv	OC010\temp_cond_salinity.csv
	PFM002655	1st	10 m	CTD	T,C	24	AaCTD 105 Fo13-10m.xls	Fo13_1of4_I1_TC_10m_hr.csv	OC010\temp_cond_salinity.csv
	PFM002655	1st	17.5 m	CTD	T,C	25	AaCTD 106 Fo13-17,5 m.xls	Fo13_1of4_I1_TC_17m_hr.csv	OC010\temp_cond_salinity.csv
	PFM002655	2nd	1.5 m	CTD	T,C	26	AaCTD 118 Fo13-1,5m.xls	Fo13_2of4_I1_TC_02m_hr.csv	OC010\temp_cond_salinity.csv
	PFM002655	2nd	10 m	CTD	T,C	27	AaCTD119 Fo13-10m.xls	Fo13_2of4_I1_TC_10m_hr.csv	OC010\temp_cond_salinity.csv
	PFM002655	2nd	17.5 m	CTD	T,C	28	AaCTD 120 Fo13-17,5m.xls	Fo13_2of4_I1_TC_17m_hr.csv	OC010\temp_cond_salinity.csv
	PFM002655	3rd	1.5 m	CTD	T,C	29	AaCTD121 Fo13-1,5m.xls	Fo13_3of4_I1_TC_02m_hr.csv	OC010\temp_cond_salinity.csv
	PFM002655	3rd	10 m	CTD	T,C	30	AaCTD122 Fo13-10m.xls	Fo13_3of4_I1_TC_10m_hr.csv	OC010\temp_cond_salinity.csv
	PFM002655	3rd	17.5 m	CTD	T,C	31	AaCTD123 Fo13-17,5m.xls	Fo13_3of4_I1_TC_17m_hr.csv	OC010\temp_cond_salinity.csv
	PFM002655	4th	6 m	CTD	T,C	32	Fo13-4_AaCTD-133_6m.xls	Fo13_4of4_I1_TC_06mhr.csv	OC010\temp_cond_salinity.csv
	PFM002655	4th	10 m	CTD	T,C	33	Fo13-4_AaCTD-134_10m.xls	Fo13_4of4_I1_TC_10m_hr.csv	
	PFM002655	4th	17.5 m	CTD	T,C	34	Fo13-4_AaCTD-135_17.5m.xls	Fo13_4of4_I1_TC_17m_hr.csv	OC010\temp_cond_salinity.csv
Fo14	PFM002656	1st	2:1:25 m	ADCP	24x(U,D)	35	ADP Fo14- 001.xls	Fo14_1of4_M1_24xUD_hr.csv	OC001\current_vel_dir.csv
	PFM002656	2nd	0.5:23.5 m	ADCP	24x(U,D)	36	ADP Fo14- 002.xls	Fo14_2of4_M1_24xUD_hr.csv	OC001\current_vel_dir.csv
	PFM002656	3rd	0.5:21.5 m	ADCP	22x(U,D)	37	ADP Fo14- 003.xls	Fo14_3of4_M1_22xUV_hr.csv	OC002\current_data_adcp.csv
	PFM002656	4th	03:01:23	ADCP	21x(U,D)	38	FO14-4_ADP.xls	Fo14_4of4_M1_21xUV_hr.csv	OC002\current_data_adcp.csv
	PFM002655	1st		CTD			missing		
	PFM002656	2nd		CTD	T,C	39	Fo14- Seabird.xls	Fo14_2of4_M1_TC_25m_hr.csv	OC010\temp_cond_salinity.csv
	PFM002656	3rd		CTD	T,C	40	FO141020Seabird.xls	Fo14_3of4_M1_TC_23m_hr.csv	OC010\temp_cond_salinity.csv
	PFM002656	4th		CTD	T,C	41	Fo14-4_SBE37_24m.xls	Fo14_4of4_M1_TC_24m_hr.csv	OC010\temp_cond_salinity.csv
Fo15	PFM002657	1st		TC	11xT	42	T3034 Fo15 april-jul2004.xls	Fo15_1of4_I1_TK_hr.csv	OC100\temperature_depths.csv
	PFM002657	2nd		TC	11xT	43	T3037 Fo15.xls	Fo15_2of4_I1_TK_hr.csv	OC100\temperature_depths.csv
	PFM002657	3rd	01:2:6:27	TC	11xT	44	AaT3039 Fo151m-27m.xls	Fo15_3of4_I1_TK_hr.csv	OC100\temperature_depths.csv
	PFM002657	4th	01:2:6:27	TC	11xT		missing		
Fo16	PFM002658	1st	1.5 m	CTD	T,C	45	AaCTD 101 Fo16-1,5m.xls	Fo16_1of4_S1_TC_2m_hr.csv	OC010\temp_cond_salinity.csv
	PFM002658	1st	10 m	CTD	T,C	46	AaCTD102 Fo16-10m.xls	Fo16_1of4_S1_TC_10m_hr.csv	OC010\temp_cond_salinity.csv
	PFM002658	1st	18 m	CTD	T,C	47	AaCTD103 Fo16-18m.xls	Fo16_1of4_S1_TC_18m_hr.csv	OC010\temp_cond_salinity.csv
	PFM002658	2nd	1.5 m	CTD	T,C	48	AaCTD 115 Fo16-1.5m.xls	Fo16_2of4_S1_TC_2m_hr.csv	OC010\temp_cond_salinity.csv
	PFM002658	2nd	10 m	CTD	T,C	49	AaCTD 116 Fo16-10m.xls	Fo16_2of4_S1_TC_10m_hr.csv	OC010\temp_cond_salinity.csv
	PFM002658	2nd	18 m	CTD	T,C	50	AaCTD 117 Fo16-18m.xls	Fo16_2of4_S1_TC_18m_hr.csv	OC010\temp_cond_salinity.csv
	PFM002658	3rd	1.5 m	CTD	T,C	51	AaCTD 124 Fo16-1.5m.xls	Fo16_3of4_S1_TC_02m_hr.csv	OC010\temp_cond_salinity.csv
	PFM002658	3rd	10 m	CTD	T,C		missing		
	PFM002658	3rd	18 m	CTD	T,C	52	AaCTD125 Fo16-18m.xls	Fo16_3of4_S1_TC_18m_hr.csv	OC010\temp_cond_salinity.csv
	PFM002658	4th	6 m	CTD	T,C	53	Fo16-4_AaCTD-136_6m.xls	Fo16_4of4_S1_TC_06m_hr.csv	OC010\temp_cond_salinity.csv
	PFM002658	4th	10 m	CTD	T,C	54	Fo16-4_AaCTD-137_10m.xls	Fo16_4of4_S1_TC_10m_hr.csv	OC010\temp_cond_salinity.csv
	PFM002658	4th	18 m	CTD	T,C	55	Fo16-4_AaCTD-138_18m.xls	Fo16_4of4_S1_TC_18m_hr.csv	OC010\temp_cond_salinity.csv
Tran-		0th		ADCP	U,V	56	Fors042r.000		
sects		1st		ADCP	U,V	57	Fors 074r.000		
		2nd		ADCP	U,V	58	Fors110r.000		
		2nd		ADCP	U,V	59	Fors111r.000		
		3rd		ADCP	U,V		missing		
		3rd		ADCP	U,V		missing		
		4th		ADCP	U,V	60	Fors000r.000 Fors001r.000		
		4th		ADCP	U,V	61-66	Fo27000r.000 (X=1,3,5,6-8)	=6 files	
		4th		ADCP	U,V	67	Fo28001r.000		
							a) ADCPBBSCfo11-001.xls		
							b) ADCPSCFo11-002.xls		

Table 1-3. Overview of the temporal aspects of data and ensuing remarks and responses of the executioner of the field programme.

Station ID				Instrument	Meas.	UTC time used consistently				File	Remarks on the	SMM's	SMM reporting
SMM	SBD	period	depth	type	params	start	hour	stop	hour	number	originally delivdata	response	SBDP-01-191
Fot1	PFM002953	1st	1.5 m	CTD	T,C	20040416	11	20040501	0	1			
	PFM002953	1st	10 m	CTD	T,C	20040416	11	20040721	7	2			
	PFM002953	1st	17.5 m	CTD	T,C	20040416	11	20040721	7	3			
	PFM002953	1st	25 m	CTD	T,C	20040416	11	20040721	7	4			
	PFM002953	1st	4-2:33 m	ADCP	16x(U,V)	20040416	10	20040720	6	5	UTC+1 wrongly stated	Corrected	Differing file name
	PFM002953	2nd	1.5 m	CTD	T,C	20040721	17	20040807	8	5	Algal growth on C-sensor	Conceded	
	PFM002953	2nd		CTD	T,C	20040721	17	20040807	8	7	Algal growth on C-sensor	Conceded	
	PFM002953	2nd	17.5 m	CTD	T,C	20040721	17	20041021	9	9			
	PFM002953	2nd	25 m	CTD	T,C	20040721	17	20041021	9	9			
	PFM002953	2nd	4-2:33 m	ADCP	16x(U,V)	20040721	16	20041030	65	10	2 days less in SICADA data		Differing file name
	PFM002953	3rd	1.5 m	CTD	T,C & P	20041021	9	20050206	7	11			
	PFM002953	3rd	10 m	CTD	T,C	20041021	9	20050206	7	12			
	PFM002953	3rd	17.5 m	CTD	T,C	20041021	13	20050206	7	13			
	PFM002953	3rd	25 m	CTD	T,C	20041021	13	20050206	7	14			
	PFM002953	3rd	4-2:32 m	ADCP	15x(U,V)	20041139	13.5	20050207	11	15	UTC+1 wrongly stated	Conceded	Not listed
	PFM002953	4th	5 m	CTD	T,C & P						Missing - specified acc. to AP	dismissed on purpose	Acknowledged
	PFM002953	4th	10 m	CTD	T,C	20050228	12.0	20050425	150	16	Unstable stratification		
	PFM002953	4th	17.5 m	CTD	T,C	20050228	12.0	20050425	150	17	Unstable stratification		
	PFM002953	4th	25 m	CTD	T,C	20050228	12.0	20050425	150	18	Format problem		
	PFM002953	4th	4-2:32 m	ADCP	15x(U,V)	20050228		20050426			Missing - specified acc. to AP	Battery leakage	Acknowledged
Fot2	PFM002954	1st	1.2 m	ROM-	U,D,T,C,S	20040420	9.5	20040720	16	19			
	PFM002954	2nd	1.2 m	ROM-	U,D,T,C,S	20040720	17.5	20041021	8	20	Format problem		CTD check failed
	PFM002954	3rd	1.2 m	ROM-	U,D,T,C,S,P	20041021	10	20050206	15	21	Algal growth on C-sensor		
	PFM002954	4th	1.5 m	ROM-	U,D,T,C,S,P	20050208	10.0	20050425	14.0	22	P in [hPa], U in [cm/s]		
Fot3	PFM002955	1st	1.5 m	CTD	T,C	20040420	10	20040720	14	23			
	PFM002955	1st	10 m	CTD	T,C	20040420	10	20040720	10	24			
	PFM002955	1st	17.5 m	CTD	T,C	20040410	10	20040720	10	25			
	PFM002955	2nd	1.5 m	CTD	T,C	20040720	16	20041019	11	26			
	PFM002955	2nd	10 m	CTD	T,C	20040720	16	20041019	11	27			
	PFM002955	2nd	17.5 m	CTD	T,C	20040720	16	20041019	11	28			
	PFM002955	3rd	1.5 m	CTD	T,C	20041019	13	20050134	11	29			
	PFM002955	3rd	10 m	CTD	T,C	20041019		20050134		30	Unrealistic salinities	Battery failure	Acknowledged
	PFM002955	3rd	17.5 m	CTD	T,C	20041019	13	20050134	11	31			
	PFM002955	4th	6 m	CTD	T,C	20050134	14.5	20050425	11.5	32	unstable stratification		Corrected data
	PFM002955	4th	10 m	CTD	T,C	20050134	14.5	20050425	11.5	33	Salinity sensor not working	Conceded	Acknowledged
	PFM002955	4th	17.5 m	CTD	T,C	20050134	14.5	20050425	11.5	34	unstable stratification		
Fot4	PFM002956	1st	21-25 m	ADCP	24x(U,D)	20040421	14	20040720	6.5	35			"Not a good
	PFM002956	2nd	3.5-23.5 m	ADCP	24x(U,D)	20040730	15.5	20041019	7	36	Moved to back water	Confirmed	position for
	PFM002956	3rd	3.5-21.5 m	ADCP	22x(U,D)	20041030	11	20050134	15	37	UD->UV; UTC+1 feilaktig angivet	Conceded	this ADCP
	PFM002956	4th	03-01-23	ADCP	21x(U,D)	20050135	11.4	20050416	10.0	38			in back-water"
		1st		CTD							Dismissal agreed		Acknow.
	PFM002956	2nd		CTD	T,C	20040730	15	20041018	16	39			
	PFM002956	3rd		CTD	T,C	20041030	10	20050134	14	40			
	PFM002956	4th		CTD	T,C	20050135	11.0	20050414	9.0	41	Data in this interval OK		Boat interference ?
Fot5	PFM002957	1st		TC	T1xT	20040420	14	20040720	12	42			
	PFM002957	2nd		TC	T1xT	20040720	14	20041019	9	43			
	PFM002957	3rd	01:2.6:27	TC	T1xT	20041019	11	20050134	13	44			
	PFM002957	4th	01:2.6:27	TC	T1xT						Dismissal agreed		
Fot6	PFM002958	1st	1.5 m	CTD	T,C	20040421	10	20040720	9	45			
	PFM002958	1st	10 m	CTD	T,C	20040421	10	20040720	9	46			
	PFM002958	1st	18 m	CTD	T,C	20040421	10	20040720	9	47			
	PFM002958	2nd	1.5 m	CTD	T,C	20040720	14	20041019	9	48			
	PFM002958	2nd	10 m	CTD	T,C	20040720	11	20041018	12	49			
	PFM002958	2nd	18 m	CTD	T,C	20040720	11	20041018	12	50			
	PFM002958	3rd	1.5 m	CTD	T,C	20041018	15	20050134	8	51	strange S transition 2->3	Acknowledged	
	PFM002958	3rd	10 m	CTD	T,C								Batt. Failure
	PFM002958	3rd	18 m	CTD	T,C	20041018	15	20041225	21	52	strange S transition 2->3	No data after 20051220	Conceded
	PFM002958	4th	6 m	CTD	T,C	20050134	11.5	20050425	8.5	53			
	PFM002958	4th	10 m	CTD	T,C	20050134	11.4	20050426	8.4	54			
	PFM002958	4th	18 m	CTD	T,C	20050134	11.5	20050425	8.5	55			
Tran-sects	North boundary	0th		ADCP	U,V	20040416		20040416		56			
	North boundary	1st		ADCP	U,V	20040721		20040721		57			
		2nd		ADCP	U,V	20041110		20041110		58	Point measurement		
	North boundary	2nd		ADCP	U,V	20041110		20041110		59			
	North boundary	3rd									Dismissed due to weather		
	East boundary	3rd									Dismissed due to weather		
	North boundary	4th		ADCP	U,V	20050426		20050426		60			
		4th		ADCP	U,V	20050427		20050427		61-66	6 EAY extra transects N Fot1	wrong coord. conceded	
	East boundary	4th		ADCP	U,V	20050427		20050427		67			

2 Materials and methods

2.1 Model forcing data – temporal scales

The generic Baltic model (AS3D) employed in this study /Andrejev and Sokolov 1989, 1990/ together with its local variant modelling the Forsmark area with a horizontal resolution of 0.1×0.1 nautical miles are both based on the primitive (sensu fundamental) Navier-Stokes equations formulated on a so-called C-grid and is thus inherently similar to many other 3D-models. The numerical implementation has however several advanced features /Andrejev and Sokolov 1997/. The oceanographic state variables are condensed into files that can be inspected and graphically rendered with a specially designed tool named DAS (Data Assimilation System). In the Öregrundsgrepen area earlier development versions of this model have been applied a number of times /Engqvist and Andrejev 1999, 2000/ and also in special studies with focus on Average Age (AvA) and trajectory analysis /Engqvist et al. 2006/ as general measures of water exchange.

An important aspect in the general modelling context is the temporal resolution of the forcing given in Table 2-1. It is seen that the imposed forcing with the highest frequency pertains to the boundary data of salinity, temperature and sea level, which have been computed by the 3D-model of the Baltic. Of these data, the sea level subset is the one with the highest potential to induce rapid changes in the interior of model domain since such changes are propagated with the speed of a long surface wave, while salinity and temperature fluctuation combine to form density variations which are propagated with the considerable slower speed of internal waves. For the long surface waves it would – under reasonable assumptions – take more than 20 minutes to travel the approximate 20 km from the boundaries to a mid-point of the model area. This in turn means that the highest expected forcing would be of the order of an hour, so this has been the chosen frequency rate at which modelled data have been saved for the ensuing comparison with measurement data.

Table 2-1. Overview of the forcing and other model data with regard to temporal resolution. FNP stands for Forsmark Nuclear Plants, DMI for Danish Meteorological Institute, FIMR for Finnish Institute of Marine Research and NLS is National Land Survey of Sweden.

				Baltic model (BAF3D)					Local model (For3D)				Remark
		data	time re-	2004 quarters				2005	2004 quarters			2005	
Forcing and other model data		source	solution	1st	2nd	3rd	4th	1st	2nd	3rd	4th	1st	
Grid of the 3D-model		NLS	-										Grids delivered 2004-06-07
Boundary forcing													
Göteborg (Öbg)	sea level	SMHI	1h										
Skagen	sea level	DMI	1h										
Forsmark model domain	sea level + SST		0.5h										Data derived from the Baltic 3D-model
Meteorological data	misc. parsers	SMHI	3h										Mesan and/or Mueller synoptic data
Freshwater discharge	whole Baltic	SMHI	mon										HBV-model data. Delivered Mar'06
	Forsmarksån	SMHI	w										
	Olandsån	SMHI	w										2005 measurements delivered Mar'06
Cooling water	volume flow	FNP	mon										
	over temp.	FNP	-										
	shut-down period	FNP	2 w										Shut-down period of reactor F1 is estimated
Ice formation & breakup		FIMR	1d										
Validation data:													
Initialization S/T data		ICES	-										Climatic data + spin-up runs
Salt & Temp profiles		SMHI	1h										
Current velocities		SMHI	1h										
Sea level data			-										No data available

The assessment of forcing data has not been without problem. The meteorological forcing data (so-called Mueller data set consisting of synoptical geostrophic wind) that have been used in earlier modelling studies /Engqvist and Andrejev 1999, 2000/ were stated by SMHI to be discontinued after 2001. To make up for this loss, so-called Mesan-data were offered to serve as a substitute. The geographical coverage of these grids is depicted in Figure 2-1. The first model runs of 2004 were thus relying on the Mesan-data. Late in 2005 it was revealed that the Mueller data set for 2004 was available again and this extension eventually also included the first half year of 2005. A scatter diagram of these two data sets for July 2004 is presented in Figure 2-2 and yields that the correlation coefficient is 0.51, which must be regarded as surprisingly low considering the amount of dependent data that ought to be shared between these two sets. A further comparison of logged wind speed at the island Örskär to the nearest corresponding grid points of the two meteorological data sets is given in Figures 2-3a and 2-3b which demonstrate that for this location the Mueller data set is evidently the more realistic of the two.

After Mueller data were made available, all simulations have eventually been performed both with the Mesan and the Mueller data sets. Generally, the simulation results and subsequent analysis concerning 2004 are based on runs with Mesan data, while for 2005 results based on the Mueller data are presented. From this rule there exist a few exceptions, however, in which results with both data sets are presented for comparison, e.g. Figures 3-8 and 3-10.

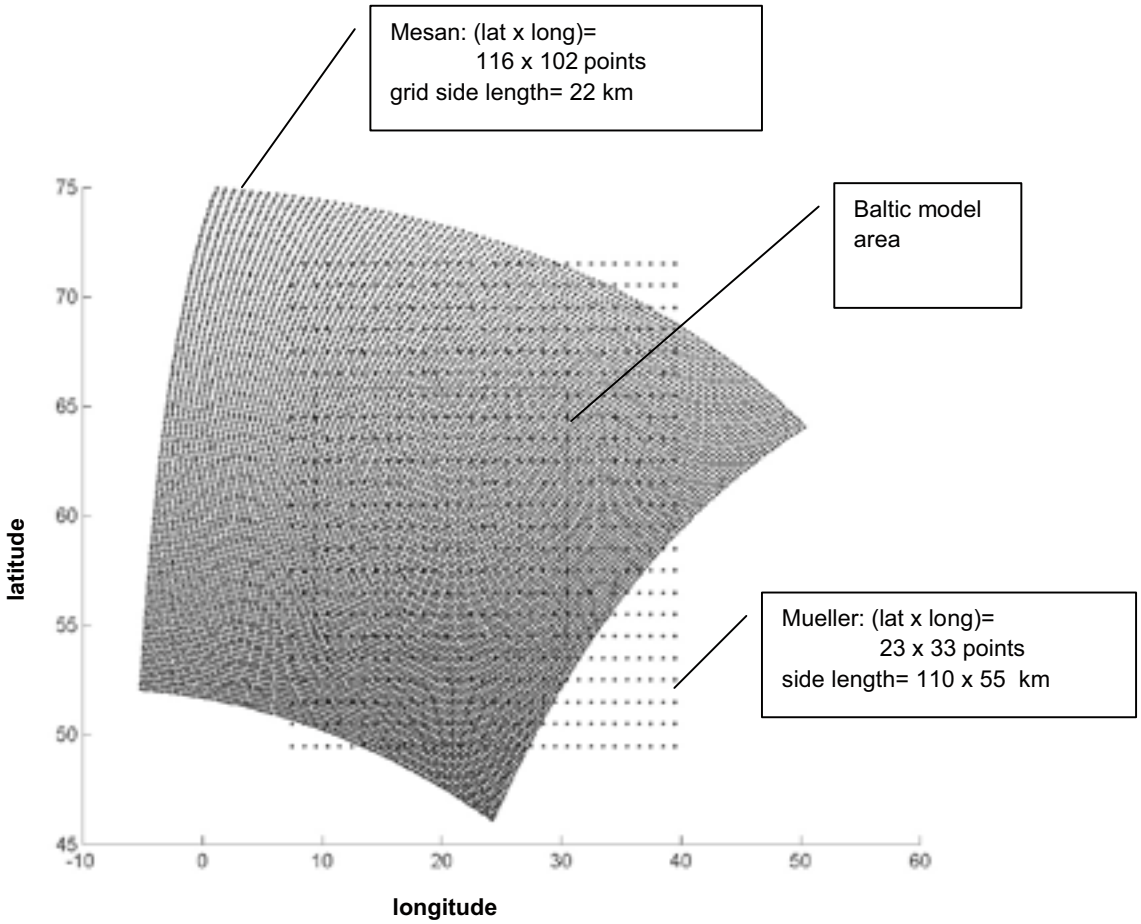

Figure 2-1. *Illustration of the transformation relationship between the two mutually rotated coordinate systems for the Mueller and the Mesan data sets. Both these sets cover the Baltic model area domain completely.*

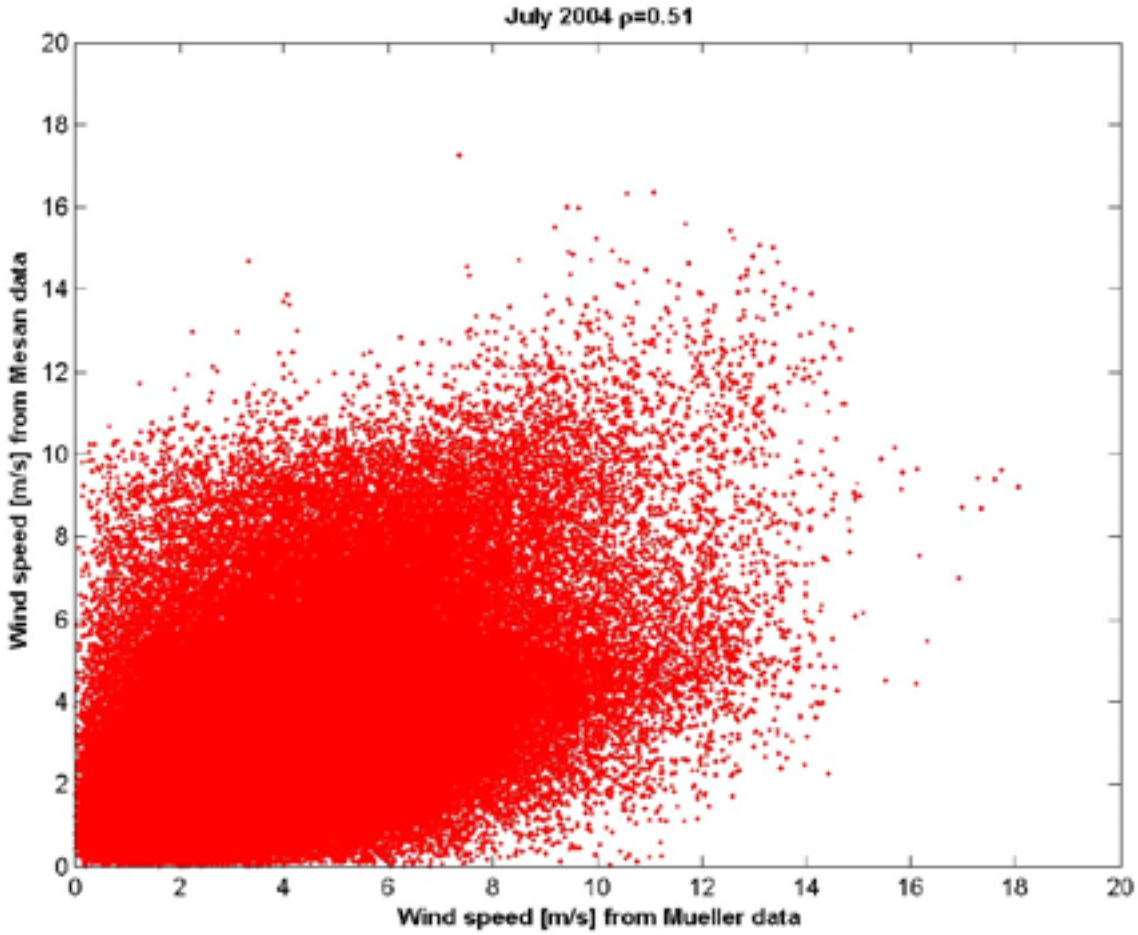

Figure 2-2. *Scatter diagram of wind speeds of all 3 h-measurements and for the entire grid for the representative month of July 2004. The Mueller data have been adjusted to match the 10 m-level of the Mesan data. This comparison results in a correlation coefficient of 0.51.*

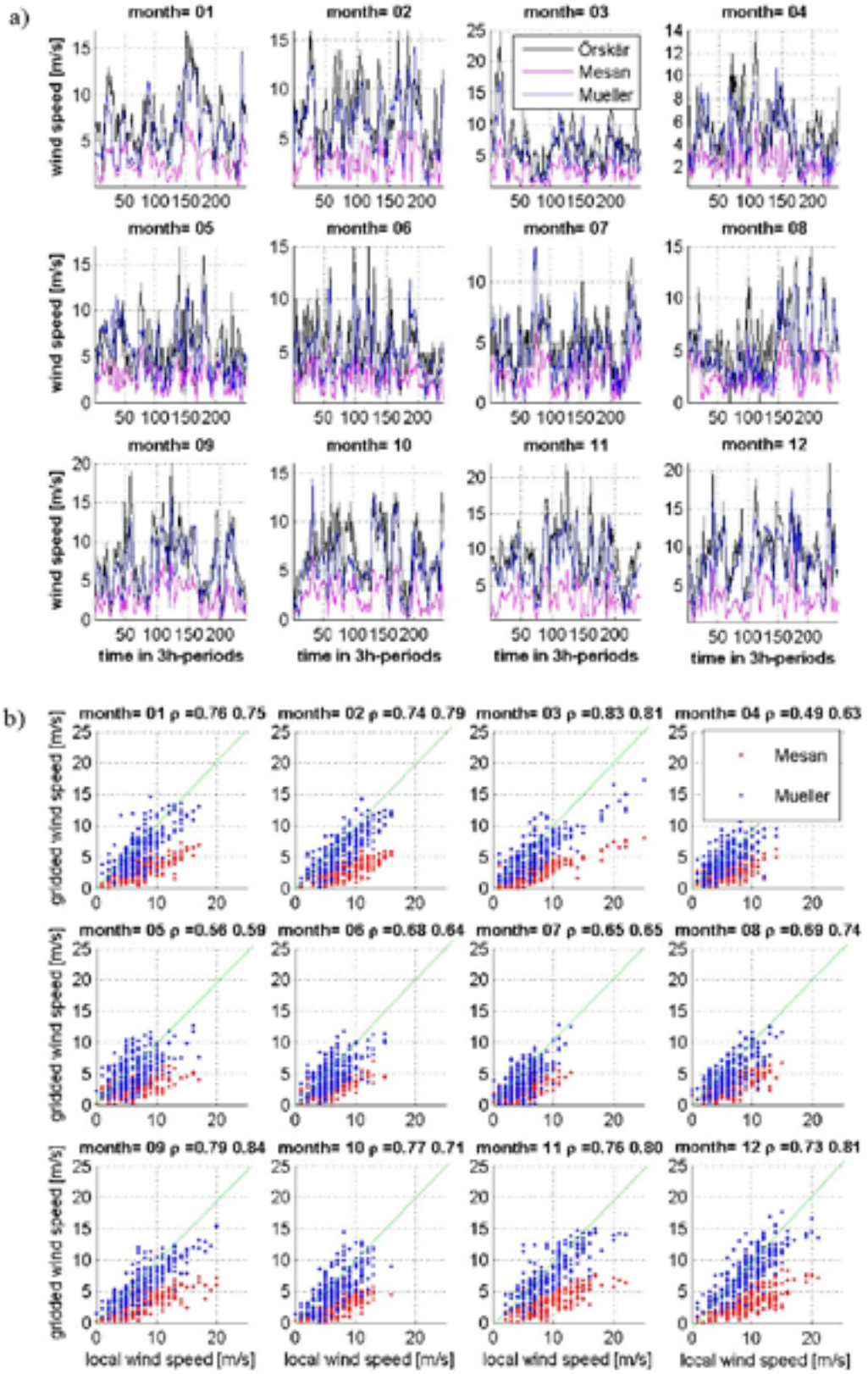

Figure 2-3a. *Comparison of the wind speed of the Mesan and the Mueller data at the grid point that is closest to the local wind station Örskär located at 60.53°N,17.38°E (or 6714750 1640990 in RT90). It is clear that at this location the wind speed of the Mueller data set is considerably more elevated than the corresponding Mesan data and conforms better with the local wind.*

2-3b. *Scatter diagram of the local wind at Örskär vs. the Mesan and the Mueller data respectively. The correlation coefficients, ρ, (given in Mesan-Mueller order on the title line above the graphs) are comparable for the two sets and are generally above the 0.7 level. It is clear that both sets underestimate the local wind but the Mesan data do so to a higher extent.*

Freshwater discharge data with weekly resolution of the two major streams Forsmarksån and Olandsån have been acquired from SMHI. Both of these streams display a marked seasonal variability, Figure 2-4.

The contemporary operation of the three reactors F1 through F3 requires cooling water which is withdrawn from the adjacent coast via an entrance canal, and after fulfilling its cooling purpose is subsequently discharged with an average overtemperature of about 10°C. However, this cooling water is of no consequence for the advent of a possible leakage of nuclides from a future repository, since when this has been established, the reactors will be shut down according to plan. The cooling water is included in this study because of its factual but rather marginal influence on the water circulation and stratification during the study period April 2005 through April 2005, see Figure 2-5.

Cooling water data have been obtained from the operators of the three nuclear plants. During the model period (April 2004 through April 2005) the discharge of both F1 and F2 has been 43 [m^3/s], while for F3 the flow rate amounts to 47 [m^3/s]. F1 and F2 were shut down during most of June 2004 while the non-operational period of F3 mainly coincided with the month of August 2004. An indication of the inlet and outlet points of the cooling water can be seen in Figure 2-5.

Ice data with a horizontal resolution of one (1) nautical mile have been obtained from the Finnish Institute of Marine Research. A snapshot example is given in Figure 2-6. Checking against local ice freeze-up and break-up observations from the SICADA data base yields concurring results and gives no reason to question the validity of this data set, see Table 2-2.

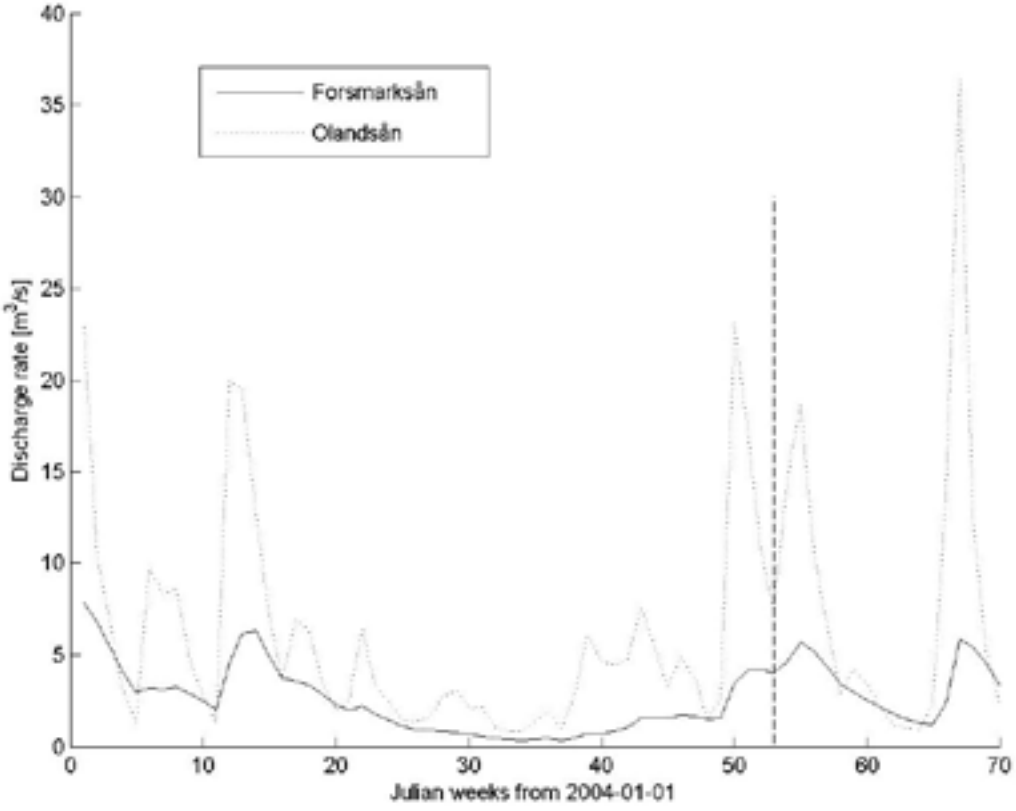

Figure 2-4. *Volume flux of the two streams that discharge into the interior of the model area. The annual averaged combined discharge of both streams amounts to 9 [m^3/s].*

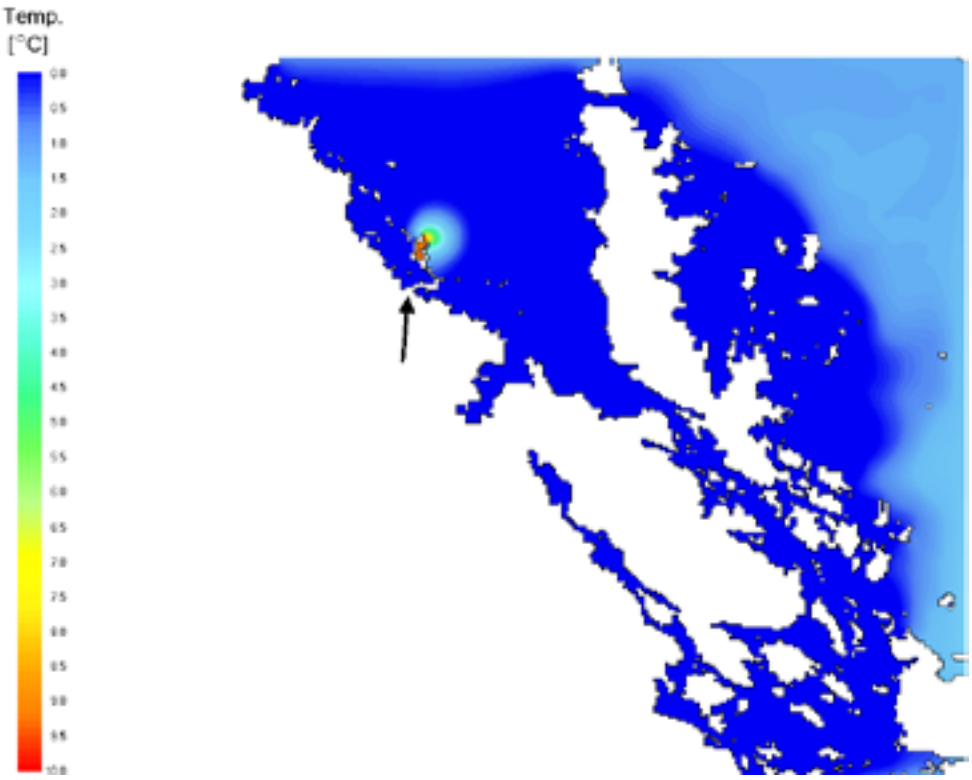

Figure 2-5. *Snapshot of the thermal plume discharged into the so-called Biotestsjön. Cooling water with an over-temperature of about 10°C is discharged at volume flux rate of approximately 130 m^3/s at two separate but close locations in the interior of this receiving embayment. This discharge is not considered to be a potential source of nuclide contamination. The approximate location of the common inlet is indicated with an arrow.*

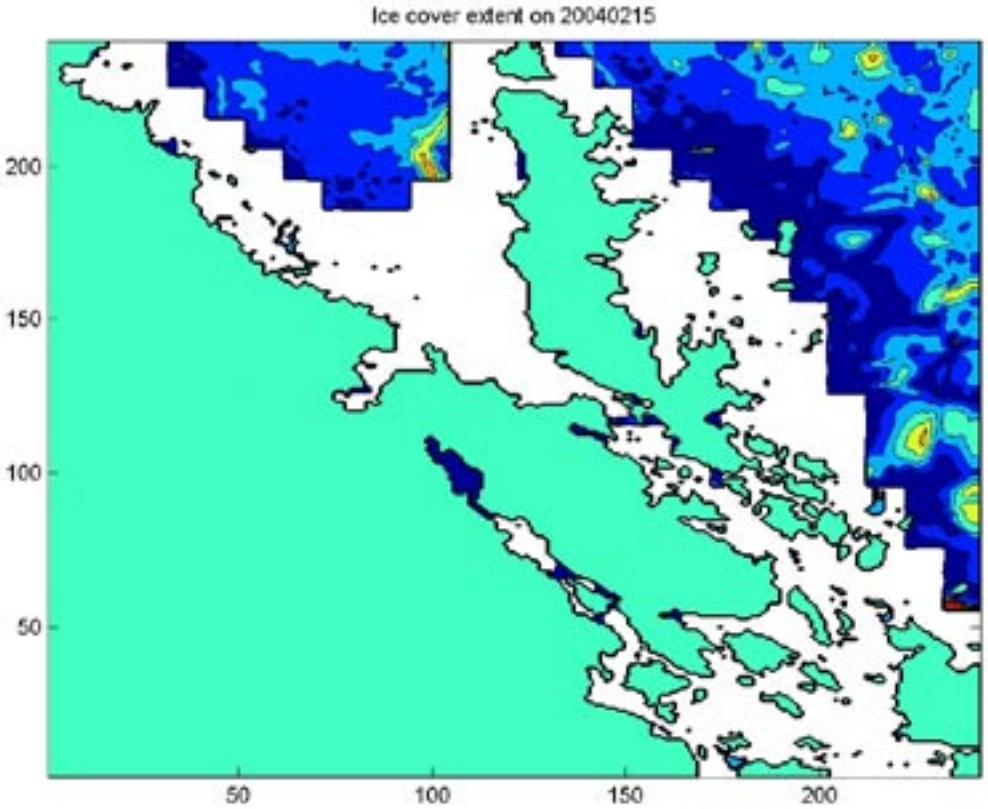

Figure 2-6. *Ice situation on February 15, 2004, with ice cover in white and land in green, as presented in the ice statistics of the Finnish Institute of Marine Research and which for this data obviously is consistent with the local ice observation in Table 2-2.*

Table 2-2. Ice data concerning the validation period from the SICADA data base.

	freeze-up	break-up
Winter period 2004/2005	2004-11-18	2005-04-09

2.2 Extraction of model data

For the two stations located on the northern boundary of the model area both the data of the Baltic model (BAF3D) and the local area model (For3D) have been saved and are available. For obvious reasons these sets do not differ by much since the latter is derived from interpolated data of the former. For the other locations the closest equivalent grid cell – both horizontally and vertically – has been chosen. This produces a problem concerning the stations Fo14 and Fo15 for which the average depth, as represented by the gridding procedure, is considerably more shallow than the actual depth at that station. With these exceptions the bulk of work has consisted of rearranging the output data of the models into appropriately formatted files suitable for statistical analysis.

2.3 Extraction of measurement data

Initially the extraction of the measurement data was hampered by the things that make data processing difficult: format changes, unmotivated change of units, data without specification, data with erroneous specification, varying depth ranges, transient data retained at the beginning and ending of a measurement period, etc. Most of these nuisances disappeared when the data were submitted into the SICADA database from which the measurement data could be retrieved in a standard format. The naming of the files is given in Table 1-2, and the time of deployment in Table 1-3.

2.4 Spectral analysis and choice of comparison time frames

In order to find an appropriate sampling rate for making the comparison with simulated salinity and temperature data without missing relevant variations and thereby producing bias (so-called alias errors), the power spectra for representative months of the different seasons have been investigated using the Fast Fourier Transform (FFT) in the Matlab toolbox. The outcome of this encompassing analysis is presented in Figure 2-7 concerning temperature and Figures 2-8 and 2-9 for salinity, from which it is clear that the bulk of the contained variance concerning salinity and temperature measurements is located in the part of the spectra that lies above diurnal rates, i.e. once a day. Thus it can be safely concluded that daily samples of measured and simulated salinity and temperature can be compared without loss of generality and introduction of spectral aliases.

In Figure 2-10 the corresponding spectrum analysis is performed on the ADCP instrument placed at station Fo11 where 15 layers of orthogonal current components are measured. Most of the variance is located on a frequency interval safely lower than one a day, however with a few exceptions. To be on the safe side all current comparisons have been conducted with a semidiurnal (12 h) sampling rate. This also applies to most of the current measurements at other locations.

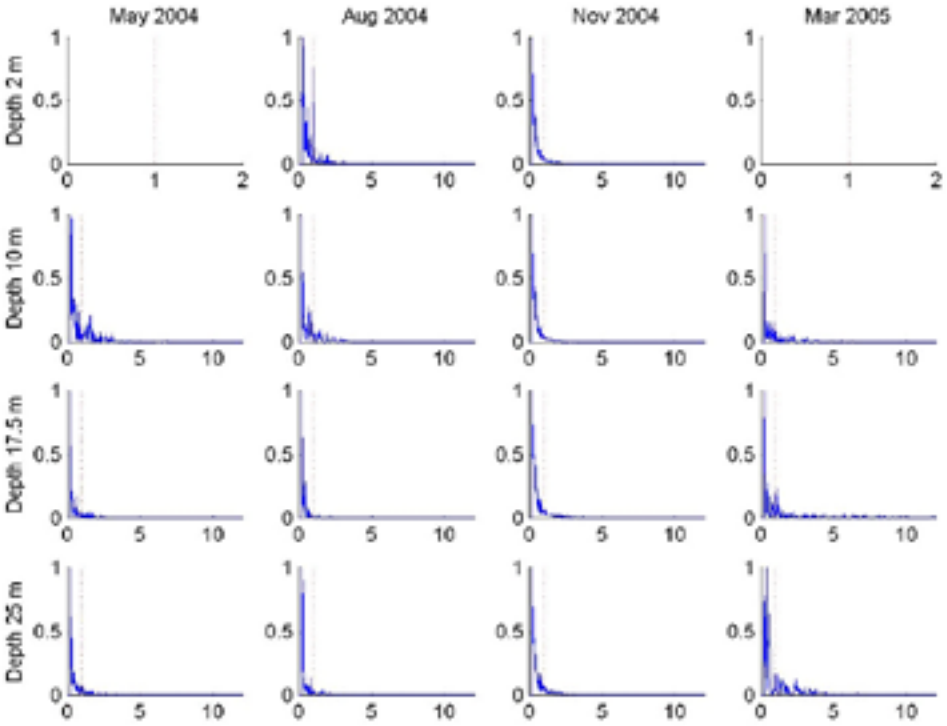

Figure 2-7. *Power spectra of the four depths and four periods of the* ***temperature*** *measurements of station Fo11. The y-axis of all diagrams is normed power spectral density. The x-axis is graded in frequency units (i.e. the number of periods per day up to the Nyquist frequency 12 per day) corresponding to hourly sampling. The diurnal frequency has been marked with a dotted vertical line. A dominant part of the variance is for most of these spectra found for longer periodicities than this. In some cases (e.g. 10-m depth in May) semidiurnal periods also contribute to some extent. Two diagrams are left blank due to missing data.*

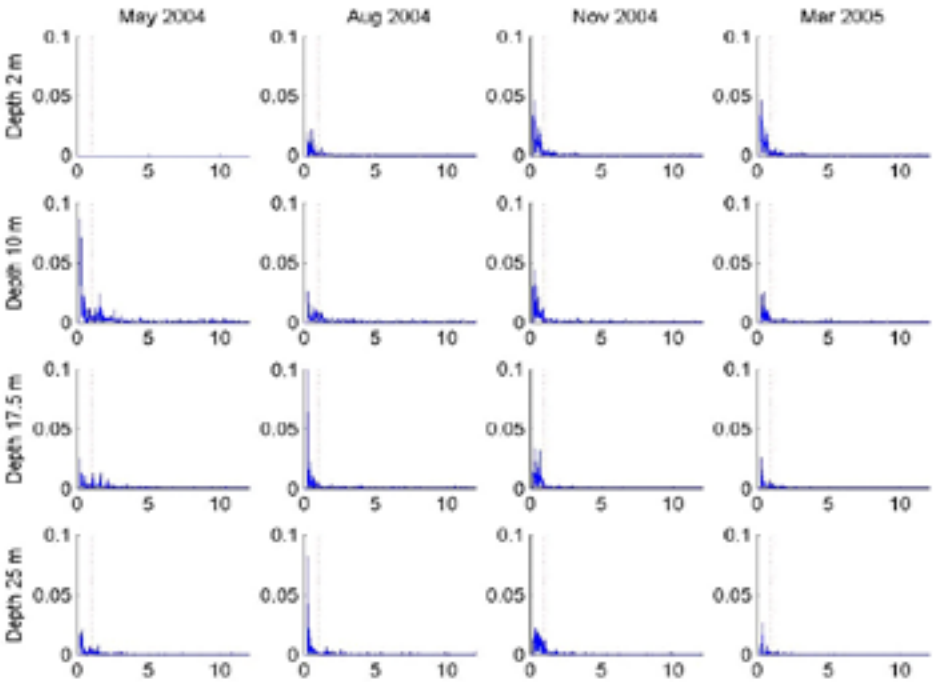

Figure 2-8. *Power spectra of the four depths and four periods of the* ***salinity*** *measurements of station Fo11. The y-axis of all diagrams is normed power spectral density. The x-axis is graded in frequency units (i.e. the number of periods per day up to the Nyquist frequency 12 per day) corresponding to hourly sampling. The diurnal frequency has been marked with a dotted vertical line and all variance except for a negligible part is found for lower frequencies than diurnal oscillations. One diagram is left blank due to missing data.*

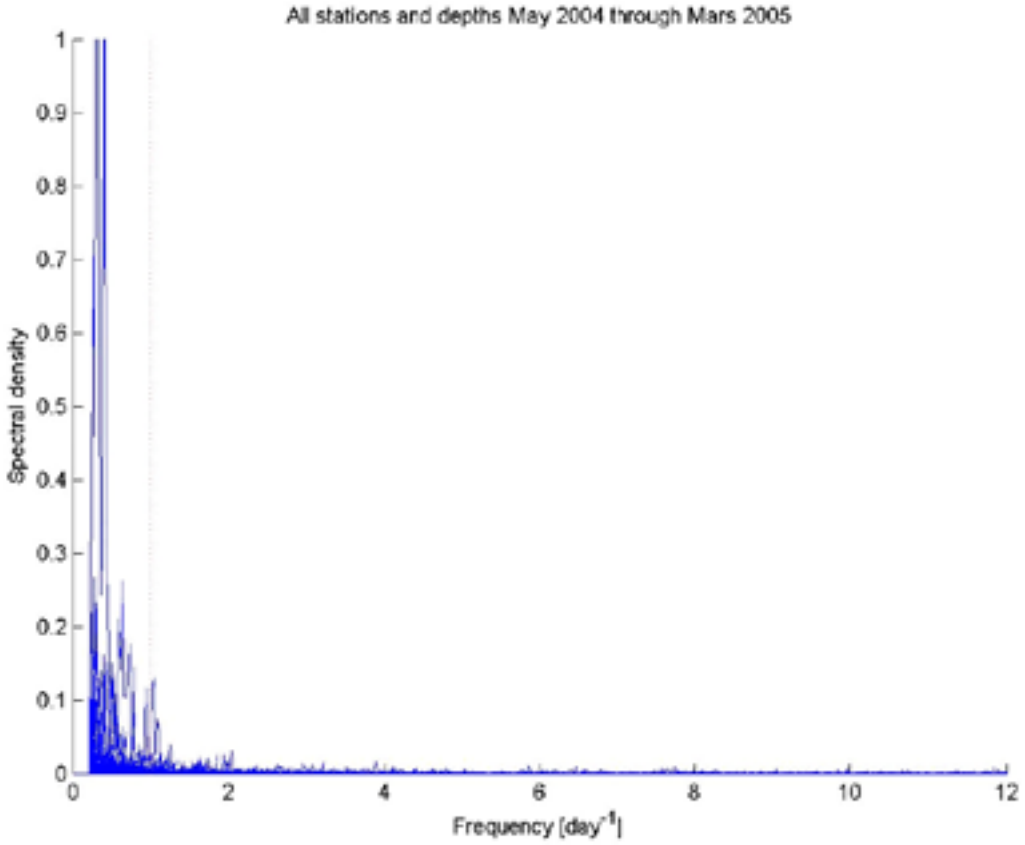

Figure 2-9. *Power spectra of all measurement depths and four periods of the salinity measurements of station Fo12 through Fo14 and Fo16 superposed. The y-axis of all curves is normed power spectral density. The x-axis is graded in frequency units (i.e. the number of periods per day up to the Nyquist frequency 12 per day) corresponding to hourly sampling. The diurnal frequency has been marked with a dotted vertical line. As for Figures 2-7 and 2-8, the dominant part of the variance is invariably for all of these spectra found for longer periodicities than this diurnal period, which thus serves as an appropriate sampling rate for comparison with simulated data.*

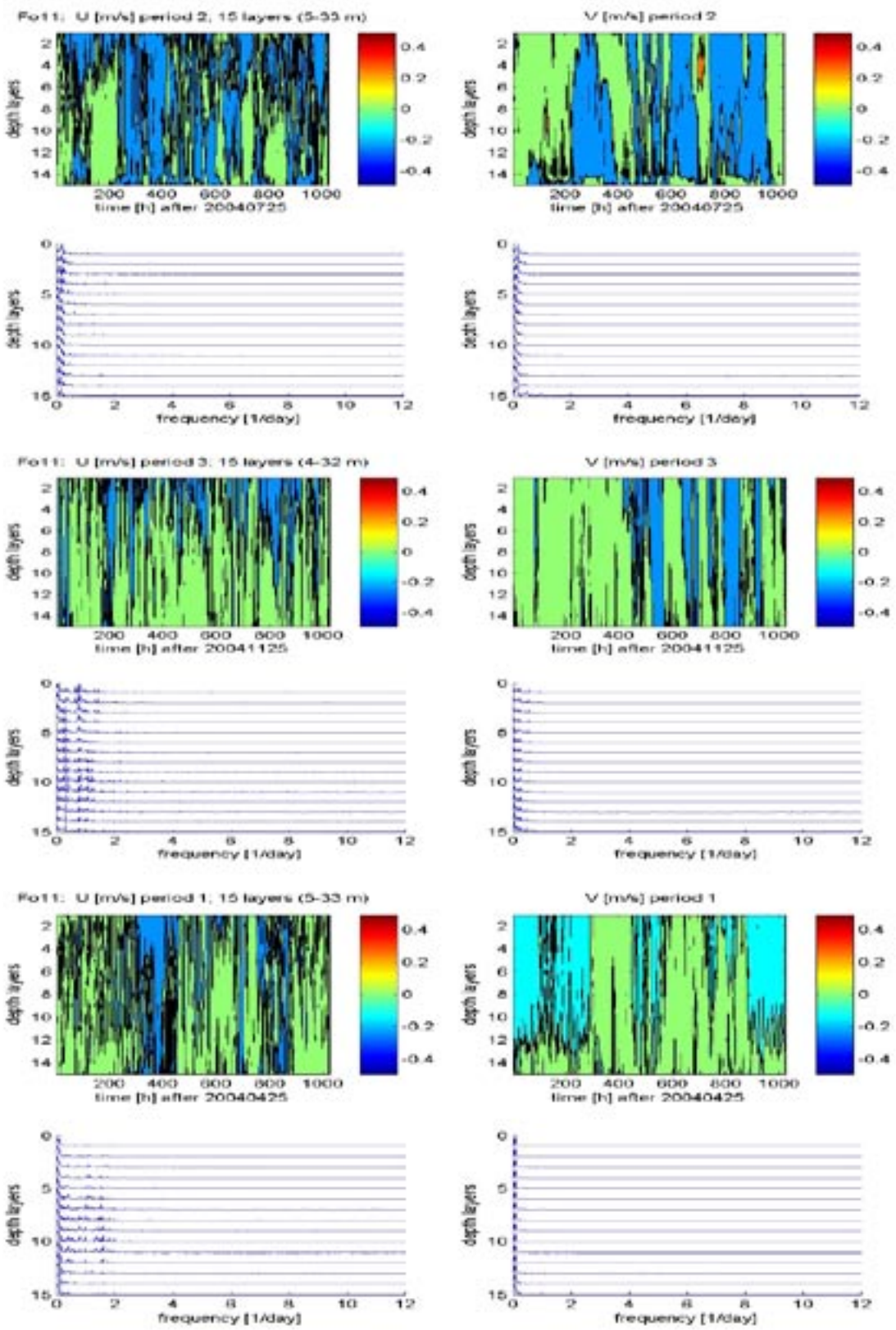

Figure 2-10. *Spectra of E/W-component (U) and N/S-component (V) of currents for each of the 15 measured layers at station Fo11 and for the three periods for which data are available. For the V-component the dominant part of the variance is found for frequencies smaller than once a day. This holds mainly also for the V-component, even though for period 1 and the top layers there is some variance attributed to near 12-h periods, i.e. frequencies corresponding to twice a day.*

2.5 Statistical methods of comparison

The method of comparison is direct and straightforward. The corresponding data as to horizontal and vertical location are extracted with their FFT-determined appropriate sampling rates and are subsequently subjected to ocular and statistical comparison. The latter consists of invoking the cross-correlation function that is supplied in the Matlab toolbox together with graphically depicted regression lines. All computed correlation coefficients are summarized and accounted for in Table 2-3. It can be pointed out that concerning the regression lines, the slopes are almost invariably less than unity, which value corresponds to a hypothetical perfect match between the data set pairs. Inaccuracy in the measurements can be shown to significantly contribute to such less-than-ideal slopes (Anders Grimvall, pers. comm.)

Table 2-3. Correlation coefficients between measured and modeled data, averaged over the various analysis intervals. Light grey fields denote 'not applicable' and dark shade that comparison was not possible to perform.

		Salinity		Temperature		U-component		V-component	
Station	depth	corr coef	N=	corr coef	N=	corr coef	N=	corr coef	N=
Fo11	1.5 m	0,23	156	0,99	215	-0,01	551	0,08	551
	10 m	-0,16	271	0,95	302	0,29	551	0,11	551
	17 m	0,11	315	0,91	302	0,22	551	-0,04	551
	25 m	0,39	315	0,87	305	0,15	551	0,07	551
Fo12	12 m	0,05	314	0,96	314	0,17	727	0,13	727
Fo13	1.5 m	0,76	255	0,96	255				
	10 m	0,42	141	0,90	182				
	17 m	0,50	255	0,87	256				
Fo14	23 m								
Fo15	1.5 m			0,94	255				
	5 m			0,94	255				
	10 m			0,87	255				
	15 m			0,83	255				
	20 m			0,81	255				
Fo16	1.5 m	0,50	242	0,96	369				
	10 m	0,04	242	0,95	291				
	18 m	-0,02	242	0,92	357				

3 Results

3.1 Overview and intercomparison of salinity and temperature measurements

First an overview of the scalar measurement entities salinity and temperature is given in Figure 3-1. The most striking feature is the noticeable fluctuations of salinity measured at station Fo16 in the 17–18 m depth bracket. Some tendencies towards unstable stratification (water with higher salinities on top of deeper layers at approximately the same temperature) can be observed, for example at Fo13. This will be scrutinized more in detail when the data of the separate station are analyzed below. The inter-comparison of salinity and temperature measurements between the stations seems otherwise consistent. The salinity levels are systematically increased towards the periphery of the model domain near the boundaries. This applies to Fo11, Fo12 and Fo16 compared to the more centrally placed stations. The surface temperatures peak at a comparatively higher value for the shallower stations F13 and F16 than for the deeper ones (Fo12 and Fo14). At station F15 only temperature was measured with a thermistor chain with eleven levels giving an improved vertical resolution. This will be examined in detail below.

3.2 Station Fo11

At the peripheral station Fo11 positioned on the eastern side of the northern boundary all four parameters (salinity, temperature and two orthogonal velocity components) are logged. A time-wise expansion of Figure 3-1 reveals that the salinity measurement at the Fo11 station (upper panel in Figure 3-2), displays a few flaws. After Julian day (JD) 250 the surface salinity measurement takes a steep dive, most likely due to growth of algae on the conductivity sensor. In the following this cause of malfunctioning will be referred to ‘epiphytal growth’. After the beginning of the third period (about JD 300) a systematic unstable stratification of the two upper instruments exceeding the stipulated inaccuracy of ± 0.1 units in the psu scale /Johansson and Morosini 2002/ can be seen. In the transition between the second and third periods, the mismatching reading of the instrument deployed at the 10–12 m level is striking. This also casts doubt on the validity on the 10–12 m measurement during the second period. The temperature measurements (lower panel in Figure 3-2) made during the spring and summer heating period (before JD 225) are consistent with a formation of a thermocline only occasionally interrupted by vertical mixing and possible up-/down-welling events. The same consistency applies to the cooling period (after JD 250) when thermally well-mixed conditions mainly prevail from the 2- to 25-m depth.

Such ‘up/down-welling’ events are partly due to wind-induced vertical mixing and partly due to Ekman dynamics that are only partially resolved by the CR-grid and never become fully developed because of the funnel-shaped deviation from a strait coast line. Neither does the FR-grid with its limited model domain facilitate Ekman dynamics to develop in the interior of the Öregrundsgrepen. The vertical mixing represents an irreversible and thus lasting effect. The wind-induced down-welling means a temporary vertical redistribution of water which on the other hand should recoil quite soon after the wind subsides. This has little lasting effect on the internal vertical distribution of the salinity and temperature fields.

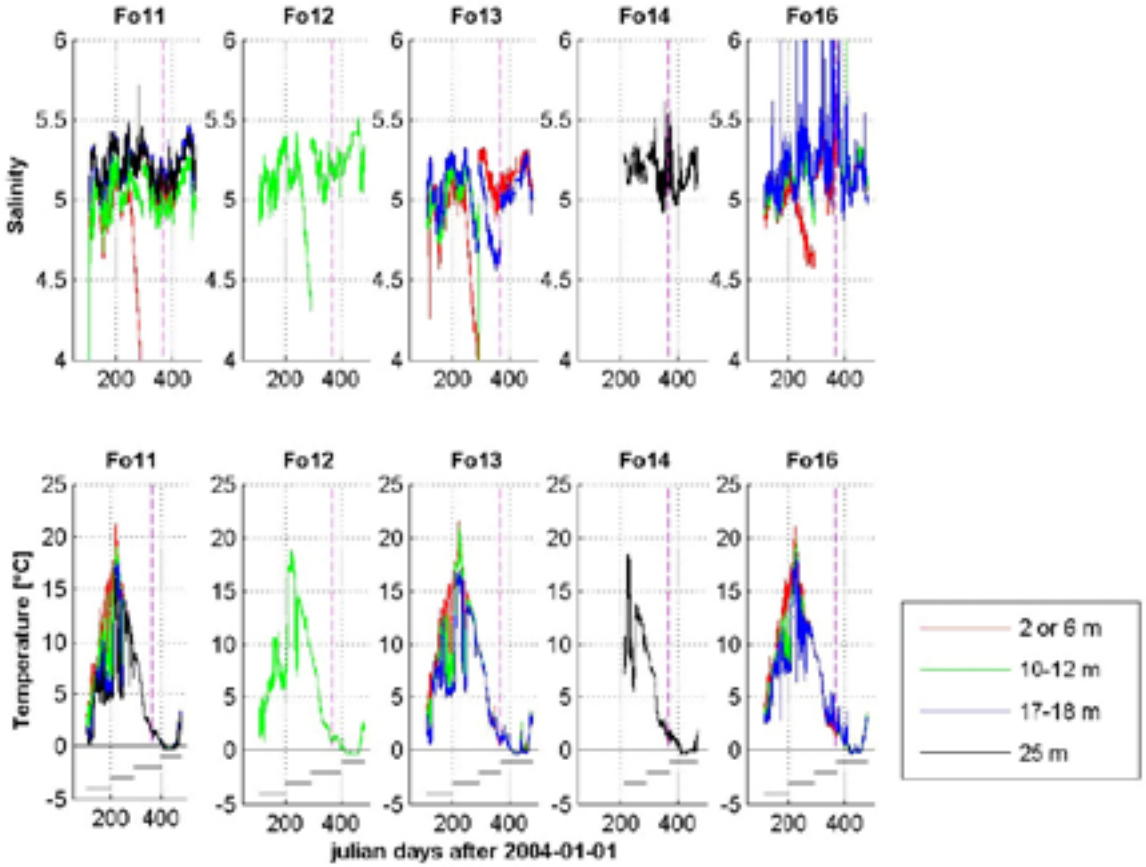

Figure 3-1. *Overview of the scalar measurement entities salinity and temperature with different colors for the different depth layers. The new year transition between 2004 and 2005 is marked with a broken magenta line. The most striking features are the rapid decline of the surface-most salinities (Fo11 through Fo13 and Fo16) and the noticeable fluctuations of salinity measured at station Fo16 in the 17–18 m depth bracket. Some tendencies of unstable stratification (water with higher salinities on top of deeper layers at approximately the same temperature) can be observed, for example, at Fo13. The inter-comparison of salinity and temperature measurements between the stations seems otherwise quite consistent with increased level of salinity towards the boundaries (Fo11, Fo12 and Fo16) compared to interior stations. The surface temperatures peak at a comparatively higher value for the shallower stations F13 and F16 than for the deeper ones (Fo12 and Fo14). At the station F15 only temperature was measured with a thermistor chain with eleven levels giving an improved vertical resolution.*

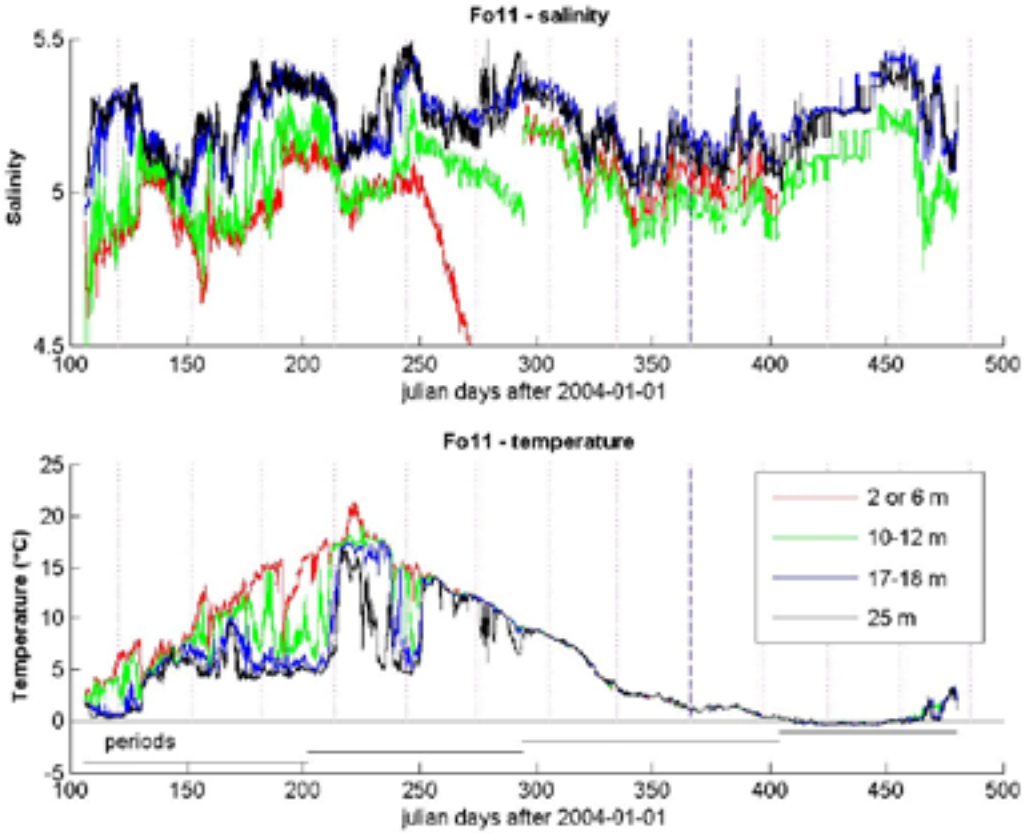

Figure 3-2. *For both panels the transition between months is indicated with red vertical dotted lines and the new year with a broken blue line. Overview of the salinity (upper panel) measurement at Fo11 station with the duration of the four measurement periods indicated beneath the temperature plot. After Julian day (JD) 250 the surface salinity measurement takes a steep dive, most likely due to growth of epiphytes on the conductivity sensor. After the beginning of the third period (about JD 300) a systematic unstable stratification of the two upper instruments that exceeds the acceptable inaccuracy of ± 0.1 units in the psu scale can be seen. Also the mismatch of the 10–12 m instrument reading in the transition between the second and third periods is striking, and casts doubt on the validity on 10–12 m measurement during the second period. The temperature measurements (lower panel) are during the heating period (before JD 225) consistent with a formation of a thermocline that is occasionally interrupted by vertical mixing and possible up-/down-welling episodes. The same applies to the cooling period (after JD 250) when thermally well-mixed conditions mainly prevail from the 2- to 25-m depth.*

In Figure 3-3 the temperature development during the entire validation period is shown with measurements at the respective depth layers together with the corresponding simulated values. The vertical curves that go down to zero temperature mark the transition between the measurement periods and are exempted from the ensuing correlation analysis. By the end of the simulation period there is a noticeable systematic difference between the two set of curves amounting to a couple of Celsius degrees. During the heating phase the model data do not mimic the notable down-welling episodes that are captured in the measurements.

Salinity curves of station Fo11 for the duration of the validation period are depicted in Figure 3-4 also with simultaneous measurements and corresponding simulated data. In addition to a general falling trend of the simulated salinity curves, there are both similarities and differences. The falling and rising salinities in the JD intervals (200–250) and (420–470) are acceptably well simulated. The upper two measurement data during period 2 (JD 250–300) have been omitted because of the evident malfunctioning due to epiphytal growth.

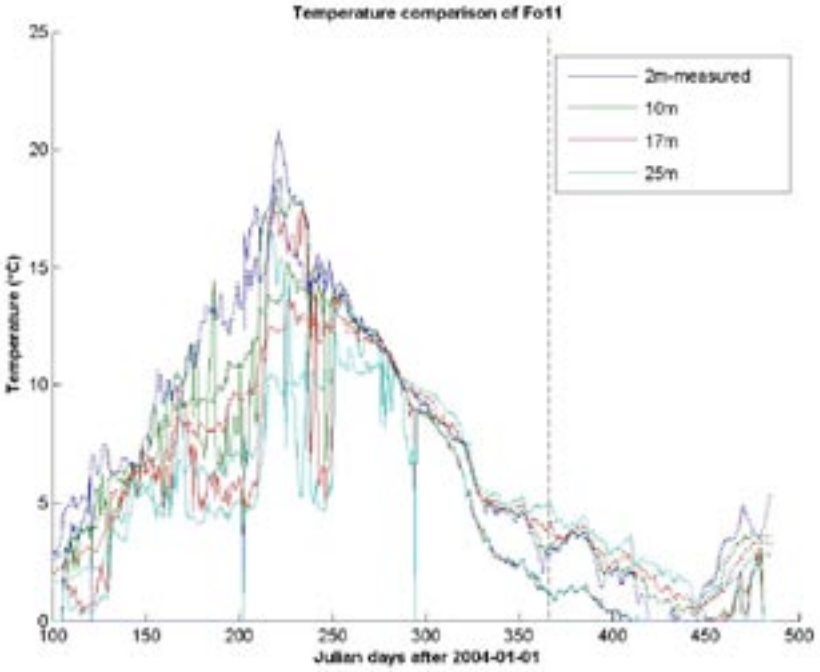

Figure 3-3. *Temperature development during the entire validation period. Solid curves are measurements of the respective depth layers, dotted lines the corresponding simulated curves. The vertical curves that go down to 0°C mark the transition between the measurement periods and are exempted from the ensuing correlation analysis. By the end of simulation period (JD 320 and onward) there is a noticeable systematic difference between the two set of curves amounting to a couple of degrees Celsius. During the heating phase the model data do not mimic the notable down-welling episodes that are captured in the measurements.*

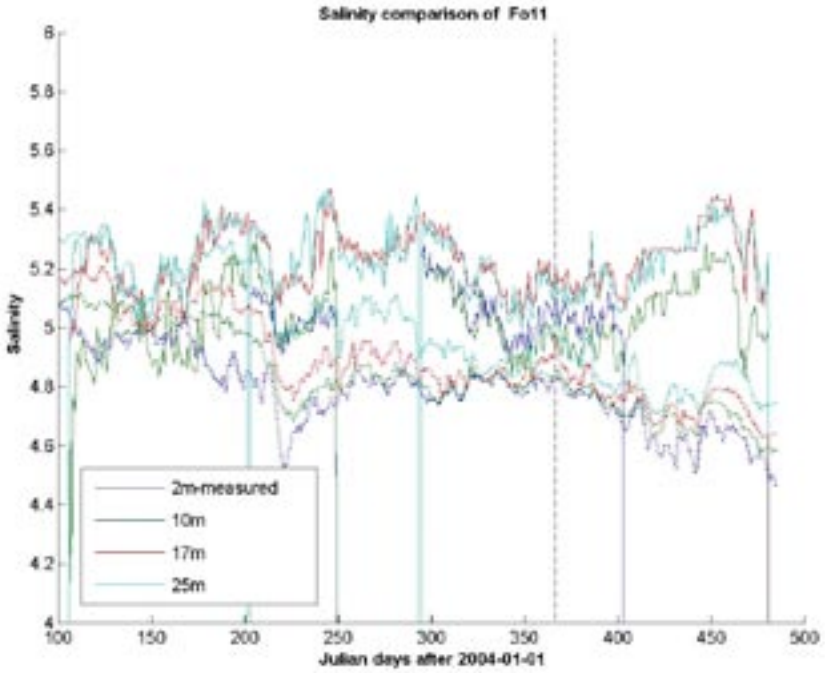

Figure 3-4. *Salinity curves of station Fo11 for the duration of the validation period. Solid lines are measurement data and dotted lines simulated data. In addition to a falling general trend of the simulated curves, there are both similarities and differences. The falling and rising salinities in the JD intervals (200–250) and (420–470) are acceptably well simulated. The upper two measurement data during period 2 (JD 250–300) have been omitted for the reasons given in the text.*

In Figure 3-5, the scatter diagram displays differences between measured and simulated temperatures at station Fo11. The agreement is obviously improved for the surface layers. The accounting of corresponding correlation coefficients is deferred to Table 2-3.

A scatter diagram between measured and simulated salinities of the station Fo11 is displayed in Figure 3-6 with the corresponding correlation coefficients also deferred to Table 2-3, and which reveals that the correlation coefficients are comparatively improved for the top and the bottom layers.

In Figure 3-7 contour diagrams of measured N/S-velocity (V-) component at station Fo11 are depicted with a semi-diurnal sampling rate compared to the corresponding simulated data. This picture foremost reveals the considerable variance in the flow field.

Contour diagrams of measured N/S-velocity (V-)component at station Fo11 are shown in Figure 3-8. These diagrams are based on the same sampling rate as in Figure 3-7 but smoothed with a 5 h-running average filter and compared to the corresponding simulated data both for the Mueller and the Mesan data sets of the meteorological forcing. At least for the Mueller data (center panel) some faint resemblance between measured and modelled data pattern emerges. The two bands with intensified negative (south-going) currents near JD 200 and 300 are mysterious. Possible explanations will be given shortly below.

In Figure 3-9 contour diagrams of measured E/W-velocity (U-) component at station Fo11 are depicted with a semi-diurnal sampling rate compared to the corresponding simulated data. As for Figure 3-7, this picture primary reveals the considerable variance in the flow field. The actual model from which data originates is For3D, forced with the Mesan meteorological data.

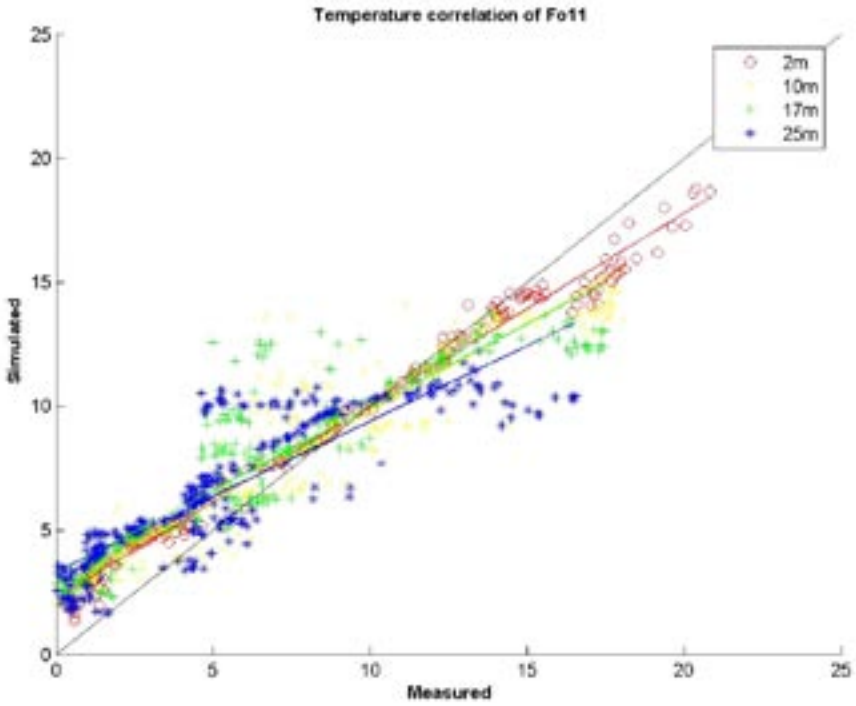

Figure 3-5. *Scatter diagram between measured and simulated temperatures at station Fo11, with regression lines and the ideal line representing a perfect match indicated as a diagonal black solid line. The agreement is obviously improved for the surface layers. The corresponding correlation coefficients are deferred to Table 2-3.*

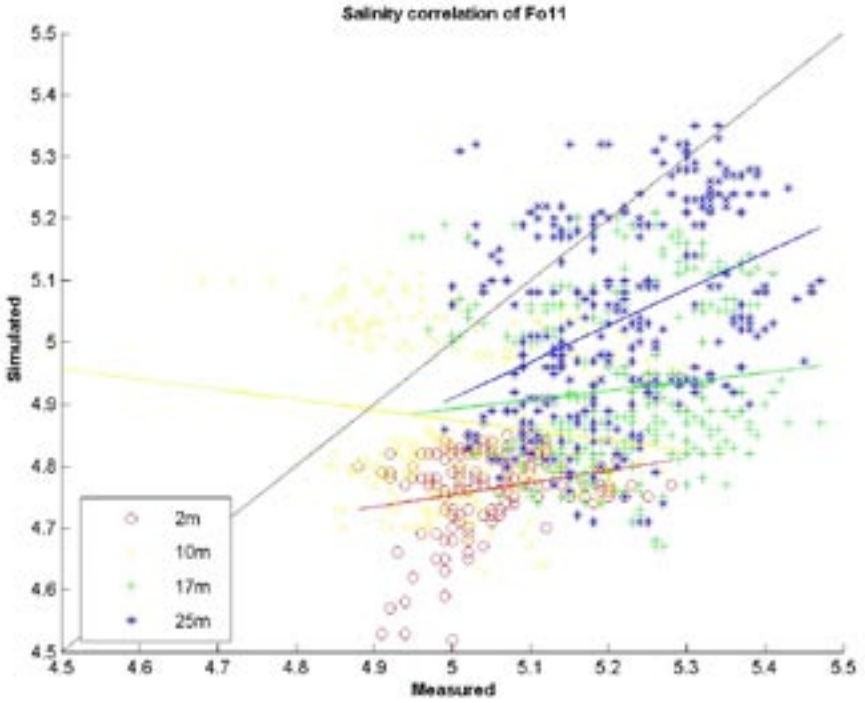

Figure 3-6. *Scatter diagram between measured and simulated salinities of station Fo11, with regression lines for the four depths and the ideal line representing a perfect match indicated as a diagonal black solid line. The corresponding correlation coefficients are deferred to Table 2-3 and reveal that the correlation coefficients are comparatively better for the top and the bottom layers verified by the negative slope of the 10 m-layer data. The bottom layer data give the best fit.*

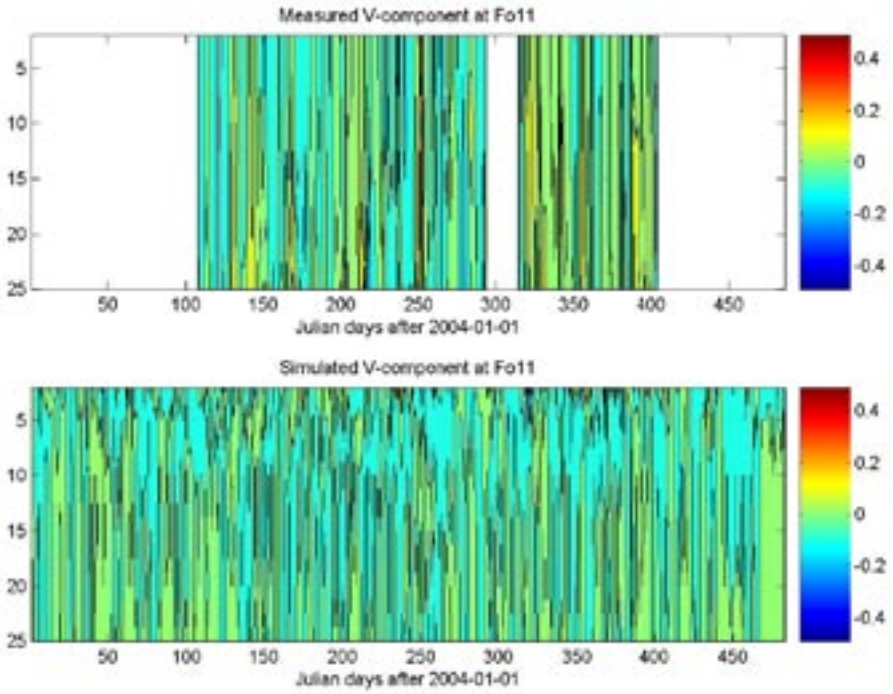

Figure 3-7. *Contour diagrams of measured N/S-velocity (V-) component at station Fo11 depicted with a semi-diurnal sampling rate compared to the corresponding simulated data. This figure reveals foremost the considerable variance in the flow field. The actual simulating model is For3D, forced with Mesan meteorological data.*

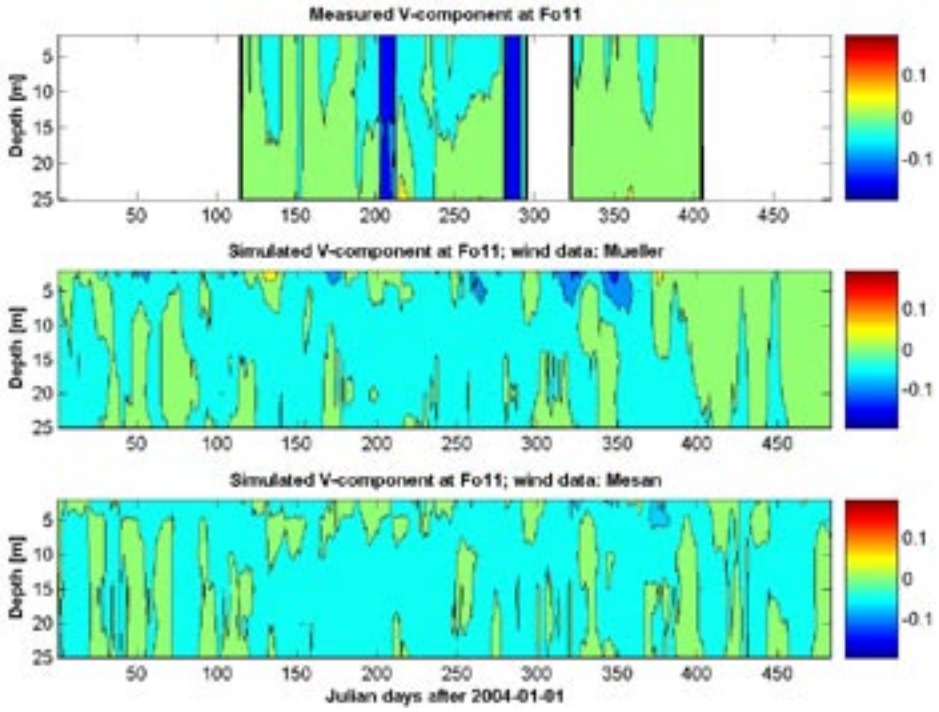

Figure 3-8. *Contour diagrams of measured N/S-velocity (V-) component at the station Fo11 with the same sampling rate as Figure 3-7 but smoothed with a 5 h running average filter and compared to the corresponding simulated data both for the Mueller and the Mesan data set. At least for the Mueller meteorological forcing (middle panel) some faint resemblance between measured and modeled data emerges. The two bands with intensified negative (south-going) currents near JD 200 and 300 are mysterious.*

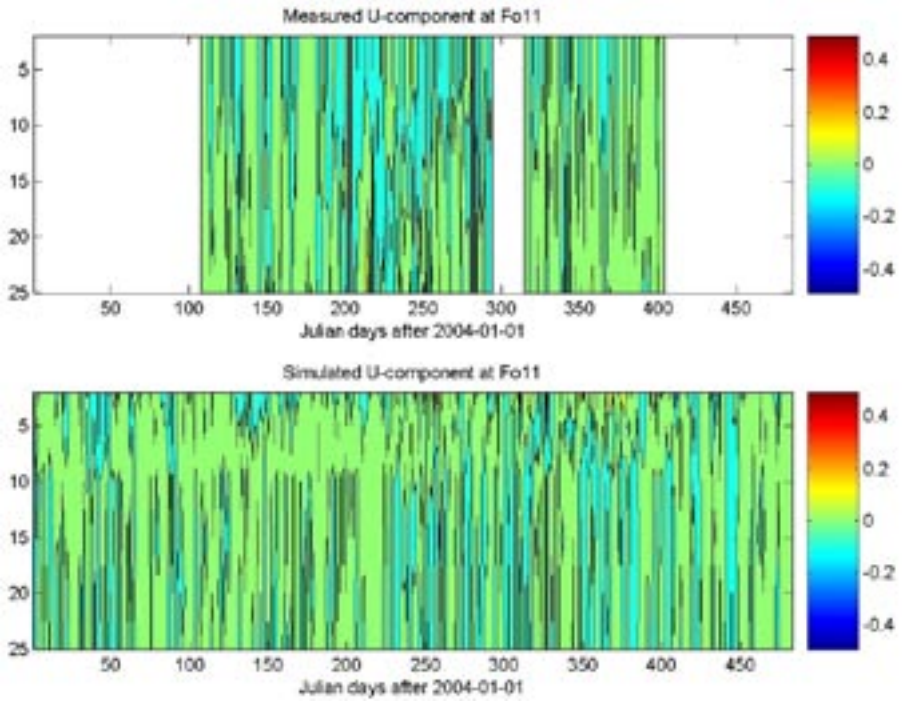

Figure 3-9. *Contour diagrams of measured E/W-velocity (U-) component at station Fo11 depicted with a semi-diurnal sampling rate compared to the corresponding simulated data. As for Figure 3-7, this picture reveals foremost the considerable variance in the flow field. The actual simulating model is For3D, forced with Mesan meteorological data.*

Contour diagrams of measured E/W-velocity (U-) component at station Fo11 can be seen in Figure 3-10 with the same sampling rate as Figure 3-9 but smoothed with a 5 h-running average filter and compared to the corresponding simulated data both for the Mueller and the Mesan data set. The resemblance of these contour patterns is less than striking. One of the bands with intensified negative (west-going) currents near JD 200 is in common with the V-component in Figure 3-8, but new such barotropic flow instances occur, some of which have a counterpart in the simulation forced with Mueller meteorological data.

The reason that these velocity anomalies are clearly visible in Figures 3-8 and 3-10 (but not in Figures 3-7 and 3-9) is that these episodes with enhanced systematic negative velocity components from surface to bottom occur adjacent in time to periods of stagnant water movements which enhance the contrast. They are thus not due to processing error but sooner to the contouring program's feature of reinforcing contrasts. A more plausible explanation than instrument anomalies would be that they may be caused by eddies (see Figure 4-1) entering into the domain. The time duration and the depth reach for these occurrences make it less probable that they are induced by ship wakes.

A scatter diagram for corresponding measurements and simulated data points in space and time for the N/S(V)-component of the current at station Fo11 is presented in Figure 3-11a. The local For3D-model is in this case forced with Mueller meteorological data. The corresponding small correlation coefficient (Table 2-3) for all layers can be perceived by ocular inspection. This is also the case when Mesan data are used. The simulated data range is noticeably greater than for the measured data.

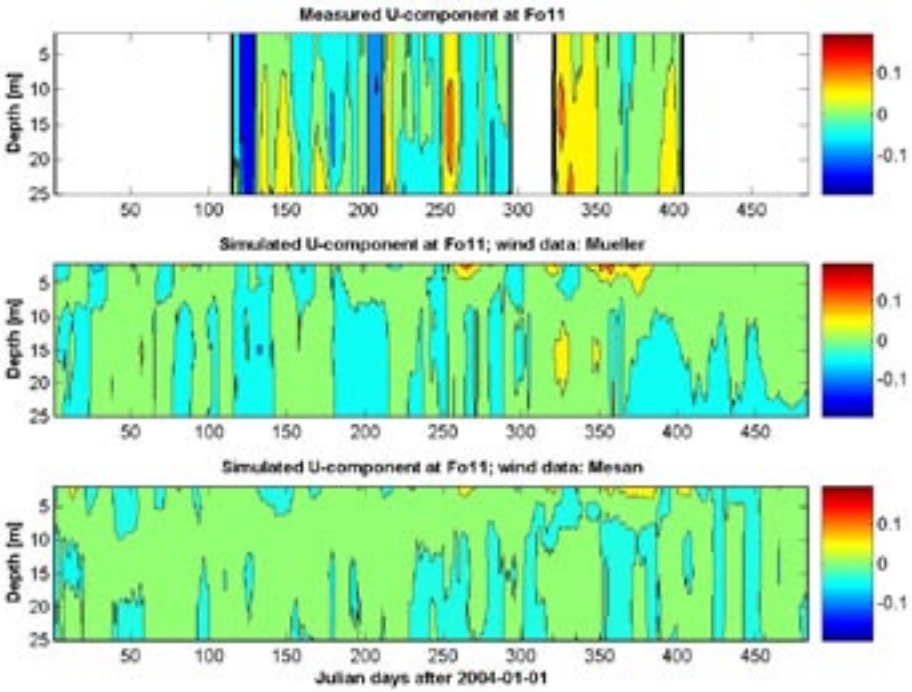

Figure 3-10. *Contour diagrams of measured E/W-velocity (U-) component at station Fo11 with the same sampling rate as Figure 3-9 but smoothed with a 5 h running average filter and compared to the corresponding simulated data both for the Mueller and the Mesan data set. At least for the Mueller meteorological forcing (middle panel) some faint resemblance between measured and modeled data emerges. One of the band with intensified negative (west-going) currents near JD 200 is in common with the V-component in Figure 3-1, but new such barotropic flow instances occur, some of which have a counterpart in the simulation forced with Mueller meteorological data.*

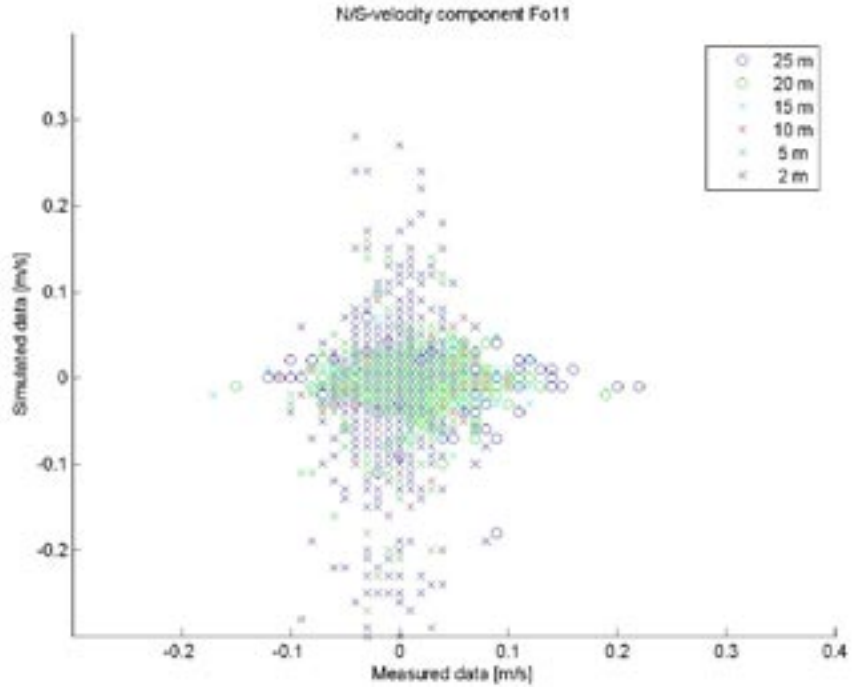

Figure 3-11a. *Scatter diagram for corresponding measurement and simulated data points in space and time for the N/S (V)-component of the current at station Fo11. The For3D model is forced with Mueller meteorological data. The corresponding low correlation coefficient (Table 2-3) for all layers can also be perceived by ocular inspection. This also holds when Mesan data are used. The simulated data range is noticeably greater than for the measured data.*

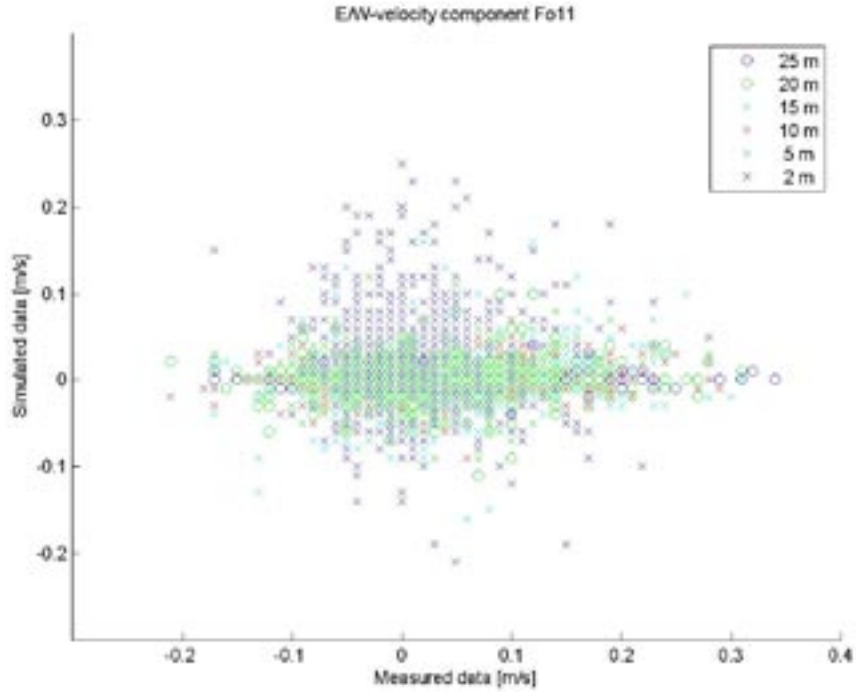

Figure 3-11b. *Scatter diagram for corresponding measurement and simulated data points in space and time for the E/W (U)-component of the current at station Fo11. The For3D model is forced with Mueller meteorological data. The corresponding correlation coefficient (Table 2-3) is considerably improved in comparison to the V-component. Contrary to Figure 3-11a, the measured data range is noticeably greater than for the simulated data.*

For the corresponding measurement and simulated data points in space and time for the E/W(U)-component of the current at station Fo11 is depicted in the form of a scatter diagram in Figure 3-11b. The high-resolution For3D-model is in analogy with the previous figure forced with the Mueller meteorological data set. The corresponding correlation coefficient (Table 2-3) is considerably improved in comparison to the V-component. Contrary to the V-component, the measured data range is noticeably greater than for the simulated data.

A comparison of current speed spectra for six depth levels is presented in Figure 3-12. The frequency distribution of the variance of the measured and simulated data is not radically dissimilar despite that the found correlation coefficients are quite small and even negative in a few instances.

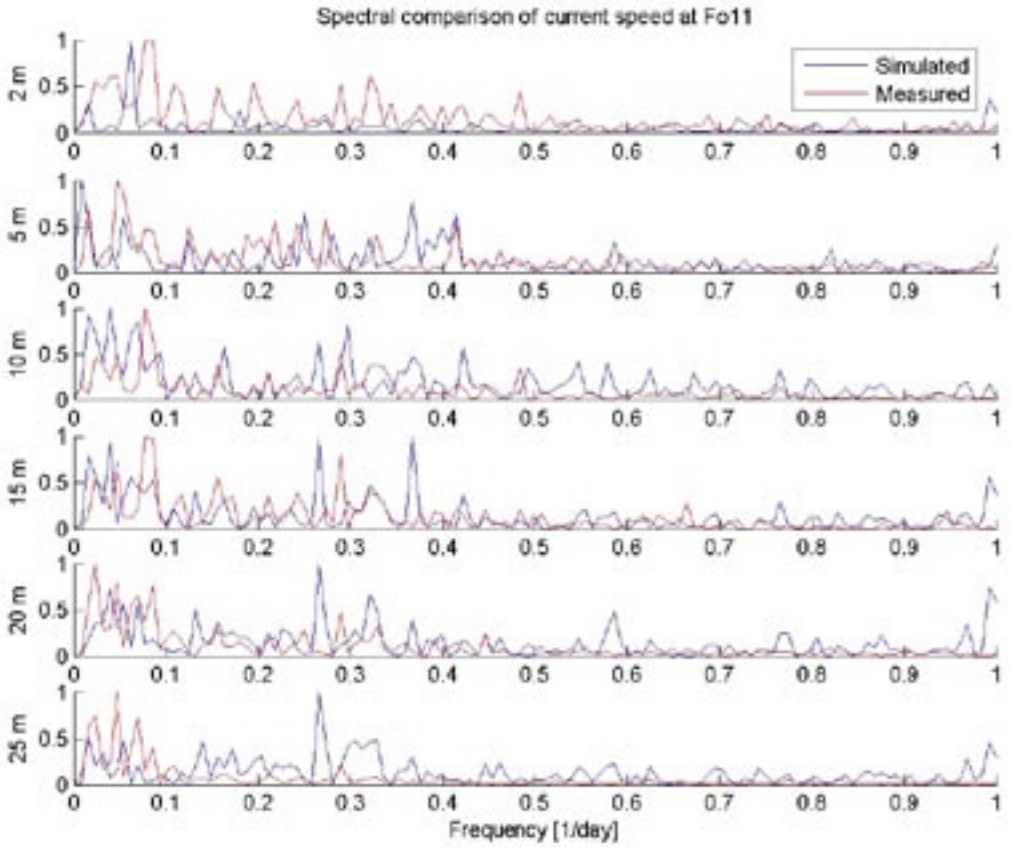

Figure 3-12. *Spectral comparison of the simulated and measured current speed at station Fo11 for the first 256 days of data and for the six depths indicated to the left of the individual diagrams. This comparison is independent of the current direction and displays that the spectral appearances are not notably dissimilar in spite of the comparatively small and even negative correlation coefficients of the U- and V-velocity components given in Table 2-3. For the bottommost layer there are an elevated spectral representation of components with a periodosity of about 3 days.*

3.3 Station Fo12

The salinity measurement during the second measurement period rapidly decreased at station Fo12 and the transition between periods 2 and 3 is disturbingly discontinuous, Figure 3-13. The latter part of salinity measurements of period 2 must thus be discarded from the statistical analysis. There is, however, good reason to believe that the instance of rapid down-welling or down-mixing by the end of July is factual since this event was captured by virtually all other instruments, e.g. Figure 3-1.

Comparison of the temperature at the 12-m depth at station Fo12 for the whole validation period (2004-04-20 through 2005-04-25) is performed in Figure 3-14. During the spring and summer heating phase (up until JD 250), the simulated data do not display the sharp transitions that are presumably connected to up-/down-welling and/or down-mixing events indicated e.g. by the rapid rise of temperature at the 12 m depth level. The only way to distinguish between these mechanisms is that vertical mixing is an irreversible effect that give a lasting redistribution on the stratification while up/down-welling entails a more temporary redistribution of water that also has the capacity to recoil as the wind forcing subsides. During the cooling phase, there is a slight but noticeable discrepancy between the two temperature curves that level off to attain approximately 1°C by the end of the validation period.

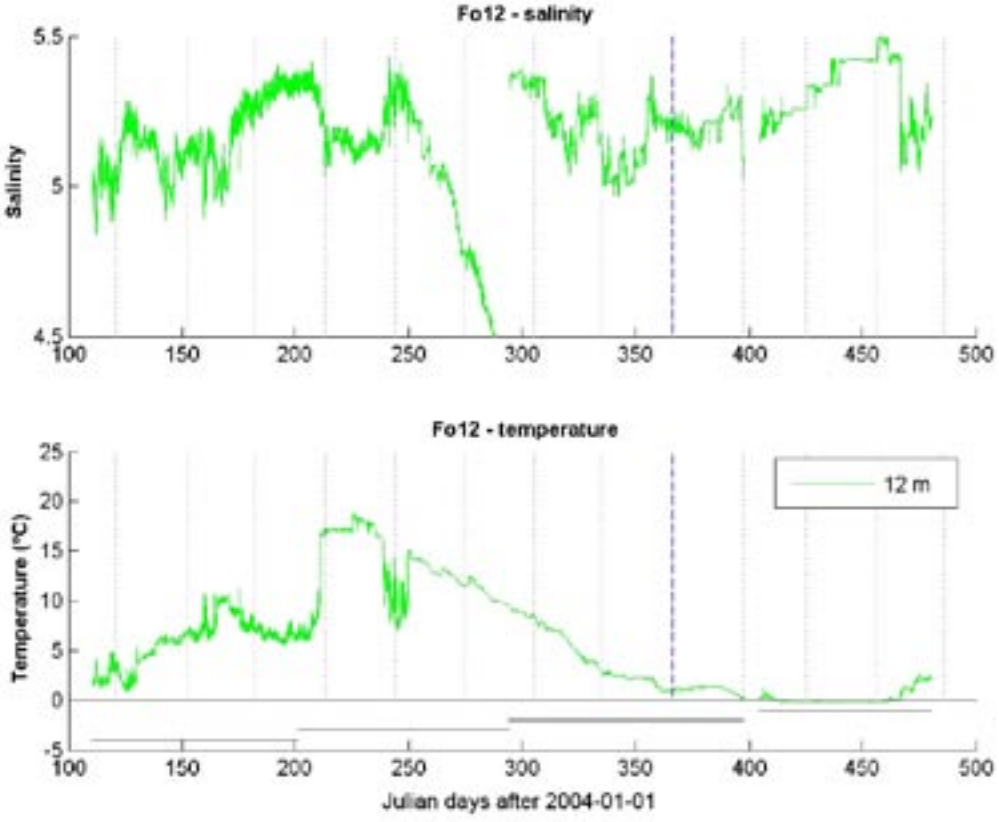

Figure 3-13. *Presentation of the salinity and temperature measurement at station Fo12 with the measurement periods indicated beneath the temperature diagram. The salinity measurement in the second period is rapidly decreasing and the transition between periods 2 and 3 is disturbingly discontinuous. The latter part of salinity measurements of period 2 must thus be discarded. There is good reason to believe that the instance of rapid down-mixing/welling by the end of July is factual since this event is captured by virtually all other instruments, Figure 3-1.*

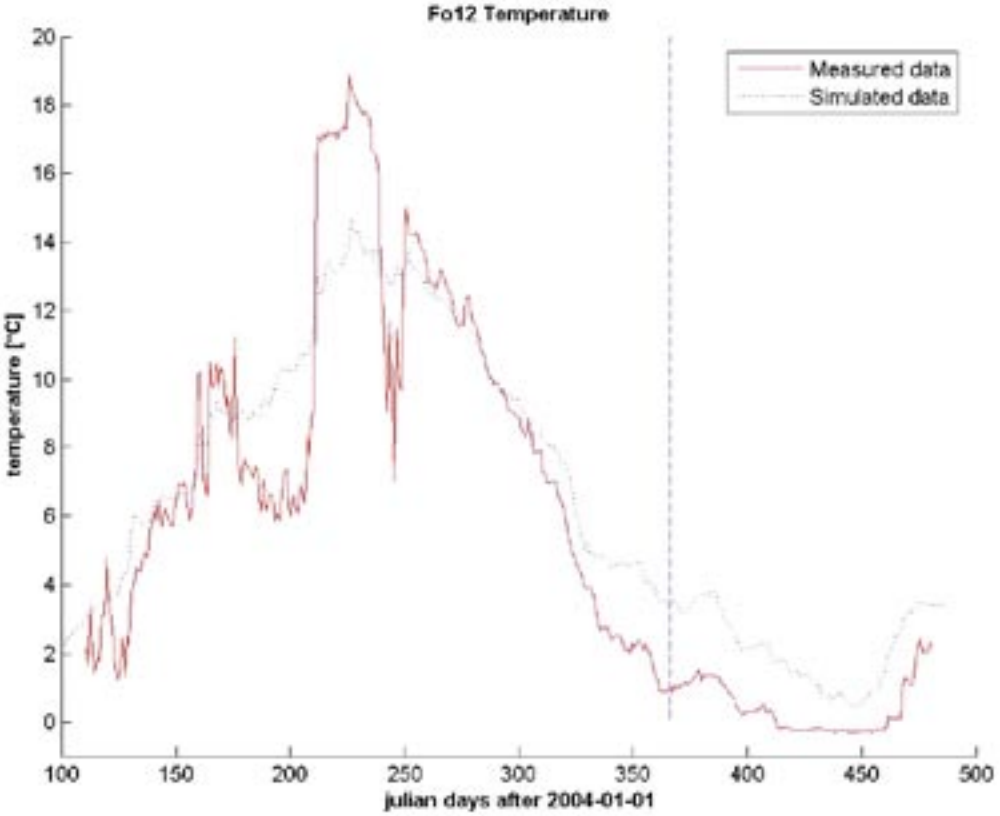

Figure 3-14. *Comparison of the temperature at 12-m depth at station Fo12 for the whole validation period (2004-04-20 through 2005-04-25). During the heating phase (up until JD 250) the simulated data do not display the sharp transitions that are most likely connected to up/down-welling events. The temperature at the 12 m depth level rapidly rises on down-welling. During the cooling phase, there is a noticeable discrepancy between the two temperature curves that levels off to attain approximately 1°C by the end of the validation period.*

A comparison of the temperature at the 12-m depth at station Fo12 is shown in Figure 3-15. The sharp salinity transitions by the end of the validation period appear suspect but cannot arguably be dismissed from partaking in the statistical analysis.

A scatter diagram of measured vs. simulated temperature at station Fo12 at 12-m depth beneath the surface can be seen in Figure 3-16. The regression line slopes less than the ideal line, which means that the average range of the simulated data is smaller than the average range of the measured data. The break-even point is about the mid range, i.e. somewhat below 10°C.

In Figure 3-17 a scatter diagram of measured vs. simulated salinity at station Fo12 at 12-m depth beneath the surface is presented. The entire validation period has been subdivided into four periods not exactly coincidental with the periods of the instrument deployment. One of these periods yields a negative correlation coefficient, while the other three are reassuringly positive. It can be seen by visually joining the mass centers of the sub-periods, that the drift towards lower salinities during the entire validation period would yield a negative overall correlation coefficient if the regression analysis were to encompass the whole validation period.

A scatter diagram of the north/south(V)- and east/west(U)-velocity components of Fo12 station at 12-m depth is given in Figure 3-18. The regression lines display a considerably smaller slope than the ideal line, but both are in fact positive.

In Figure 3-19 a spectral comparison of the simulated and measured current speed at station Fo12 for the data of the first 256 days is presented. This comparison is independent of the current direction and demonstrates that the spectral appearances are not notably dissimilar in spite of the comparatively small but positive correlation coefficients of the U- and V-velocity components.

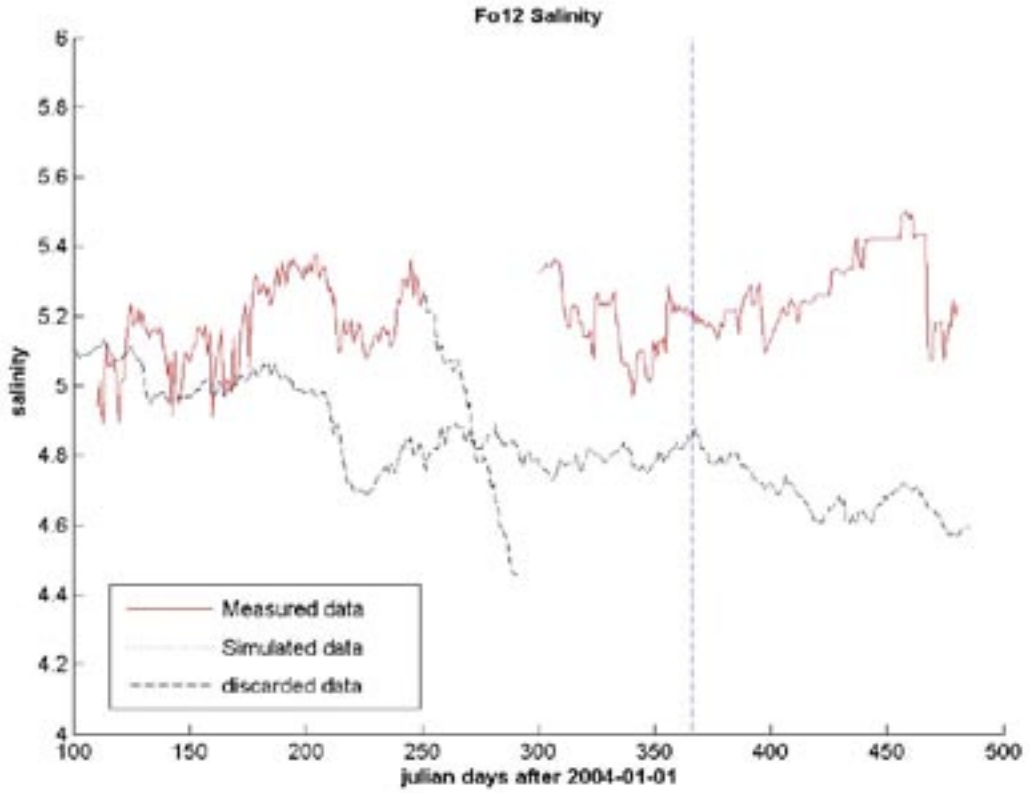

Figure 3-15. *Comparison of the salinity at 12-m depth at station Fo12. The part of the measured data that is invalidated has been drawn in black. The sharp salinity transitions by the end of the validation period seem suspect but cannot be dismissed. Vertical broken line indicates the new year transition.*

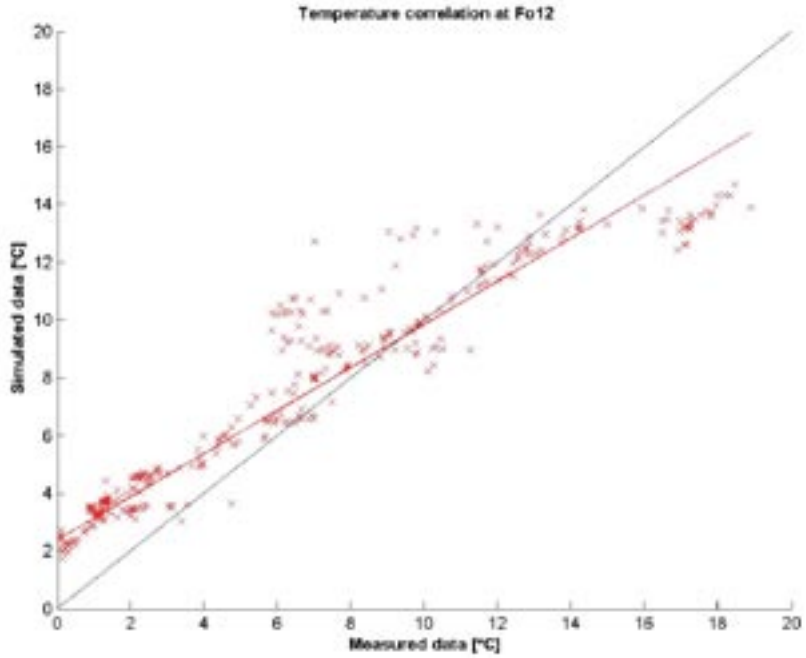

Figure 3-16. *Scatter diagram of measured vs. simulated temperature at station Fo12 at 12-m depth beneath the surface. The regression line (red) slopes less than the ideal line (black), which means that the range of the simulated data is smaller than the range of the measured data. The break-even point is about the mid range, i.e. somewhat below 10°C.*

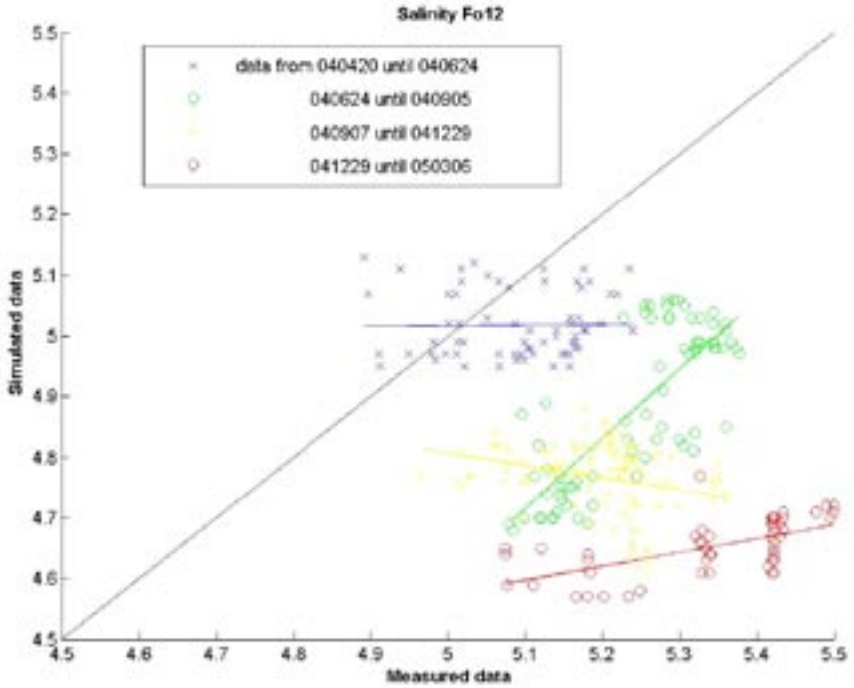

Figure 3-17. *Scatter diagram of measured vs. simulated salinity at station Fo12 at 12-m depth beneath the surface. The period has been subdivided into four periods that do not coincide exactly with the periods of the instrument deployment. One of these periods yields negative correlation coefficients (yellow circles), the other three positive with the blue line close to zero. The systematic drift towards lower salinities during the entire validation period gives a negative overall correlation coefficient for the whole period.*

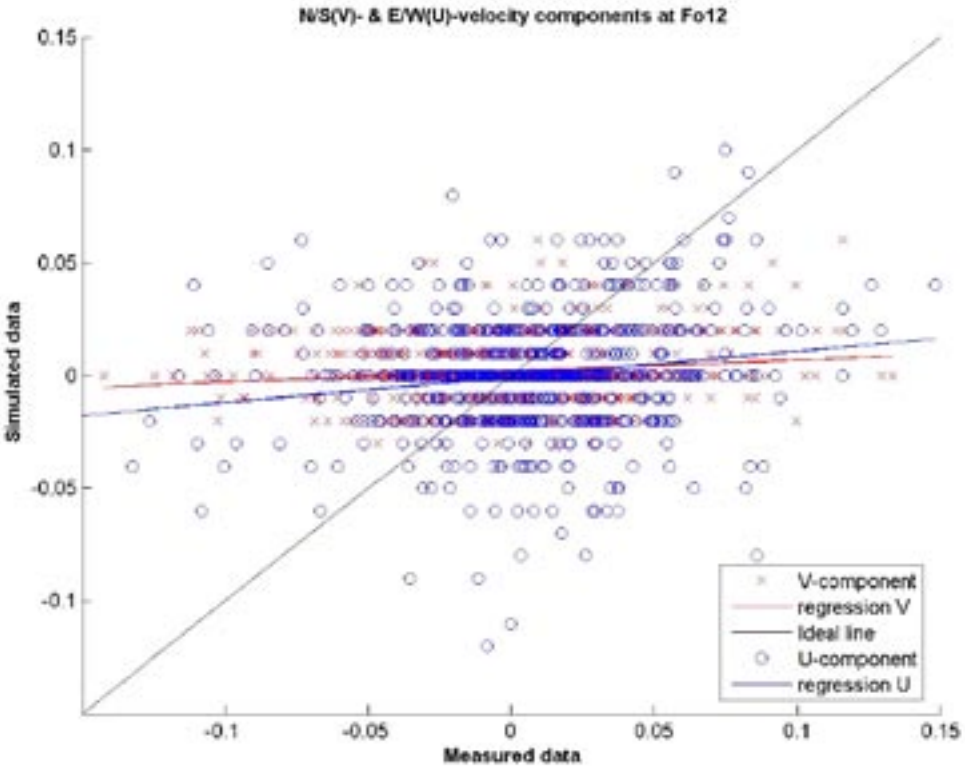

Figure 3-18. *Scatter diagram of the north/south(V)- and east/west(U)-velocity components of station Fo12 at 12-m depth. The regression lines display considerably less slope than the ideal line, but are both positive.*

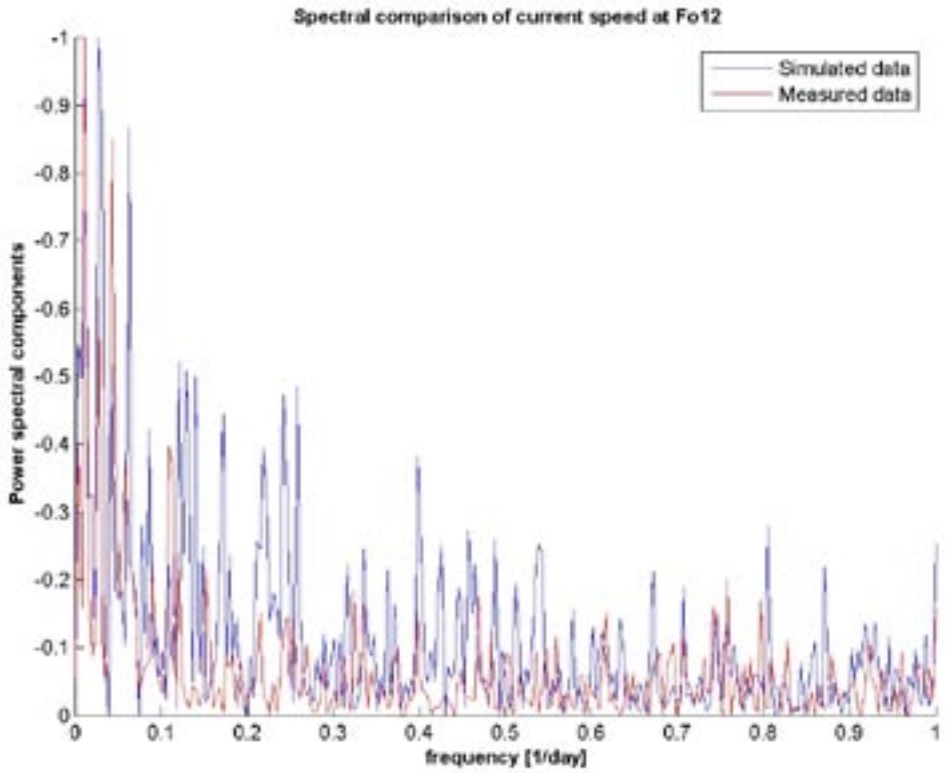

Figure 3-19. *Spectral comparison of the simulated and measured current speed at station Fo12 for the first 256 days of data. This comparison is independent of the current direction and displays that the spectral appearances are not notably dissimilar in spite of the comparatively small but positive correlation coefficients of the U- and V-velocity components.*

3.4 Station Fo13

In the salinity and temperature diagram of station Fo13 (Figure 3-20), the measured salinity levels on all levels of the second period decreased rapidly and the transition between periods 2 and 3 is also alarmingly discontinuous. The latter part of salinity measurements of period 2 thus had to be discarded from further analysis. From period 3 and onward, with short temporal exceptions, there are regimes of unstable stratification that decisively exceed the acceptable inaccuracy of 0.1 in the psu-scale. Concerning the temperature measurements, there is good reason to believe that the instance of rapid down-mixing/welling by the end of July is factual since this event was captured by virtually all other instruments.

A comparison of measured and simulated Salinity for the four depth sites of station Fo13 are depicted in Figure 3-21. As for stations Fo11 and Fo12, the up- and down-welling events during the heating phase in springtime and early summer are not well simulated, neither regarding magnitude nor phase. During the autumnal cooling period the vertical well-mixed conditions are well captured by the model as is the rate of heat loss, but there is a systematic difference of a couple of degrees Celsius. By the end of the simulation the renewed heating of the water column starts roughly simultaneously, but the modelled heating process is somewhat faster.

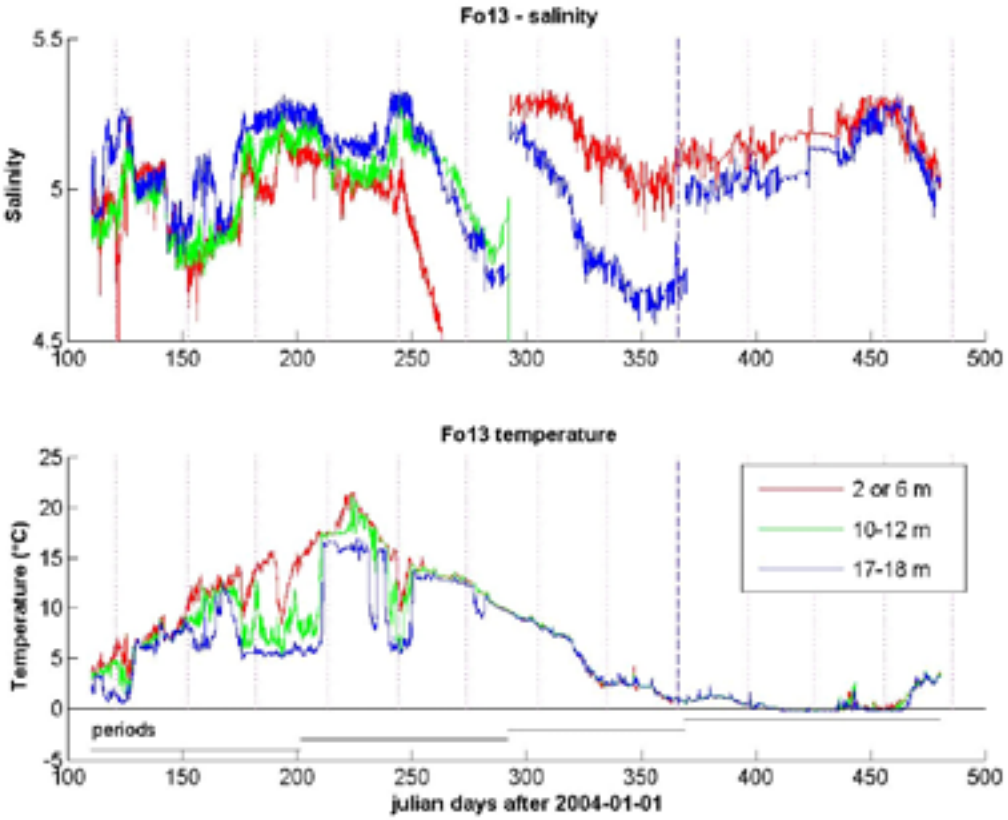

Figure 3-20. *Salinity and temperature measurements at station Fo13 with the measurement periods indicated beneath the temperature diagram. The measured salinity levels on all levels of the second period decrease rapidly and the transition between periods 2 and 3 is disturbingly discontinuous. The latter part of salinity measurements of period 2 must thus be discarded. From period 3 and onward, most of the time there is a regime of unstable stratification decisively exceeding the acceptable inaccuracy of 0.1 in the psu-scale. Concerning the temperature measurements, there is good reason to believe that the instance of rapid down-welling by the end of July is factual since this event is captured by virtually all other instruments.*

The salinity dynamics of corresponding measured and simulated data for the same depth sites of station Fo13 are compared in Figure 3-22. The rapid decline of the salinity after JD 250 is also taking place in the model, but the vast mismatch of salinities on the transition to the third validation period makes these data questionable to the point that this period should be discarded from the ensuing correlation analysis. The simulation that begins on January 1, 2005, has been performed with Mueller data while for 2004 Mesan data were used. For these last four months the model performs quite well, in particular by capturing the down-welling event between JD 450–500 both to date and magnitude.

In Figure 3-23 scatter diagrams of measured and simulated salinity and temperature are presented. These plots are subdivided into three periods of which only two are valid for salinity at 10-m depth because of instrument failure. Regression lines display the same pattern as for Fo11 and Fo12, namely the reflection of systematically decreasing salinity with time. The notable exception is the salinity of the last period at 17-m depth, which show replenished salinity levels. This is most likely due to the increased wind forcing by using Mueller instead of Mesan data. As for the corresponding scatter plots of Fo11 and Fo12, the correlation levels of the salinities are considerably improved on the shorter term intervals, also due to the above-mentioned steadily decreasing Baltic salinities of the top layers. The slope of the regression lines is clearly adopting closer to the ideal line with increasing depth, while the contrary applies to the correlation coefficient (Table 2-3).

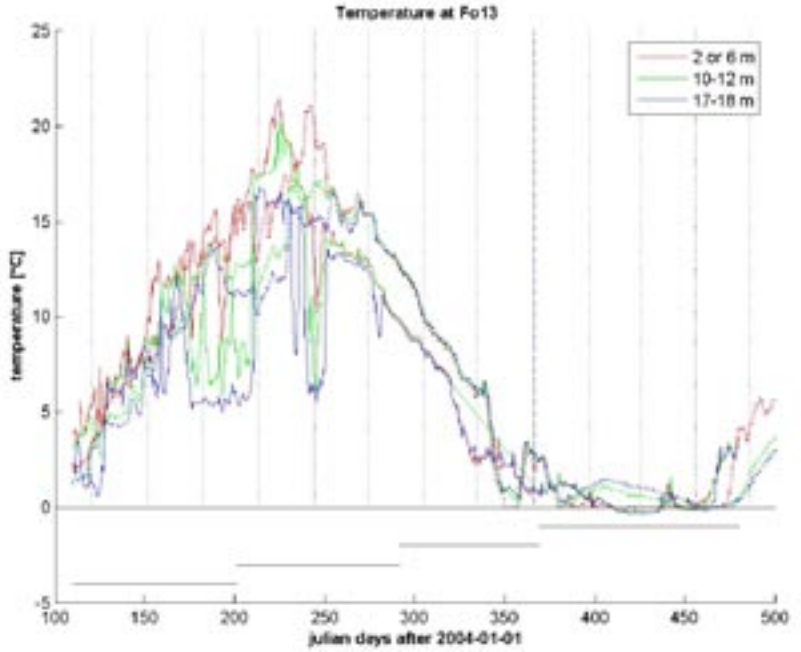

Figure 3-21. *Temperature comparison of measured (solid lines) and simulated (dotted lines) data for the indicated depth sites of station Fo13. As for stations Fo11 and Fo12, the up-/down-welling events during the heating phase during springtime are not well simulated, neither regarding magnitude nor phase. During the fall cooling period the vertical well-mixed conditions are well captured by the model as is the heat loss intensity, but there is a difference of a couple of degrees Celsius. By the end of the simulation the heating of the water column starts at the same time but the modeled heating process is faster.*

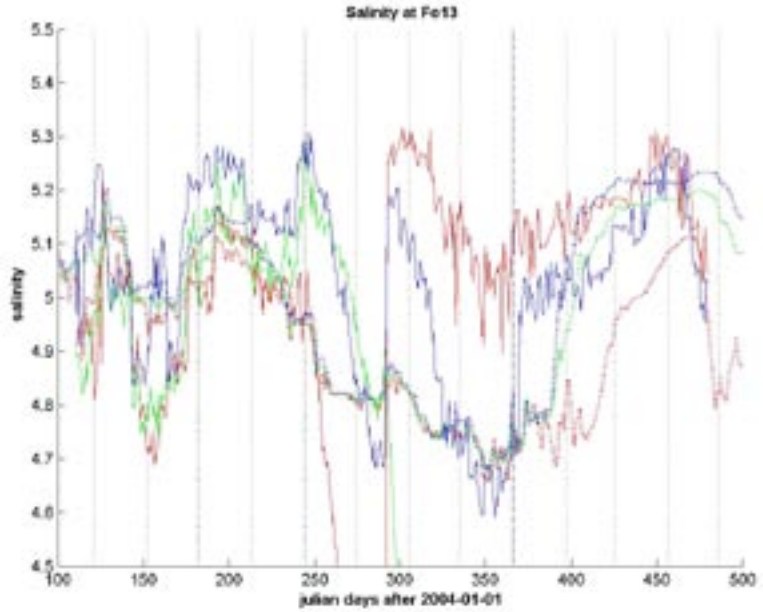

Figure 3-22. *Salinity comparison of measured (solid lines) and simulated (dotted lines) data for the indicated depth sites of station Fo13. The rapid decline of the salinity after JD 250 is also taking place in the model, but the vast mismatch of salinities on the transition to the third validation period makes these data questionable and this period has been discarded from the ensuing correlation analysis. The simulation of 2005 (marked by the vertical black broken line) has been performed with Mueller data while for 2004 Mesan data were used. For this last four months the model performs quite well, in particular by capturing the down-welling event between JD 450–500 both as to date and magnitude.*

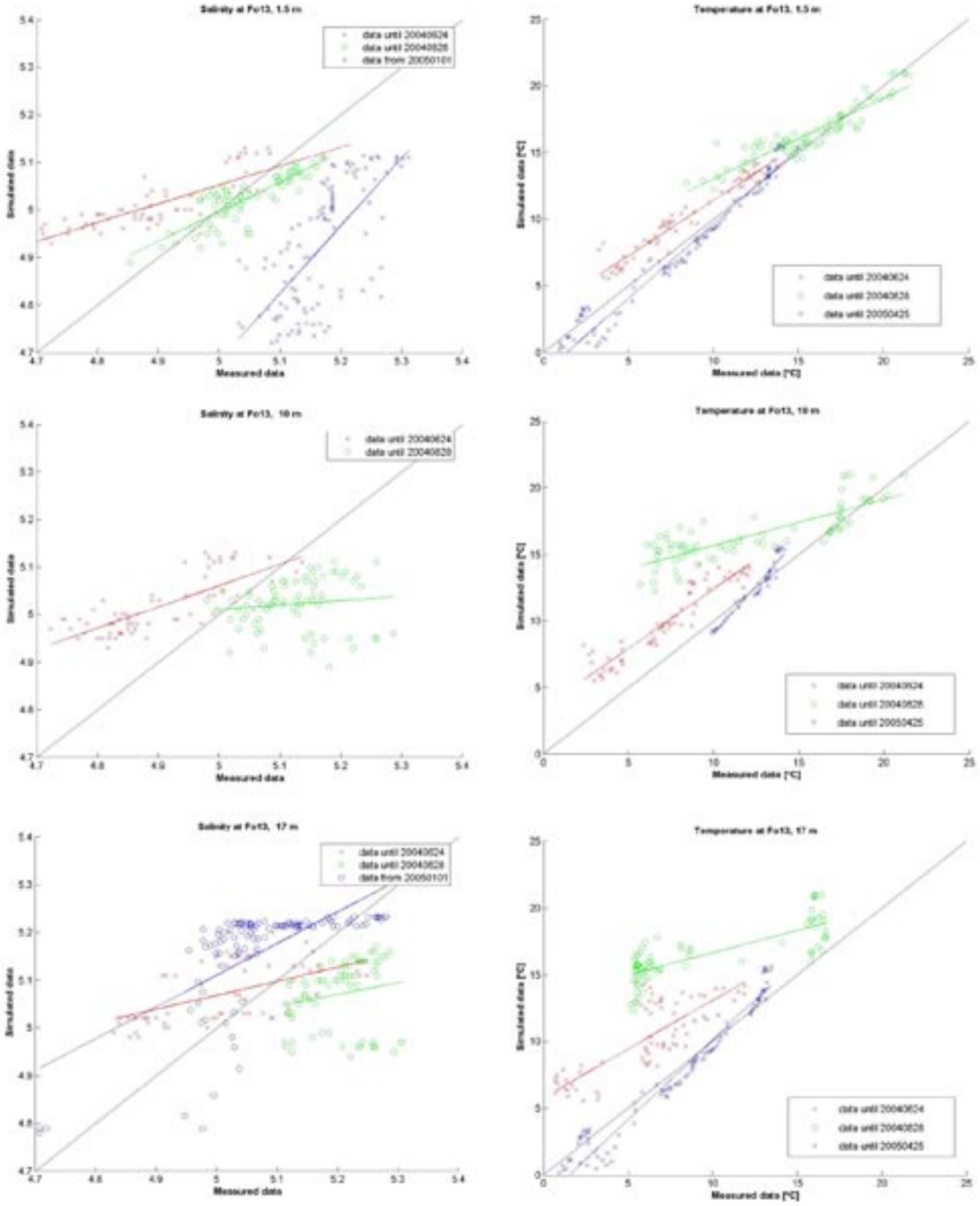

Figure 3-23. *Scatter diagrams of measured and simulated salinity and temperature subdivided into three periods (only two for salinity at 10-m depth because of instrument failure). Regression lines are also displayed. As for the corresponding scatter plots of Fo11 and Fo12, the correlation is of the salinities is better on the short term due to overall decreasing Baltic values. The slope of the regression lines is clearly adapting closer to the ideal line with increasing depth, while the contrary applies to the correlation coefficient (Table 2-3).*

3.5 Station Fo14

The placement of this station was intended to check the through-flow of the strait Öregrundssund. For unclear reasons this station was relocated in stages towards the western side of strait and it was only later that it was found that the actual secluded locations were completely off the mainstream flow, see Figure 3-24a–c. These three presented transects all pass north of this station (Fo14). It is clear that the varying placement of this station is very susceptible to small changes in width of the back-going current and does not, as was the original intention, reflect the intensified current branch that flows through the deepest part of the strait Öregrundsund. Even worse was that the average depth of the corresponding grid cell turned out to be only a fraction of the actual depth due to the local bottom heterogenic bathymetry. This completely invalidates a fair comparison of the salinity and temperature at 23-m depths, since no such depths exist in the model realm. Despite this, the salinity and temperature time development has been plotted in Figure 3-25. The salinity curve for period 3 shows notable fluctuations that continue into period 4. The temperature curve shows that the above-mentioned up-/down-welling periods during spring also penetrate into this central part of the modelling domain.

This instrument also seems to have been the object of curious local residents since it displays a dramatic change in regime during the third measurement period, most likely due to human interference. This can be seen from Figure 3-26, in which the East/west(U)-component and north/south(V) component are contoured employing a low-pass filter with running average over a 10 h-window. The disparate flow patterns of these notably different regimes of the four measurement periods are conspicuous. There is no sign of intensified bottom current in the north/south(V)-component, which would have been expected if the instrument had been placed in the mainstream flow.

3.6 Station Fo15

Station Fo15 was endowed with a thermistor chain that had 11 sensors covering the depth range from 1 m to 27 m. Contour plots (time vs. depth) of the *measured* and temperature development at station Fo15, starting from JD 110 is given in the upper panel of Figure 3-27, while the lower panel analogously depicts the *simulated* temperature development at station Fo13. This is because the depth of the model grid at the site of Fo15 in the model is considerably more shallow than the actual depth. The comparison has thus been made with the simulated temperature data of the station Fo13 in the close vicinity, see Figure 1-2. This station is located in a symmetric position with regard to deeper mid-rift in the north/south-direction of the embayment; no thresholds but mere open water separate these locations. The measured data, in spite of the diurnal sampling rate for the comparison, display a higher degree of temporal variability, more pronounced towards the surface, than the modelled one. The corresponding scatter diagrams for the five different layers available for comparison, limited by the number of model layers, are shown in Figure 3-28. In spite of considerable aberration of singular data points, the regression lines indicate an overall good agreement, substantiated also by the high correlation coefficients in Table 2-3.

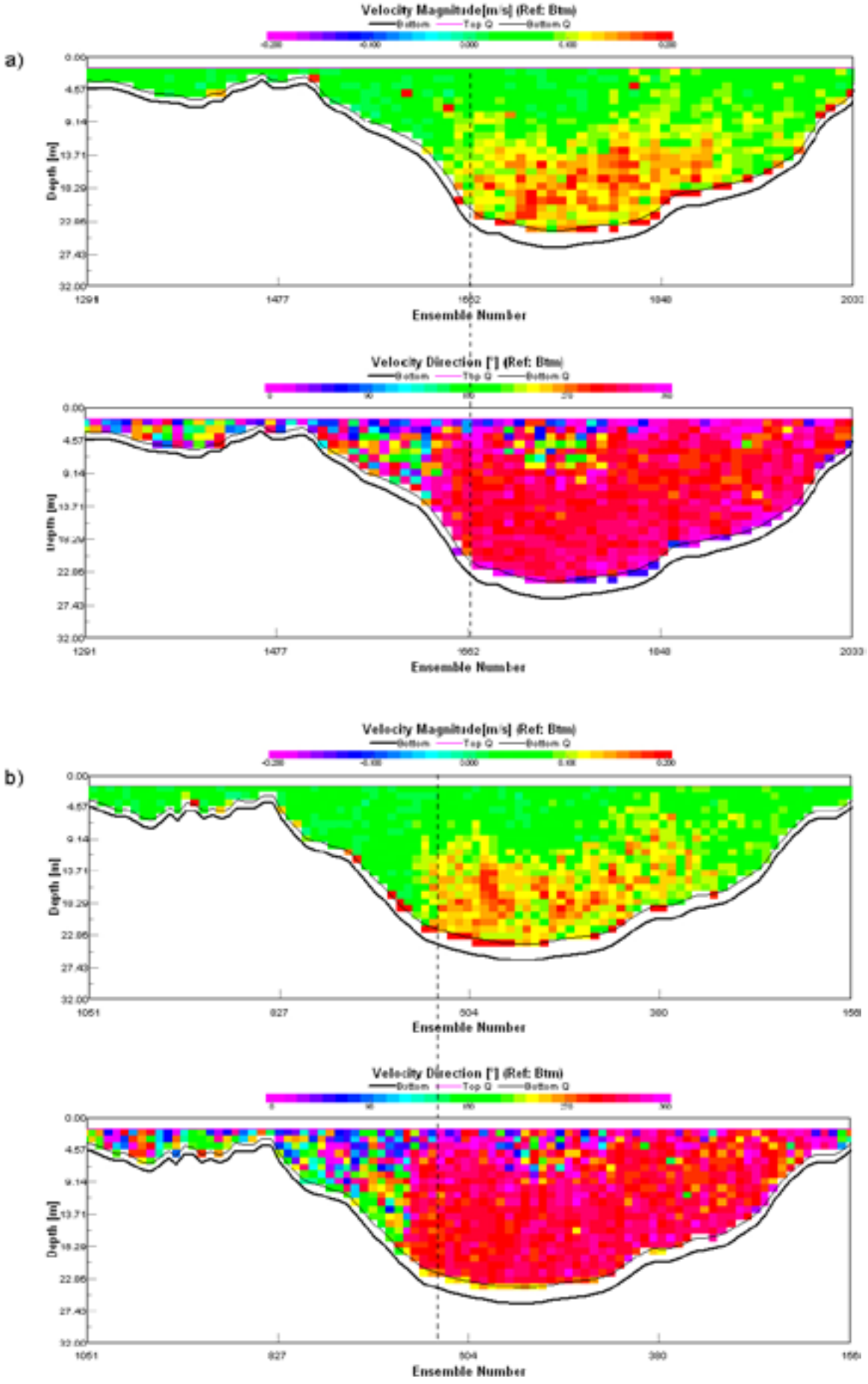
a)
Velocity Magnitude[m/s] (Ref: Btm)
Bottom
Top Q
Bottom Q
Depth [m]
Ensemble Number
Velocity Direction [°] (Ref: Btm)
b)

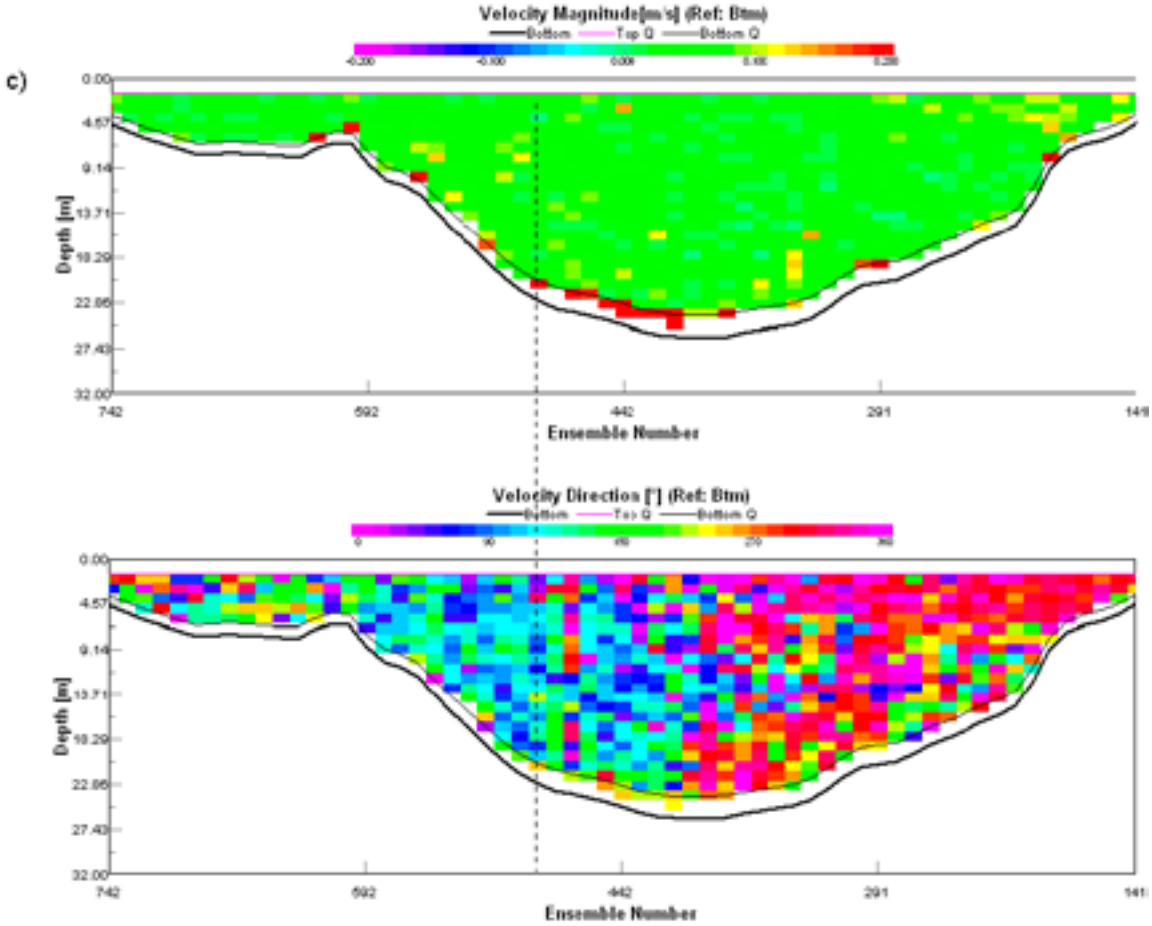

Figure 3-24a–c. *Three ADCP transects revealing the currents near Fo14. In all three pairs of transects the upper panel displays the current velocities (ranging from –0.2 to 0.2 ms^{-1}) and the lower in each pair the current direction ranging from 0°–360°. The vertical axis in all three pairs of diagrams denotes depth and ranges from 0 to 32 m. These transects all pass north of this station Fo14 near the position indicated by broken lines. It is clear that the varying placement of this station is very susceptible to small changes in width of the back-going current and does not, as was the original intention, reflect the intensified current branch that flows through the deepest part of the strait Öregrundsund.*

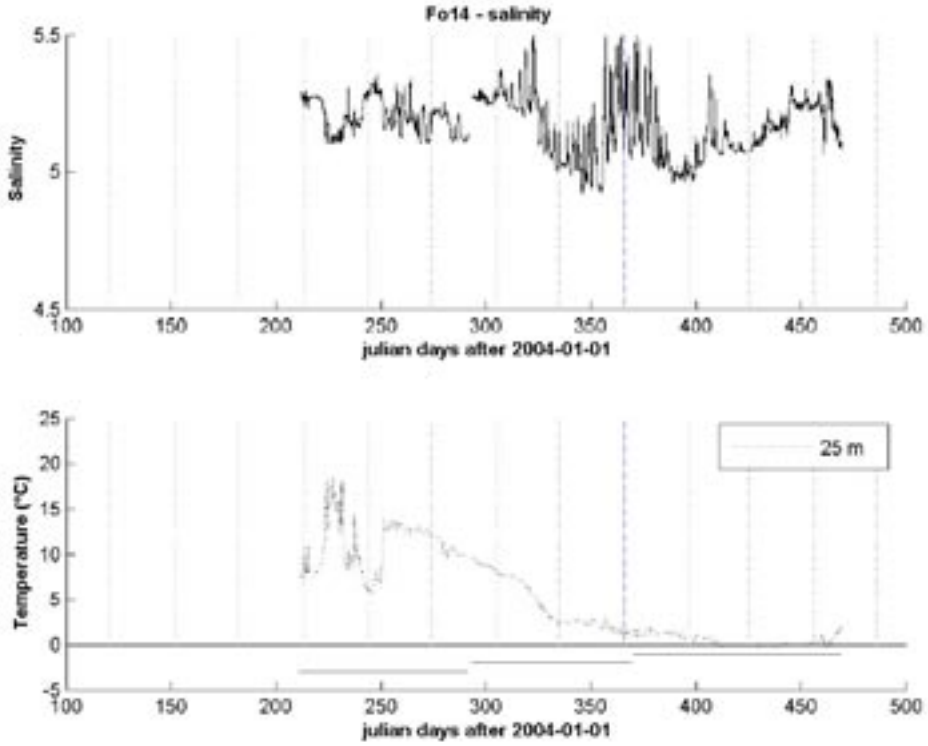

Figure 3-25. *(Upper diagram) Salinity at station Fo14 measured at 23 m depth. Around the transition to the new year (marked with a broken black line) there are notable fluctuations that continue into period 4. (Lower diagram) Temperature development starting from period 2.*

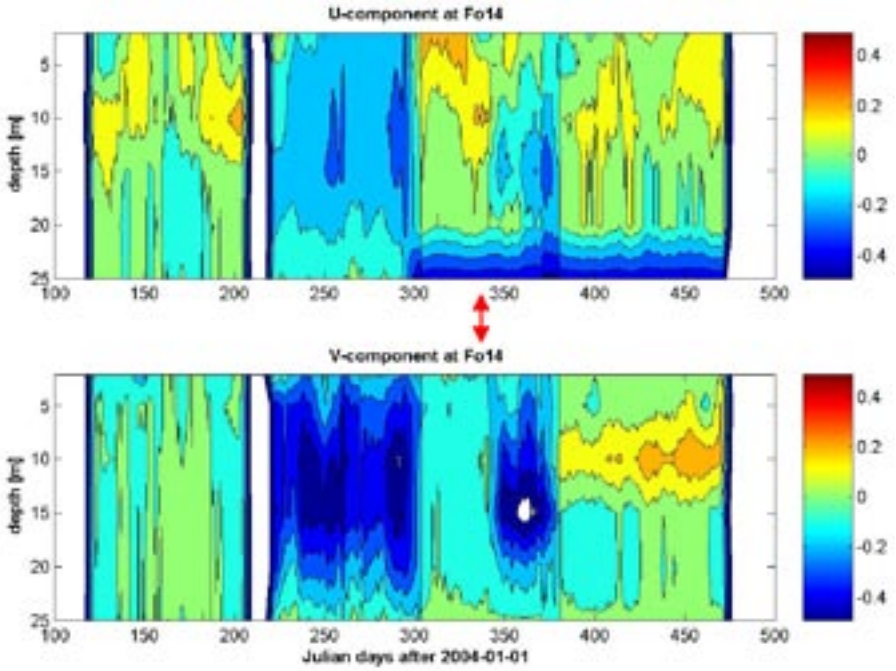

Figure 3-26. *East/West(U)-component (upper panel) and North/South(V)-component (lower panel). In this low-pass filter (performed with running average over a 10 h-window), the differing regimes between the validation periods is conspicuous. Also note the changed regime in the middle of the third measurement period, indicated by a red double headed arrow. There is no sign of the anticipated intensified bottom current in the V-component that should occur if the instrument placement had reflected the through-flow of the Öregrundsund strait.*

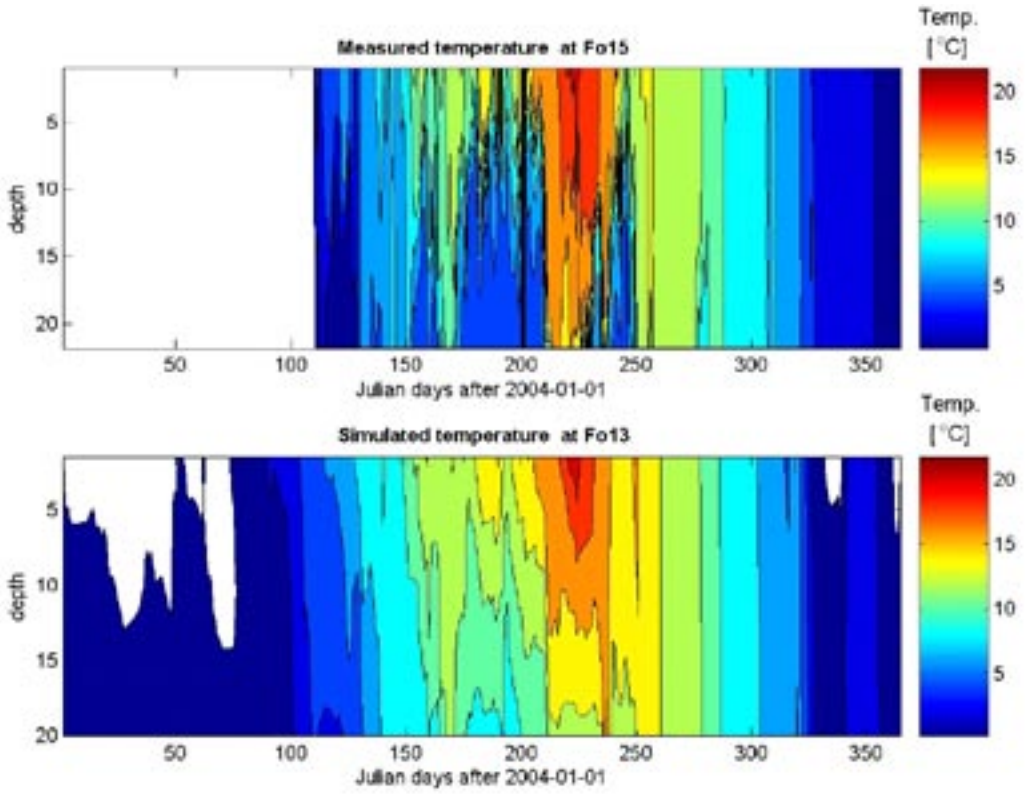

Figure 3-27. *(Upper panel) Contour plot (time vs. depth) of the* ***measured*** *temperature development at station Fo15, starting from JD 110. Missing data are marked with white color. (Lower panel) Contour plot (time vs. depth) of the* ***simulated*** *temperature development at station Fo13. Since the gridded depth at the site of Fo15 is considerably more shallow, the comparison has been made with the simulated nearby station Fo13. Temperatures below zero are indicated with white.*

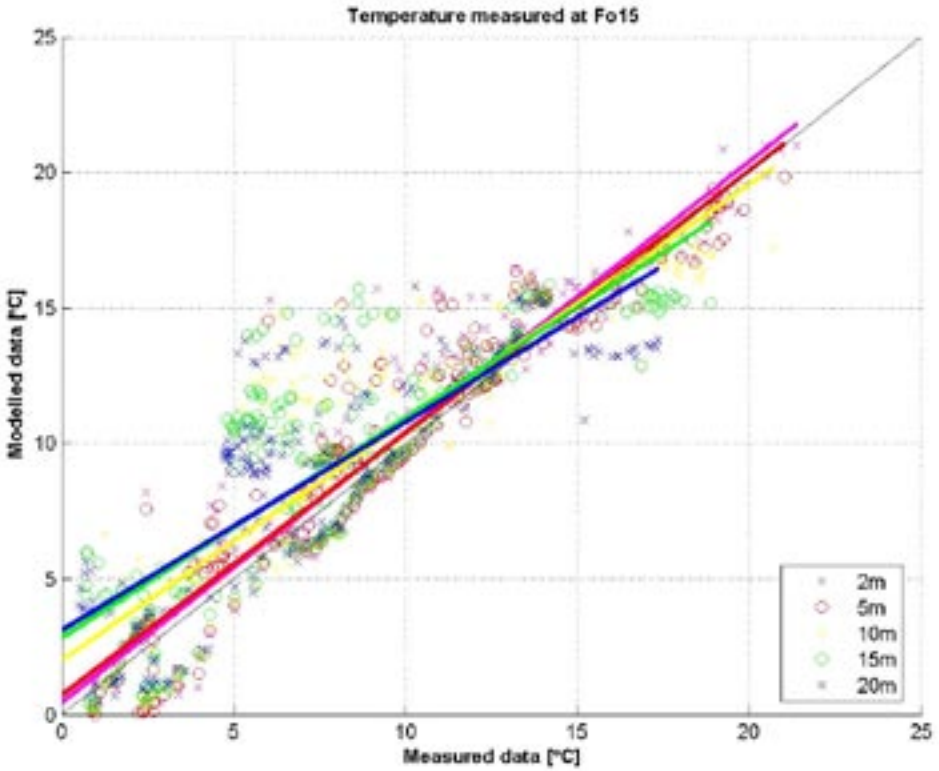

Figure 3-28. *Scatter diagrams of measured vs. simulated temperature data for the five different layers. In spite of considerable aberration of singular data points, the regression lines indicate an overall good agreement, substantiated also by the correlation coefficients in Table 2-3.*

3.7 Station Fo16

In the overview of the conjoined measurement effort of station Fo16, the salinity dynamics shows rapid fluctuation for all three layers but this is particularly pronounced for the bottom layers, Figure 3-29. The steady decrease of salinity during period 2 applies to all three layers and is most accentuated for the surface layer. The mismatching transition from period 2 to 3 gives an unequivocal indication. After the transition to the new year, well-mixed conditions prevail with approximately the same reading of all three instruments. The *temperature* development in the same figure shows stratified conditions during the spring heating phase with the same homogenizing vertical mixing event near JD 210 when the bottom layers almost instantaneously attain the surface temperature. The lasting effect excludes down-welling as a plausible explanation. During the autumnal cooling phase a thermally well-mixed water column is permanent until the end of the fourth and last measurement period

In Figure 3-30a a comparison is made between measured and simulated temperature development for the three depths at station Fo16. The same homogenizing vertical mixing event near JD 210 is well captured by the model as is the cooling phase and the temporal heating in the middle of the third period. The 10 m-line for period 3 is not valid due to instrument malfunction.

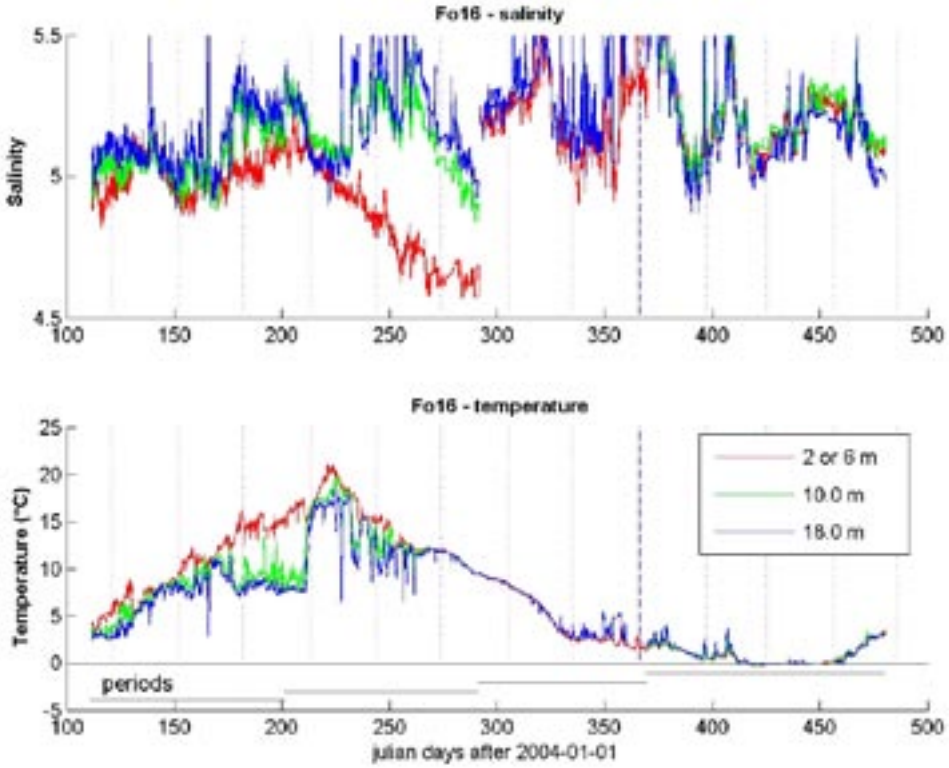

Figure 3-29. *Overview of the conjoined measurement effort of station Fo16. The salinity dynamics (upper panel) shows rapid fluctuation for all three layers but is particularly pronounced for the bottom layers. The salinity scale truncates some of the elevated measurements but has been retained in order to facilitate comparison. The decrease of salinity during period 2 applies to all three layers but is most accentuated for the surface layer. The mismatch in the transition between periods 2 and 3 is a clear indication of this. After the transition to the new year (marked with vertical black broken line) well-mixed conditions prevail. The* ***temperature*** *development (lower panel) shows temperature stratified conditions during the spring heating phase with the same homogenizing vertical mixing event near JD 210 when the bottom layers almost instantaneously attain the surface temperature. During the autumnal cooling phase a thermally well-mixed water column is persistent until the end of the last period.*

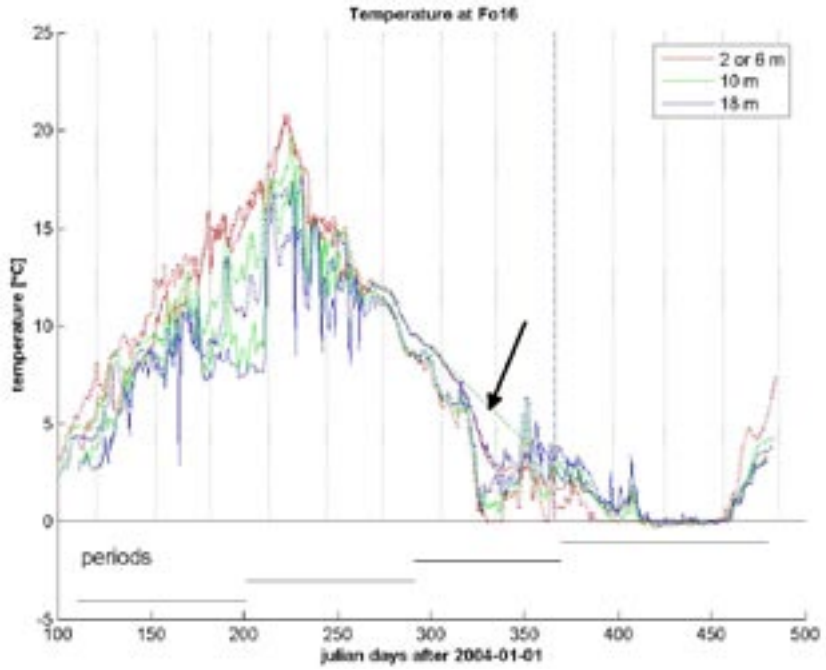

Figure 3-30a. *Comparison of temperature development for the three depths at station Fo16. The downmixing event near JD 210 is well-captured by the model as is the cooling phase and the temporal heating in the middle of the third period. The 10 m-line for period 3 has been drawn broken and marked with an arrow to indicate that this only a straight line connecting the sections of this curve that are regarded as valid.*

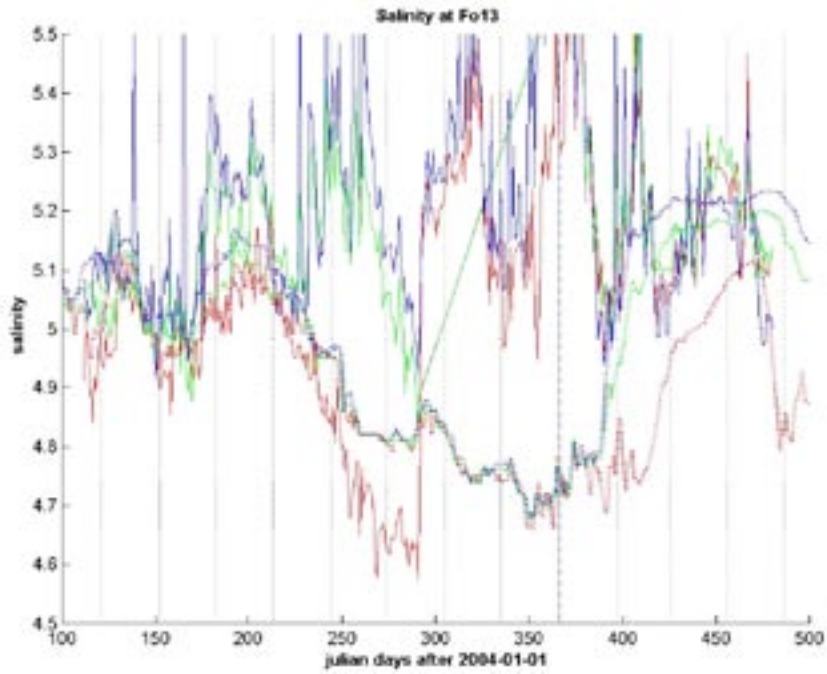

Figure 3-30b. *Comparison of salinity development for three depths at station Fo16. During the second period a rapid decline in salinity occurs for all three instruments, followed by a huge mismatch in the transition to period three. It is problematic that part of this decline is also simulated by the model, but not by far to the extent that the measurements indicated, which is certainly caused by growth of epiphytes. The straight broken green line during period 3 is an interpolation of the data of the third period that has been discarded. The fourth period takes place entirely in 2005 and for this year the Mueller wind data have been used.*

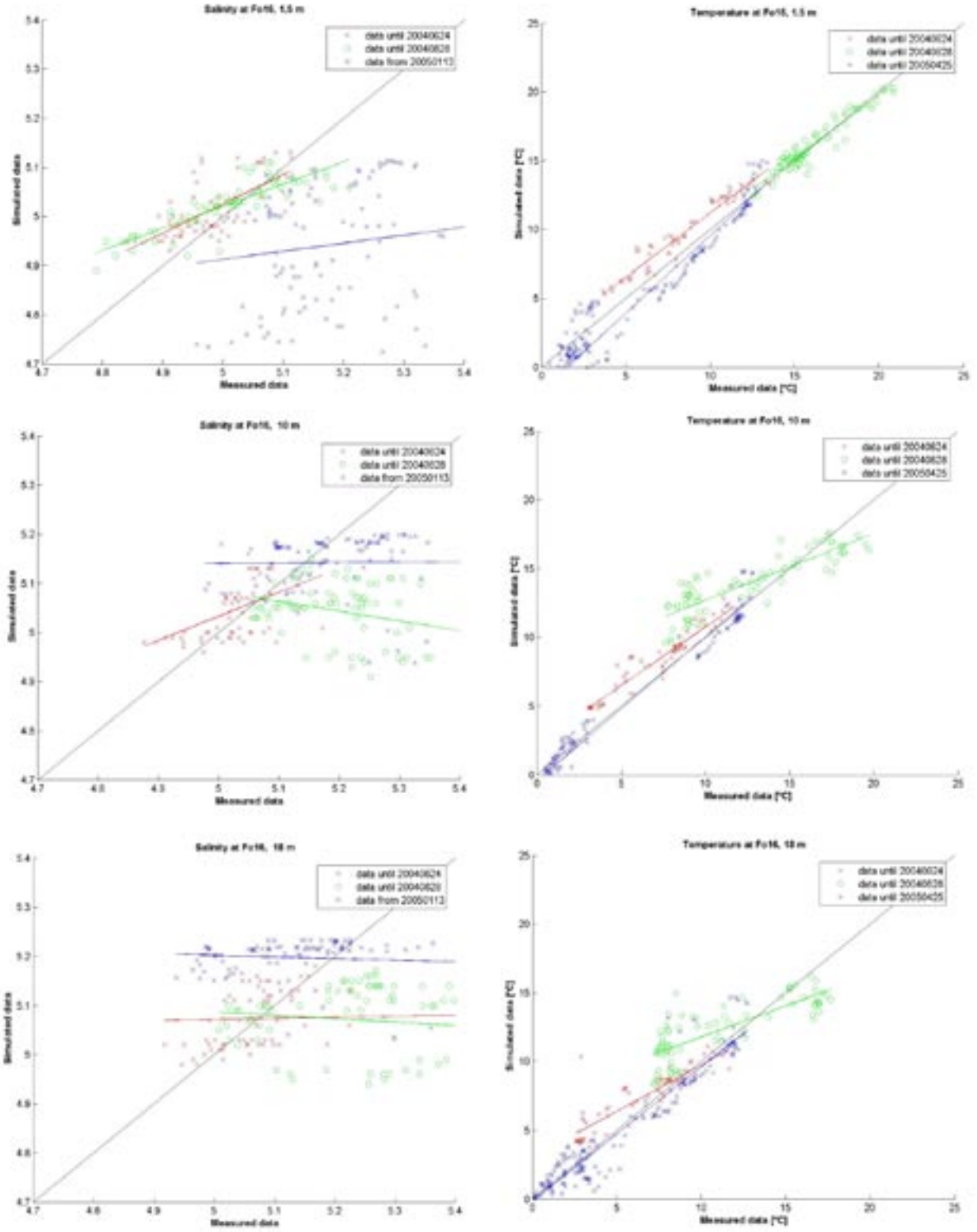

Figure 3-31. *Scatter diagrams of salinity (left panels) and temperature (right panels) of Fo16 with most of period 2 exempted for the salinity plots, cf. Figure 3-30a and b. No data for period 3 at the 10 m-level have been used. The corresponding regression lines are also displayed. As for the corresponding scatter plots of the stations Fo11, Fo12 and Fo13, the correlation of the salinities is better on short terms due to overall decreasing Baltic values. The slope of the regression lines for the temperatures is clearly adapting closer to the ideal line with decreasing depth, while the contrary applies to the correlation coefficient (Table 2-3).*

The corresponding comparison of the salinity development for three depths at station Fo16 is shown in Figure 3-30b. During the second period there occurs a rapid decline in salinity for all three instruments. This is followed by a huge mismatch in the transition to period three. It is problematic that part of this decline is also simulated by the model but not to the extent that the measurements indicate. This is most likely caused by epiphytal growth. As for temperature, the data of the third period have been discarded. The fourth period takes place entirely in 2005 and for this year the Mueller wind data have been used.

In Figure 3-31 scatter diagrams of salinity and temperature of the Fo16 stations are displayed. Most data of period 2 are exempted for the salinity plots due to the cited reasons, see Figure 3-30b. No data for period 3 at the 10 m-level have been used. The corresponding regression lines are also provided. As for the corresponding scatter plots of the stations Fo11, Fo12 and Fo13, the correlation of the salinities is better on short terms due to overall decreasing Baltic values. The slope of the regression lines for the temperatures is clearly adopting closer to the slope of the ideal line with decreasing depth, while the contrary applies to the correlation coefficient (Table 2-3).

3.8 Transects

Four transects with a ship-mounted ADCP instrument have been performed along the easternmost part of the northern boundary. In addition to the special studies near station Fo14, another transect along the southern part of the eastern boundary has been completed. All these transects were done under sufficiently calm weather conditions and can thus not be considered as representative of the average water circulation along these transects. Figure 3-32a shows a transect along the northern boundary taken 2004-04-16 passing close to the station Fo11. The velocity in all these diagrams is rendered as one panel for the current speed and another for the current direction. The sloping interface to the east separating north-flowing surface water from south-flowing bottom water is an indication of baroclinic and possibly also geostrophic water movements deflected by the presence of the nearby Örskär island. The next transect was taken 2004-07-21 (Figure 3-32b) and shows feeble current speed with a distinct upper well-mixed layer most clearly revealed by the current direction contrast. The Fo11 station seems to have been inadvertently placed in the middle of a gradient zone of changing directions. The white vertical bar in both diagrams is the result of lost bottom tracking and are deemed to be little consequence. The third transect of 2004-11-10 (Figure 3-32c) shows that in spite of very feeble currents, distinct baroclinic conditions prevail at the deepest part of the transect. The last of the northern boundary transects was recorded 2005-04-26 (Figure 3-32d) and renders a south-going jet-like bottom current that passes through the Fo11 location. The distance from east to west of the transect is about the same as the side length of the Baltic model grid cells.

Finally, a transect along the eastern boundary was performed 2005-04-27 (Figure 3-33). On this part of the model domain the water depths are scantily charted due to military considerations. The surface currents are on this occasion mainly flowing northwards while the deeper layers go in the opposite direction.

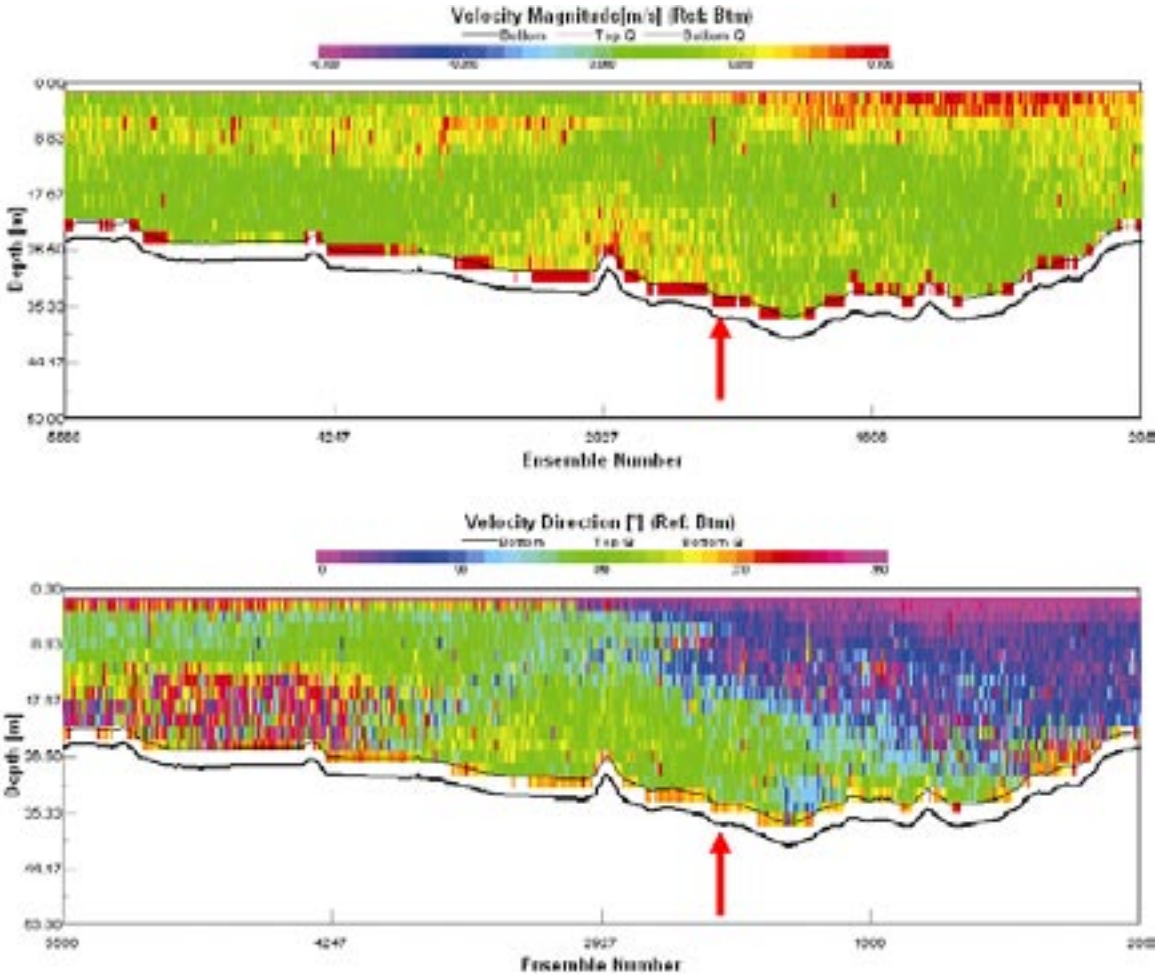

Figure 3-32a. *Transect along the northern boundary taken 2004-04-16. The location of station Fo11 is indicated with red arrows. The velocity in all these diagrams (a through d) is rendered as current speed (upper panel in the four pairs) ranging from –0.1 to 0.1 ms^{-1} and current direction (lower panel in the same pair) ranging from 0° to 360°. The vertical axis denotes depth from 0 m to 53 m. The sloping interface to the east separating north-flowing surface water from south-flowing bottom water is an indication of baroclinic (and possibly geostrophic) water movements sensing the presence of the nearby Örskär island.*

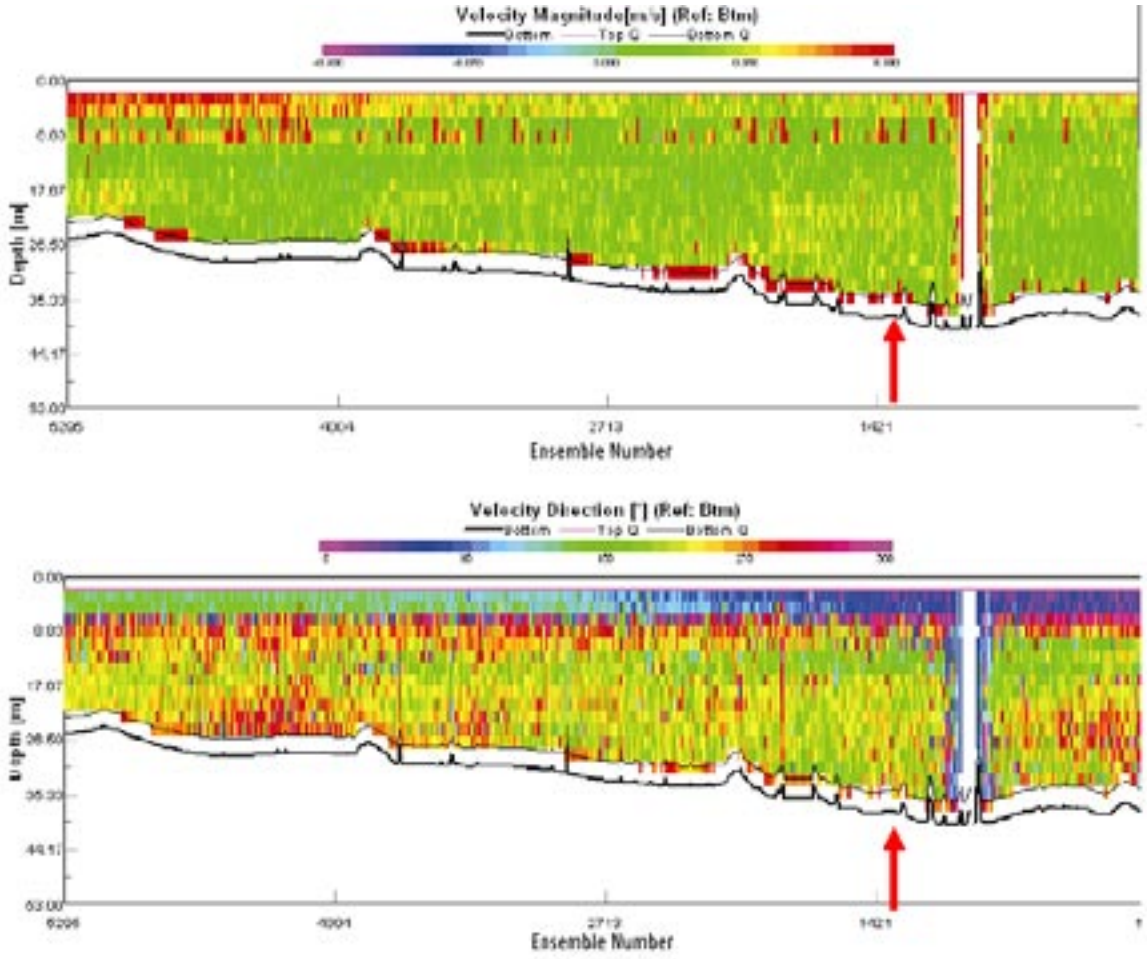

Figure 3-32b. *Transect taken 2004-07-21 with feeble current speed and with a distinct upper well-mixed layer revealed by the current direction diagram. For axis legend, see Figure 3-32a. The location of station Fo11 is indicated with red arrows and seems to be in the middle of a gradient zone of changing directions. The white vertical bar in both diagrams is the result of lost bottom tracking.*

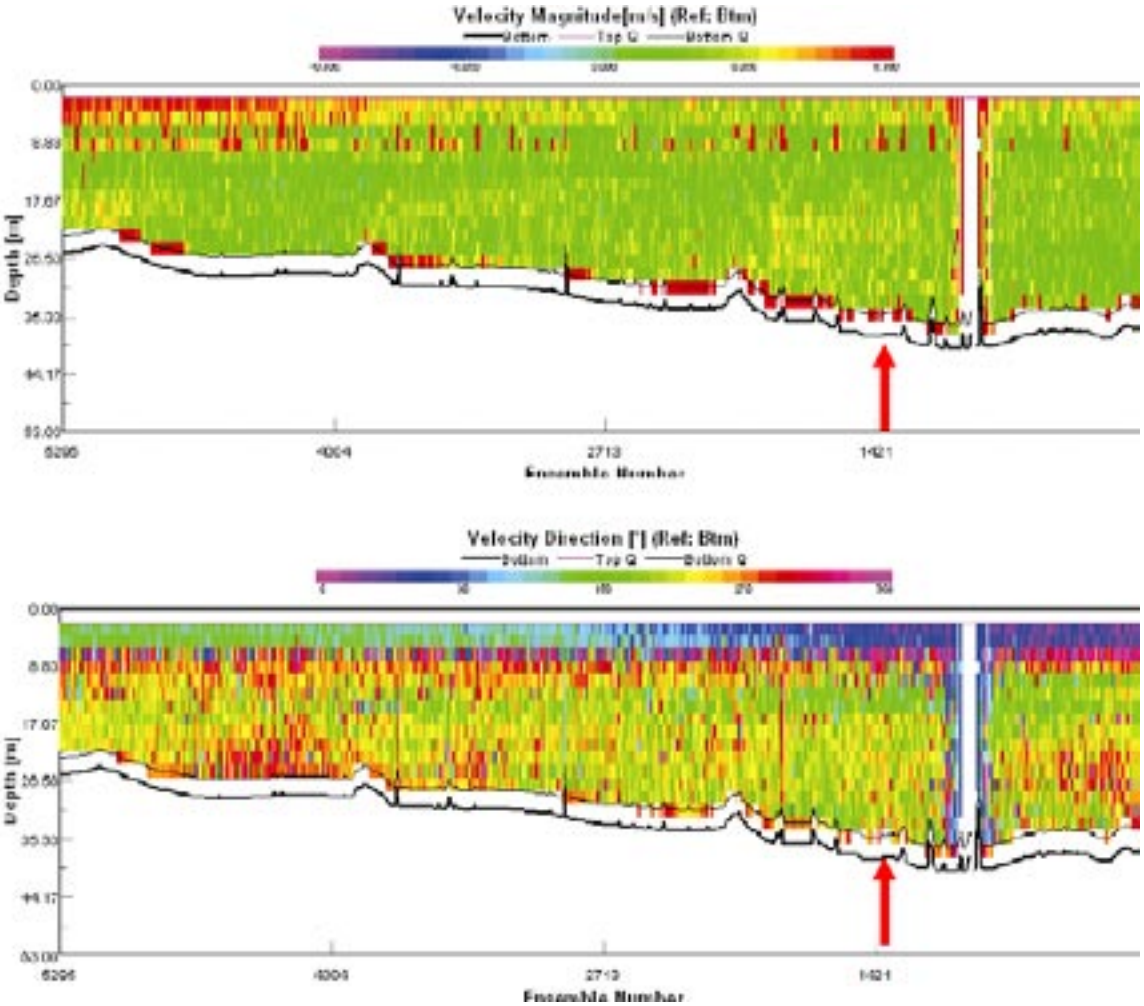

Figure 3-32c. *Transect of 2004-11-10. For axis legend, see Figure 3-32a. In spite of very feeble currents, baroclinic conditions prevail at the deepest part of the transect. The location of station Fo11 is indicated with red arrows.*

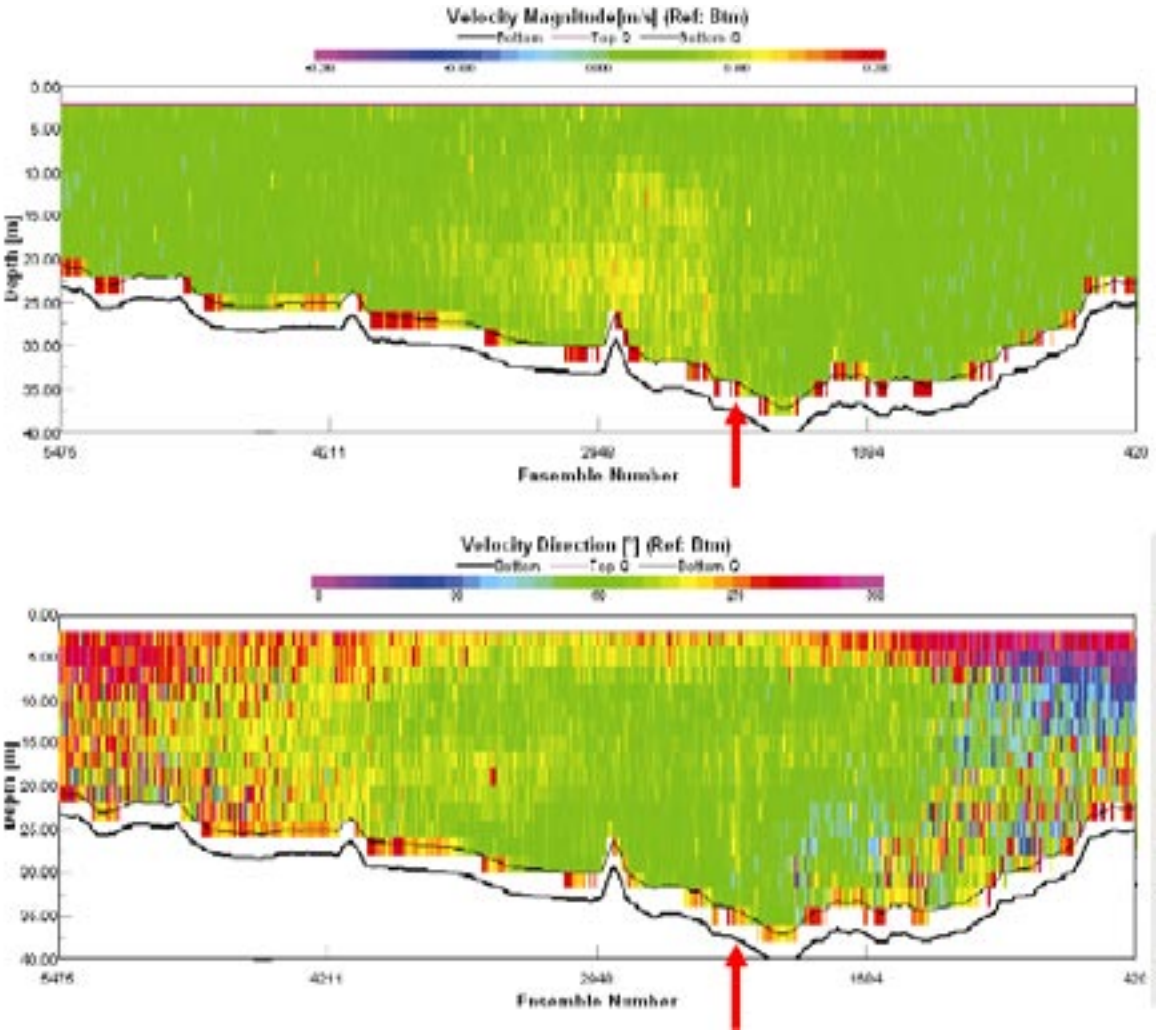

Figure 3-32d. *Last of the northern boundary transects recorded 2005-04-26. For axis legend, see Figure 3-32a. A south-going jet-like bottom current passes through the Fo11 location. The location of station Fo11 is indicated with red arrows. The distance from east to west is about the same as the side length of the Baltic model.*

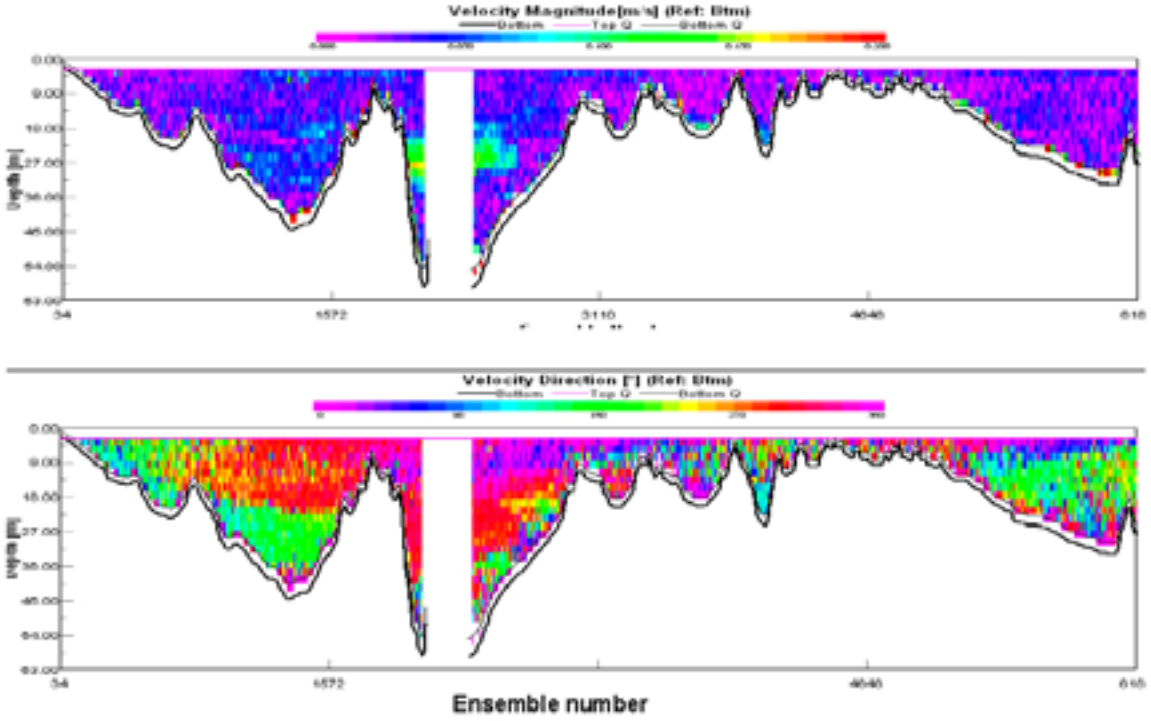

Figure 3-33. *Transect along the eastern boundary taken 2005-04-27. The south starting point corresponds to the left of the picture. The velocity in all these diagrams is rendered as current speed (upper panel) and current direction (lower panel). The surface currents are on this occasion mainly flowing northwards while the deeper layers go in the opposite direction.*

4 Discussion

4.1 Current comparison

The observed currents at the various depths at the two stations Fo11 and Fo12 give mainly positive correlations with the simulated flows decomposed into the orthogonal U- and V-components, Table 2-3. The east/west(U)-component is decisively better correlated than the V-component. This could be due to the deflection of the flow by the vicinity of the land in the east, i.e. the island Örskär, see Figure 3-32a through d. The Baltic model resolves 2 nautical miles (n.m.) and the local model one tenth n.m. A snapshot result of a separate study /Engqvist 2007/ with an intermediary grid resolution of one quarter of a n.m. (463 m) is shown in Figure 4-1, in the form of a vector display of the surface flow field averaged over the month of March 2004. This shows that the south-going large-scale coastal current produces a time-persistent eddy to the east and the residual currents flow mainly to the west if one looks to the east of the island Örskär at the latitude of the northern boundary. This is substantiated in Figures 3-8 and 3-10, which show that the U-component is greater than the V-component and that the former is most of the time negative, i.e. flowing to the west. To recollect, the station Fo11 was relocated to the east outside the leading sector of the lighthouse (Engelska grundet) in order to lower the probability of ship interference. With the exception of the top layer the correlation levels of the U-component at Fo11 are fairly good and in agreement with what could be expected under the given circumstances.

The same condition also applies to the current measurement at Fo12 at 12-m depth. The correlation coefficients are positive but small, mostly lying in the 10–20% interval. It has been argued /Andrejev and Sokolov 1989/ that spectral comparison possibly would be the most adequate way of evaluating modelled current results against measurements. If the current direction information is moreover made irrelevant by comparing only the speed of the current,

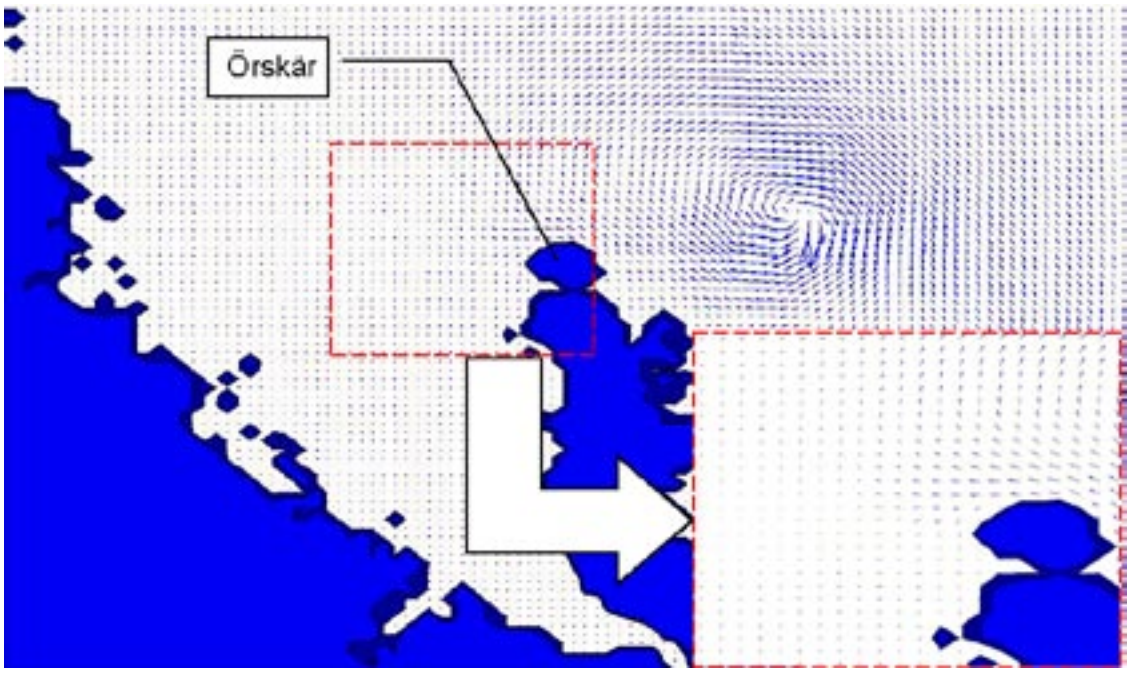

Figure 4-1. *Residual surface flow in March 2004, simulated with a model that has a horizontal resolution of ¼ nautical mile. Note the persistent eddy east of Örskär. The inset magnified flow picture (lower right corner) shows that along the northern boundary the average flow sets mainly towards east.*

then the overall spectral appearances can be compared irrespective of possible bathymetrical forming and deflection of the flow field. A spectral agreement with regard to the distribution of the variance (Figure 3-19) then should be a reflection of a balanced set of forcing (Table 2-1) both to its relative magnitude and temporal resolution. If so, the statistical distribution of velocities should also be mainly congruent. This means that the Eulerian slushing back and forth of water passing through the measurement site would be contributing in a similar manner to that of the local water exchange within an allowance of phase and time.

In general there are two main reasons for the found dissimilarities. The *first reason* is that these stations are located on the boundary interface between the coarse and the finer scale models. This means that the coarser resolution of the Baltic model will mostly influence the flow field. This is however modified to some extent when letting the boundary data (ZTS-file) force the finer resolved local model. The differences between the currents of the two models at the same sites are small. The *second reason* is related to the intrinsic variability of flow field. In a similar validation in Ålandian waters (Delet) two current meters were deployed for more than one month's time and located about 75 m apart. The correlation between these measurements on 3 m and 10 m depths respectively was found to be on the average 20%, while for each of these four time series the correlation with modelled components was approximately the double /Engqvist 2007/. The conclusion must be that the model struck a reasonable compromise between these measurements.

This cited evaluation also cast some doubts on the validity of the ADCP meter, since on the same site but with different meter ranges the correlation was not 100% as it should, but a mere 75% /Engqvist 2007/. This underscores the fact that ADCP measurements are based on averages of a large number of samples and thus are connected with a standard deviation that need not be small. The events of radically intensified currents, from surface to bottom, in Figures 3-8 and 3-10 turns on closer inspection to consist of a couple of hours of persistently and systematically increased currents with regard to depth that can only be given a plausible oceanographic explanation if large-scale eddies are invoked, as was argued for station Fo11, but could also be due to interferences (e.g. instrument anomalies) outside the present validation scope.

This also applies to the unfortunate placement of station Fo14. Not only was it relocated off the deeper channel on a site for which the depth of the grid is so much shallower that a comparison of currents was made impossible. In addition, during the third measurement period, the current regime was so radically changed that again an extraneous interfering factor must have been involved.

The transects (Figures 3-32a–d and 3-33) also confirm that there are current features that the larger grid cells of the Baltic model do not resolve. There are no obvious contradictions between the near-coinciding measurements of the currents along the northern boundary transect with boat-mounted ADCP vs. the point measurement with the same kind of instrumentation at station Fo11.

4.2 Temperature evaluation

The temperature dynamics displays a distinct seasonal curve that invariably peaks in summer and has a minimum during winter. This is the basic explanation why most models are capable of producing temperature data for which the correlations are quite good. The presently simulated temperature data are no exception with a correlation with a grand average above 90% (Table 2-3). This favorable achievement is however mitigated when looking at the decreasing correlations with depth. The rather crude formulation of the heat exchange through the air/water interface ignores the radiation portions of heating and cooling. Moreover, the ice formation and melting have been prescribed from data and not computed by the models. This part of the model formulation can certainly be improved, and in later versions the full equations of the /COHERENS 2004/ formulation have been implemented. The reason it has not been

included in this validation effort is because central data (e.g. nebulosity and irradiation) were missing in the employed (Mesan) meteorological data set. Temperatures are routinely measured with thermistor sensors that do not get clogged by biological growth of epiphytes and can thus be regarded as an example of a fully reliable metrological device.

4.3 Salinity validation

It seems that the most pertinent validation entity is the salinity, because salt is an almost ideal tracer of water exchange. It lacks state transitions (at least at the salinity levels occurring in normal coastal waters) and is from a chemical point of view basically inert. The good correlations obtained at the inner station Fo13 that on the average are on the 60% level thus bears a very favorable testimony to the model's capacity to simulate of the bulk of water exchange of the entire Öregrundsgrepen bay. From other studies of coastal embayment around the Baltic coast /e.g. Engqvist 1996/ and the same experience from other Scandinavian sites of investigation /Stigebrandt 1990, Stigebrandt and Aure 1990/, it is well established that the most effective mode of water exchange is the so-called intermediary exchange that is driven by relative density differences between the inside and the outside of an embayment. Since the salinity is the dominant factor in determining the varying horizontal density gradients, it follows that good salinity correlations mean that the water has been exchanged accordingly in both reality and in the model.

The malfunction of the salinity sensors for instruments in the photic zone near the surface, in particular during the production season in summer, is a known hazard (Björn Kjerfve, pers. comm.) impeding all salinity measurements based on conductivity measurement as a proxy for salinity. In this study there have been several occasions when this ailment has occurred while the salinity seems to be decreasing for regular oceanographic reasons. This enhances the difficulty to discriminate between which salinity data should be retained for the statistical analysis and which should be discarded. The well-considered result of such deliberation is given in Table 4-1.

As a bonus, the executioner of the field program (SMHI) undertook a series of complementary salinity and temperature measurements so as to produce profiles of these entities /Lindow 2005/ by casting an assumingly well-calibrated CTD instrument at the stations while the deployed meters were still in operation before and after lifting the instruments for data retrieval. Regarding the Fo11 station, the outcome was that the differences were outside the allowed inaccuracy of 0.1 in the psu-scale only a couple of instances. To the contrary, salinity comparisons for Fo12 both before and after redeployment were off by 1 and 0.2 units respectively. This confirms the earlier noted deficiency by growth of epiphytes that seemingly not to a sufficient degree had been removed during service. Concerning salinity comparison of the remaining stations, five of 18 such accounted pairs of possible comparison fell outside the allowed inaccuracy with three of those pertaining to the surface layer.

The found good correlations pertain however to time periods approximately coinciding with the duration of the measurement periods, i.e. of the order of a couple of months. From Figure 3-23 it is clear that for the two top instruments the measured salinity on the average decreases with time. This is doubtless a reflection of the Baltic model that cannot uphold the salinity of the top layers, since the same phenomenon can be seen in Figures 3-4 and 3-17. This is ultimately due to the delicate salinity balance of discharges of freshwater and the vertical mixing provided by the wind that is inherently difficult to maintain on extended time scales in any model (Kristofer Döös, pers. comm.). Off the coast east of Öregrundsgrepen the collective freshwater of all major rivers discharging into the Bothnian Bay passes with a few months of delay since their entering into the coastal waters. The induced residual south-flowing current is however occasionally interrupted by wind-induced reverse currents. This sets the modelling challenge in perspective and in the final analysis the good correlations of salinity at the inner station Fo13 must be regarded as an approval of the cascaded model approach in this encompassing validation test.

Table 4-1. Overview of the data that for various reasons have been discarded from the statistical analysis and thus also should properly be stricken from the SICADA data base. Discarded and missing data are marked in shading. The depths of the profiling instruments are indicated according to the convention: surfacemost position : depth interval : bottom-most position.

			Duration	discarded	Duration	discarded	Duration	discarded	Duration	discarded
	param.	depth [m]	1st period	mean. data	2nd period	mean. data	3rd period	mean. data	4th period	mean. data
Fo11	salinity	1.5	2004-04-16		2004-07-21	2004-08-01	2004-10-21		Missing	
			2004-05-01		2004-09-07	2004-09-07	2005-02-28		data	
	salinity	10	2004-04-16		2004-07-21	2004-07-21	2004-10-21	2005-02-17	2005-02-28	
			2004-07-21		2004-09-07	2004-09-07	2005-02-28	2005-02-28	2005-04-25	
	salinity	17.5	2004-04-16		2004-07-21	2004-08-23	2004-10-21		2005-02-28	
			2004-07-21		2004-10-21	2004-10-21	2005-02-28		2005-04-25	
	salinity	25	2004-04-16		2004-07-21	2004-08-23	2004-10-21		2005-02-28	
			2004-07-21		2004-10-21	2004-10-21	2005-02-28		2005-04-25	
	velocity	05:02:33	2004-04-16		2004-07-21		2004-11-09		Missing	
			2004-07-20		2004-10-20		2005-02-07		data	
Fo12	salinity	12	2004-04-20		2004-07-20	2004-08-26	2004-10-21		2005-02-28	
			2004-07-20		2004-10-21	2004-10-21	2005-02-28		2005-04-25	
	velocity	12	2004-04-20		2004-07-20		2004-10-21		2005-02-28	
			2004-07-20		2004-10-21		2005-02-28		2005-04-25	
Fo13	salinity	1.5	2004-04-20		2004-07-20	2004-07-20	2004-10-19		2005-01-04	
			2004-07-20		2004-10-19	2004-10-19	2005-01-04		2005-04-25	
	salinity	10	2004-04-20		2004-07-20	2004-09-08	C-data		C-sensor	
			2004-07-20		2004-10-19	2004-10-19	unreliable		failed	
	salinity	17.5	2004-04-20		2004-07-20	2004-07-20	2004-10-19		2005-01-04	
			2004-07-20		2004-10-19	2004-10-19	2005-01-04		2005-04-25	
Fo14	velocity	02:01:25	2004-04-21		2004-07-30		2004-10-20		2005-01-05	
			2004-07-22		2004-10-19		2005-01-04		2005-04-15	
	salinity	25	Missing		2004-07-30		2004-10-20		2005-01-05	
			data		2004-10-18		2005-01-04		2005-04-14	
Fo15	temp.	1:2.6:27	2004-04-21		2004-07-20		2004-10-19		purposely	
		tc	2004-07-20		2004-10-19		2005-01-04		dismoissed	
Fo16	salinity	1.5	2004-04-21		2004-07-20	2004-08-30	2004-10-19	2004-10-19	2005-01-04	
			2004-07-20		2004-10-19	2004-10-19	2005-01-04	2005-01-04	2005-04-25	
	salinity	10	2004-04-21		2004-07-20	2004-08-30	Missing		2005-01-04	
			2004-07-20		2004-10-18	2004-10-18	data		2005-04-25	
	salinity	18	2004-04-21		2004-07-20	2004-08-30	2004-10-18		2005-01-04	
			2004-07-20		2004-10-18	2004-10-18	2004-12-25		2005-04-25	

5 Conclusions

The major shortcoming of this modelling approach is the inaptitude of the Baltic model to maintain the salinity concentration over the present extended modelling period consisting of 16 consecutive months. As for the prospect of using these models for estimates projected into the far distant future, this does not constitute an insurmountable obstacle since the density structure of the Baltic will for such projections most likely only be available in general terms that are suitable for data assimilation /Westman et al. 1999/.

A measurement effort to resolve the large-scale current patterns revealed by the boat-mounted ADCP transects would have fallen far outside the admissible economic frames. The velocity comparisons of the two stations on the northern boundary have not corroborated the model's simulated velocities, but on the other hand have not falsified them either. The Baltic model does not yet fully resolve all the oceanographic near-shore relevant features.

The good temperature correlations could have been anticipated and were confirmed within the allowance of the found decreasing correlations towards the bottom.

The most virtuous outcome of the local fine resolution model is the found surprisingly good correlation of the inner station, Fo13. This ascertains that the overall salinity dynamics is realistically simulated by the local model notwithstanding the long-term less well-simulated forcing of the surface salinity entering through the border in the vicinity of the island Örskär. The influence of this land can arguably influence the flow and salinity fields at station Fo 11, as vouched for by the transects taken along the northern boundary.

For these reasons this present analysis of the validation programme shows that salinity and temperature dynamics at one interior station, Fo13, are broadly consistent with the measurements. This indicates that the modelling approach is adequately designed, but cannot be considered to constitute complete approval of the model methodology. For such approval to be closer obtained, corroborating evidence would be desirable for at least one more interior point, which the unfortunate placement of station Fo14 has forfeited.

6 Acknowledgements

We thank in the first place Ulrik Kautsky and Tobias Lindborg, both affiliated with SKB, for the confidence of giving us the opportunity to design and analyse this validation program. We also thank Sara Karlsson, local ecologist at Forsmark for lending us a helping hand on several occasions. She and Regina Lindborg have also given many valuable points of view on the first manuscript version as has a nonymos external reviewer on a later version. We extend our gratitude also to Björn Becker and Robert Hillgren, both of SMHI, for a positive and helpful attitude and for sharing their expertise on field assays.

7 References

Andrejev O, Sokolov A, 1989. Numerical modelling of the water dynamics and passive pollutant transport in the Neva inlet. Meteorologia i Hydrologia, 12, 78–85, (in Russian).

Andrejev O, Sokolov A, 1990. 3D baroclinic hydrodynamic model and its applications to Skagerrak circulation modelling. 17th Conf. of the Baltic Oceanographers, Proc., 38-46, 23, 280–287.

Andrejev O, Sokolov A, 1997. The data assimilation system for data analysis in the Baltic Sea. System Ecology contributions No. 3. 66 pp.

Andrejev O, Myrberg K, Lundberg P, 2004a. Age and renewal time of water masses in a semi-enclosed basin – application to the Gulf of Finland, Tellus, 56A, 548–558.

Andrejev O, Myrberg K, Alenius P, Lundberg P, 2004b. Mean circulation and water exchange in the Gulf of Finland – a study based on three-dimensional modelling. Boreal Env. Res., 9, 1–16.

COHERENS, 2004. EU Marine Science and Technology Programme, Contract No MAS3-CT97-0088.

Engqvist A, 1996. Long-term nutrient budgets in the eutrophication of Himmerfjärden estuary. Estuarine, Coastal & Shelf Science, 42, 483–507.

Engqvist A, Andrejev O, 1999. Water exchange in Öregrundsgrepen – A baroclinic 3D-model study. SKB TR-99-11, Svensk Kärnbränslehantering AB.

Engqvist A, Andrejev O, 2000. Sensitivity analysis with regard to variations of physical forcing including two possible future hydrographic regimes for the Öregrundsgrepen. A follow-up baroclinic 3D-model study. SKB TR-00-01, Svensk Kärnbränslehantering AB. 44 pp.

Engqvist A, Andrejev O, 2003. Water exchange of the Stockholm archipelago – A cascade framework modeling approach. J. Sea Res., 49, 275–294.

Engqvist A, Andrejev O, Döös K, 2006. Modelling water exchange and contaminant transport through a Baltic coastal region. Ambio, XXXV, 435–447.

Engqvist A, 2007. Den svenska modelleringsinsatsen. In: T Kohonen & J Mattila (Eds.) Mesoscale water quality models as support for decision making in the archipelagos of Turku, Åland and Stockholm, BEVIS final report. Forskningsrapporter från Husö Biologiska Station, No.118. pp. 20–62, (in Swedish).

Johansson L, Morosini M, 2002. Metodbeskrivning för Oceanografiska mätningar. SKB MD 364.009, (in Swedish).

Lindborg T, Lindborg R, Löfgren A, Söderbäck B, Bradshaw C, Kautsky U, 2006. A strategy for describing the biosphere at candidate sites for repositories of nuclear wase: linking ecosystems and landscape modeling. Ambio, XXXV, 418–424.

Lindow H, 2005. Forsmark site investigation Oceanographic measurements. SKB P-05-149, Svensk Kärnbränslehantering AB.

Omstedt A, 1999. Forecasting ice on lakes, estuaries and shelf seas. In: J S Wettlaufer, J G Dash and N Untersteiner (Eds.) Ice physics and the natural environment, NATO ASI Ser., Vol. I 56. Springer-Verlag, Berlin. pp. 185–207.

SKB, 2001. Site investigations. Investigation methods and general execution programme. SKB TR-01-29, Svensk Kärnbränslehantering AB.

Stigebrandt A, 1990. On the response of the horizontal mean vertical density distribution in a fjord to low-frequency density fluctuations in the coastal water. Tellus, 42A, 605–614.

Stigebrandt A, Aure J, 1990. De ytre drivkrefternas betydning for vannutskiftningen i fjorderne fra Skagerrak til Finnmark. Rapport FO 9003, Havforskningsinstituttet, Nordnes (N). 24 pp.

Westman P, Gustafsson B, Wastegård S, Omstedt A, Schoning K, 1999. Salinity change in the Baltic Sea during the last 8500 years: Evidence, causes and models. SKB TR-99-38, Svensk Kärnbränslehantering AB.

ISSN 1404-0344
CM Digitaltryck AB, Bromma, 2008